EXPERIMENTAL STUDY ON THE INVESTIGATION OF STRENGTHENING THE INSUFFICIENT REINFORCED CONCRETE BEAM-COLUMN JOINTS BY POST-TENSIONING

Özgür YURDAKUL

Master of Science Thesis

Civil Engineering Program

August 2015

This study was supported by Anadolu University Scientific Research Projects Commission under grant No. 1210F169.

JÜRİ VE ENSTİTÜ ONAYI

Özgür Yurdakul'un "**Experimental Study on the Investigation of Strengthening the Insufficient Reinforced Concrete Beam-Column Joints by Post-Tensioning**" başlıklı **İnşaat Mühendisliği** Anabilim Dalındaki, Yüksek Lisans Tezi 20.08.2015 tarihinde, aşağıdaki jüri tarafından Anadolu Üniversitesi Lisansüstü Eğitim- Öğretim ve Sınav Yönetmeliğinin ilgili maddeleri uyarınca değerlendirilerek kabul edilmiştir.

		Adı-Soyadı	**İmza**
Üye (Tez Danışmanı)	**:**	**Doç. Dr. Özgür AVŞAR**	**…….**
Üye	**:**	**Prof. Dr. Alper İLKİ**	**…….**
Üye	**:**	**Yard. Doç. Dr. Kıvanç TAŞKIN**	**…….**

Anadolu Üniversitesi Fen Bilimleri Enstitüsü Yönetim Kurulu'nun …… tarih ve …… sayılı kararıyla onaylanmıştır.

Enstitü Müdürü

ABSTRACT

Master of Science Thesis

EXPERIMENTAL STUDY ON THE INVESTIGATION OF STRENGTHENING THE INSUFFICIENT REINFORCED CONCRETE BEAM-COLUMN JOINTS BY POST-TENSIONING

Özgür YURDAKUL

Anadolu University
Graduate School of Sciences
Civil Engineering Program

Supervisor: Assoc. Prof. Dr. Özgür AVŞAR

2015, 117 pages

The efficiency of proposed strengthening methods using externally applied post-tension rods and CFRPs in the reinforced concrete external beam-column joints is investigated. Seven full-scale specimens were tested in the laboratory. One of the tested specimens, which is the reference specimen of well-detailed joint, complies with the current code requirements. On the other hand, remaining specimens have certain deficiencies resulting from lack of shear reinforcement in the joint and poor material properties such as low strength concrete and the presence of plain round bars. All specimens were subjected to quasi-static cyclic loading in the laboratory and different levels of structural damage were observed. A ductile response with the damage concentrated in the beam was found in the well-detailed specimen. However, the reference specimen of substandard joints displayed a brittle behavior with severe damage mostly in the joint while the rest of the RC components were almost in their elastic range. Depending on the damage type, the damaged members of both substandard and well-detailed reference specimens were repaired by CFRPs wrapped with different configurations. While one specimen was retrofitted by CFRPs, before the occurrence of damage, four of them were strengthened by externally applied post-tensioning. After testing all specimens, the ultimate lateral load capacity was improved considerably by proposed retrofit techniques. Experimental studies show that, lateral force capacities of the retrofitted specimens were mostly improved by either axial load in the post-tensioned rods or the number of CFRPs layers.

Keywords: Post-tension, beam-column joint, retrofit, CFRPs, repair

ÖZET

Yüksek Lisans Tezi

YETERSİZ KESME DAYANIMINA SAHİP BETONARME KİRİŞ-KOLON BİRLEŞİM BÖLGELERİNİN ARDGERME İLE GÜÇLENDİRİLMESİNİN DENEYSEL YÖNTEMLE İNCELENMESİ

Özgür YURDAKUL

Anadolu Üniversitesi
Fen Bilimleri Enstitüsü
İnşaat Mühendisliği Anabilim Dalı

Danışman: Doç. Dr. Özgür AVŞAR

2015, 117 sayfa

Betonarme kiriş-kolon birleşim bölgelerinde dıştan uygulanmış ard-germe çubuğu ve CFRPs ile güçlendirmenin etkinliği bu çalışmada araştırılmıştır. Yedi tam ölçekli numune laboratuvarda test edilmiştir. Deney numunelerinden bir tanesi, iyi tasarlanmış birleşimimn referans numunesi, güncel yönetmelik şartlarına uygun tasarlanmıştır. Diğer numunelerde birleşim bölgesinde kesme donatısının olmaması, düşük beton dayanımı ve düz donatı bulunması gibi önemli zayıflıkları mevcuttur. Tüm deney numuneleri tersinir tekrarlı yatay yükler altında test edilmiş ve farklı hasar seviyeleri gözlenmiştir. Güncel yönetmeliğe göre dizayn edilen numunede sünek kiriş hasarı gözlenirken, yönetmeliğe uygun olarak tasarlanmayan birleşim bölgesinin referans numunesinde göçme, numunenin diğer elemanları elastik bölgede iken birleşimde kesme hasarı şeklinde gözlenmiştir. Hasar tipine göre her iki referans numunenin hasarlı elemanları CFRPs ile onarılmıştır. Numunelerden bir tanesi CFRPs ile güçlendirilirken, dört adeti dıştan uygulanmış ard-germe çubuğu ile güçlendirilmiştir. Tüm numuneler test edildikten sonra, önerilen yöntemler ile numunelerin yatay yük kapasitelerinde önemli bir artış bulunmuştur. Gerçekleştirilen deneysel çalışmalar göstermiştir ki, numunelerin yatay yük kapasiteleri ard-germe çubuklarındaki eksenel yük ve birleşimdeki CFRPs katmanı sayısına bağlıdır.

Anahtar Kelimeler: Ard-germe, birleşim, güçlendirme, CFRPs, onarım

This thesis is dedicated to my family

ACKNOWLEDGEMENT

I am deeply grateful to my supervisor Assoc. Prof. Dr. Özgür AVŞAR for his guidance, invaluable suggestions and technical expertise. Learning from him not only scientifically but also personally was a great honor for me.

I would like to express my endless gratitude to thesis committee members Prof. Dr. Alper İLKİ and Assist. Prof. Dr. Kıvanç TAŞKIN for their time, offering helpful comments.

I am thankful to my colleagues Res. Asst. Onur TUNABOYU and Res. Asst. Burak EVİRGEN for not only their help and contributions but also friendship.

It is a pleasure to thank to İlkay KARA (HAS BETON A.Ş.) and Adil TEKE (SELKA BETON A.Ş.) for their support during the study. I am also grateful to BASF company for providing strengthening materials.

This study is supported by Anadolu University Scientific Research Projects Commission under grant no: 1210F169, which is also acknowledged.

Last, but not least, I want to thank to the staff of machine shop, but especially to Zülfükar ERTEKİN, Günay MERT and Mutlu BAŞ. I also would like to convey my appreciation to Erdoğan ÖZKAN and İbrahim TUNÇ for their help in the laboratory.

Finally, I wish to dedicate this thesis to my parents Gonca and Özkan YURDAKUL. This study would be nothing without their unconditional support and enduring love.

Özgür YURDAKUL

August 2015

TABLE OF CONTENTS

LIST OF FIGURES

LIST OF TABLES

LIST OF SYMBOLS

A	:	Area (mm^2)
d	:	Distance from extreme compression fiber to centroid of longitudinal tension reinforcement (mm)
Δ	:	Displacement
ΔF	:	Change in the axial force of rods (kN)
E	:	Young's modulus of reinforcement bar (MPa)
ε	:	Strain (mm/mm)
f	:	Strength (MPa)
F	:	Force (kN)
γ	:	Joint shear strain (rad)
K	:	Stiffness (kN/mm)
L	:	Gauge length (mm)
μ	:	Ductility
N	:	Axial load (kN)
P	:	Axial force in the one post-tension rod (N)
s	:	Spacing of transversal reinforcement in the joint (mm)
σ	:	Normal stress (MPa)
τ	:	Shear Stress (MPa)
T	:	Tensile force (MPa)
V	:	Shear force (MPa)

Subscript and superscript

c	:	Compression
CFRP	:	Carbon fiber reinforced polymer
d	:	Diagonal
d1,2	:	Number of rods
h	:	Horizontal
ini	:	Initial
j	:	Joint
jh	:	Joint shear force
jmax	:	Joint maximum

max	:	Maximum
p	:	Peak-to-peak
PT	:	Post-tension
st	:	Stirrup
*		Displacement in terms of drift ratio
t	:	Tension
u	:	Ultimate
v	:	Vertical
xy	:	Prediction
y	:	Yield
0.80	:	20% reduction of maximum lateral load

CHAPTER 1

1. INTRODUCTION

1.1. Overview

Field reconnaissance after damaging earthquakes in Turkey (Marmara 1999, Bingöl 2003, Van 2011) showed insufficient seismic performance in reinforced concrete (RC) structures built with low strength concrete (8-10 MPa), inadequate or no transverse shear reinforcement in the beam-column joints, plain round bars and improper hook detailing of bars [1]. Because of poor seismic performance of frames, devastating brittle failure can occur in the members. These local damages can thus actuate the global failure mechanism, which brought the requirement to investigate behavior of substandard members. The beam-column joint region needs specially interest in buildings with indicated deficiencies as it can be the critical and possibly the weakest link according to capacity design or hierarchy of strength considerations [2]. Several attempts thus far have been made to investigate the behavior of beam-column assembles under seismic action. However, assuming the rigid joint panel zone is still the most common tendency, which neglects the contribution of inelastic response of the joint to the overall structural performance.

According to the capacity design principles, a ductile response is expected from RC structures by the occurrence of nonlinear behavior in the beam-ends through the formation of plastic hinges. To meet such failure mode, the beam-column joint must prevent their integrity and have an ability of transferring the seismic forces to the other members under seismic action [2]. Because of indicated deficiencies, brittle joint failure modes can be observed while the rest of the RC components were in their elastic range. This, of course, results in poor energy dissipation and sudden decrement in the response quantities such as strength and stiffness. It is therefore important to pay enough attention on the design of beam-column joint.

Several guidelines such as American Concrete Institute (ACI) 352-2002 [3], Turkish Earthquake Code (TEC) 2007 [4] describes the design of joint in detail.

However, most of the existing buildings are constructed with certain deficiencies and they do not comply with the current code requirements. Therefore, many studies have been performed to investigate the behavior of non-seismically designed joints. Most of the available literatures on the deficient beam-column joints focus on buildings constructed prior to developing earthquake resistant design details in the 1970s. However, the tested specimens in the previous studies still do not represent the most of building stocks in Turkey even though they do not comply with former building standards. Because, buildings designed according to pre-1970 construction practice were normally constructed with lack of shear reinforcement in the joint. On the other hand, most of the building stock in the Turkey constructed with not only lack of transverse reinforcement in the joint but also low strength concrete. Hence, there exists scarce number of contributions representing the Turkish building stock, which brought the requirement to understand the response of the joints in such deficient buildings.

A sufficient response should be expected even in the buildings with several deficiencies in order to satisfy life-safety performance requirement. For this reason, developing a feasible retrofit strategy become more of an issue so as to improve the seismic performance of such buildings. The well-known retrofit techniques in the literature can be categorized into two main groups namely; "System Retrofit" and "Member Retrofit". While the system retrofit technique is used to reduce the seismic demand of the building by adding extra load resisting elements such as base isolation, steel brace and shear wall, the individual elements of deficient building are upgraded in local retrofit technique [5,6,7]. System retrofit technique is generally more efficient compared to member retrofit technique since the overall capacity of the building is enhanced. However, cost efficiency of the retrofit strategy should be taken into account. Therefore, member retrofit technique can be carried out for certain cases depending on the need for retrofitting [7]. Beam-column joint is one of the most critical structural members, which can be upgraded by member retrofit technique in non-seismically designed buildings since they are the key components to ensure the structural integrity. Nevertheless, issues of cost, difficulties in the application and transmission of joint forces to the rest of the members in some retrofit techniques are still among the limitations of the joint

strengthening technique. Therefore, the retrofit of deficient joints remains the most challenging and current task of today.

RC frames containing some of the indicated deficiencies may be exposed to brittle type of failure at local level such as failure of beam-column joint. This can result in moderate to severe structural damage or even the total collapse of moment-resisting frame buildings. RC buildings with moderate to severe structural damage after the earthquakes should be demolished or repaired depending on the damage level. Different techniques exist in repairing of the damaged RC members according to their damage level. Repairing the non-structural components can be sufficient for lightly damaged RC buildings. Moderately damaged RC buildings can only be serviceable after the application of sufficient structural repairing techniques. However, the effectiveness of different repairing techniques to moderately and severely damaged RC joints must be investigated in detail.

1.2. Research Objective and Scope

The current study was supported by Anadolu University Scientific Research Projects Commission under grant No. 1210F169. It aims to minimize the damage in the joint of existing building during damaging seismic action by using different retrofit techniques. These are externally applied post-tension rods and CFRPs.

Within the content of this study, seismic behavior of both benchmark and rehabilitated RC beam-column joints is investigated through laboratory tests under combined effect of axial load and quasi-static cyclic lateral load. Therefore, seven full-scale test specimens, which are taken from the inflection points of the frame, were tested. They represent the exterior beam-column assembly. The top-end of the column was subjected to quasi-static reversed cyclic loading, which is considered to be the representative earthquake force. The results of the research lead us to understand the behavior of RC beam-column joints, CFRP repaired joints and joints strengthening with either CFRPs or post-tensioning technique.

This study mainly aims to examine experimentally if the usage of post-tension rods in the joint panel can be efficient to retrofit the non-seismically designed joints. Because, most of the structures in the building stock of Turkey did not comply with the design principles of both current and former earthquake codes. Therefore, six

specimens constructed with certain deficiencies such as lack of shear reinforcement, plain round bars and low strength concrete. In addition, the viability of the proposed method should be ensured. Therefore, while six of them were built with column and in plane beam, one of the tested specimens also consisted of transverse beam to demonstrate the on-site application of the retrofit by post-tension.

The second purpose of the research is to investigate the behavior of joints, which were retrofitted by carbon fiber-reinforced polymer (CFRP).

The third objective of this study is to develop an applicable CFRPs repair technique for moderate or severe damaged joints. It is known that moderate or severe damage can be observed in the buildings with indicated deficiencies during even moderate earthquakes [1]. This study therefore intended to develop a feasible repair technique for different damage types in the joint.

Finally, the response of joints designed according to current code requirements was also intended to be investigated. Hence, one of the tested specimens was designed according to TEC 2007 [4]. It was also repaired with CFRPs after certain level of damage.

Based on the research interest in this study, the following objectives can be drawn.

1. To develop a new, efficient and cost effective strengthening solution by using conventional structural materials for deficient joints.
2. Investigating the efficacy of post-tensioning technique to improve the response quantities of joint.
3. To ensure the viability of strengthening with post-tension for existing structures.
4. To investigate the contribution of CFRPs on the strength and ductility for non-seismically designed joints.
5. To present a rational and applicable way to wrap CFRPs during repair process.
6. To investigate the behavior of both substandard and well-designed RC corner beam-column joints.

1.3. Manuscript Organization

This research context is organized in seven chapters. The output of the study and its context was presented in this chapter. The next chapters are introduced as follows.

Chapter 2 summarizes the current state of information on the deficient joints. It also gives a general review on the response of joints including load transfer mechanism and the joint failures in recent earthquakes.

Chapter 3 presents an extensive literature survey on the seismic behavior of both the well-designed and deficient joints. It summarizes data found in the literature on the retrofit of deficient joints. The prior experimental studies performed to repair the damaged joints are also investigated in this chapter.

Chapter 4 describes the details of experimental programs including construction of the specimens, manufacture of the test set up, assembly of the test set up, measuring, instrumentation and loading procedure.

Chapter 5 presents monitored response parameters and damage patterns in terms of hysteric response and pictures of test specimens, respectively.

Chapter 6 deals with the discussion of current experimental results. The overall performance of both well-designed and substandard reference specimens is compared with repaired/retrofitted specimens in this section. Test results for the effectiveness of retrofit schemes are discussed in terms of the response quantities such as strength, stiffness, stiffness degradation, ductility and energy dissipation capacity of the specimens.

Chapter 7 introduces summary of conducted study and concluding remarks drawn from this research. Suggestions for future research are also included in this chapter.

CHAPTER 2

2. BEAM-COLUMN JOINT: BACKGROUND

The current state of deficient joints is presented in this section. The given sections involve joint failures in the past earthquakes, major group of deficiencies and load transfer mechanism of the joint.

2.1. Deficient Beam-Column Joint: Need For Research

Reinforced concrete buildings constructed with no or inadequate consideration of seismic effects, which are commonly referred to as gravity-load-designed buildings, constitute a significant portion of the building inventory in many countries and pose a significant risk for society [8]. Under these circumstances, the necessary precautions should be taken immediately to avoid further losses. However, the performance of such deficient members should be known under the seismic action. Most of the existing studies on the behavior of the beam-column joints have mostly focused on well-detailed assemblies. There exists limited number of contributions on the joints, which were constructed according to pre-1970s construction practice. However, the presented studies still do not fully represent the deficient RC buildings in Turkey even though they do not comply with the former building standards. In addition, they emphasized significance of taking necessary precautions for such buildings. Hence, a study including the response of deficient joints in Turkey and their retrofit has a vital importance. Even though the application of joint retrofit technology with conventional or new materials begun in the past, limitations of each strengthening technique still remain the most challenging part of today. Therefore, an efficient, viable and practical strengthening solution is required to meet the increased demand. This study is conceptually proposed to retrofit the substandard RC beam-column joints with externally applied post-tension rods. An additional study on the response of both well-detailed and deficient joints, repair of them, and strengthening of the non-seismically designed joints by CFRPs were also conducted.

2.2. Load Transfer Mechanism

2.2.1. Mechanism of shear resistance

Under seismic excitation, beam-column joint is subjected to large shear stress due to the internal forces developed at member ends (Figure 2.1).

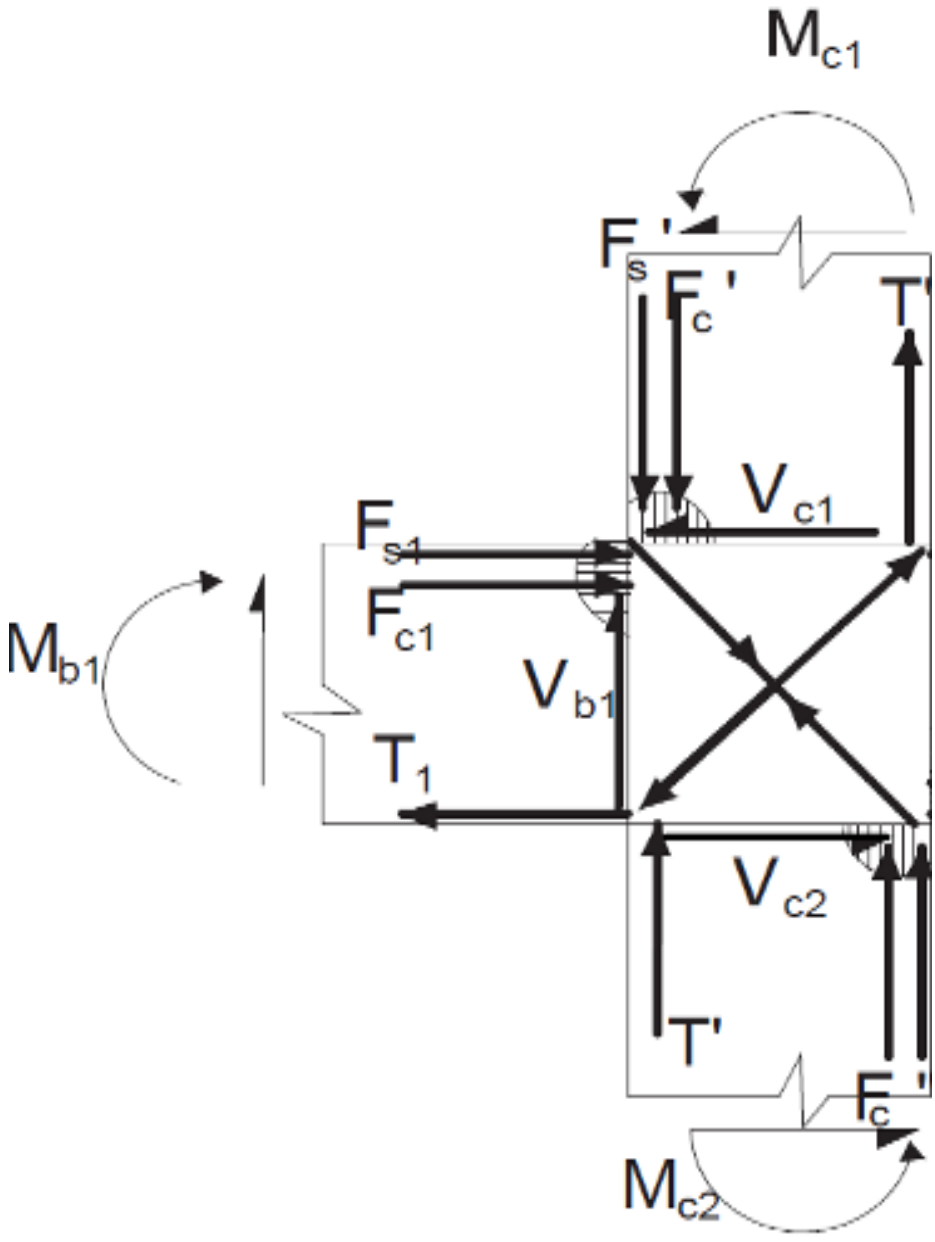

Figure 2.1. Mechanism of shear resistance [9]

The shear force demand in the joint can be written from the equation of equilibrium, which is visually presented in Figure 2.1 (Equation 2.1).

$$V_j = F_{s1} + F_{c1} - V_{c1} \quad (2.1)$$

As the force T_1 equals to the sum of the forces F_{s1} and F_{c1}, Equation 2.1 can be rearranged to new form, Equation 2.2.

$$V_j = T_1 - V_{c1} \quad (2.2)$$

V_j, T_1, V_{c1} denotes joint shear force, tensile force in the beam reinforcement bar, horizontal load applied at beam-column assembly, respectively. The parameter, V_{c1}, is monitored column tip load (column shear force) by load cell during the experiment. The tensile force in the longitudinal reinforcement of beam (T_1) can be obtained from either measured data in strain gauges that located in the beam longitudinal bars or section analysis. In this study, the tensile force in the beam (T_1) was calculated in both ways. For more information, the method proposed by Park and Pauley [10] should be investigated in calculation of joint shear force.

2.2.2. Mechanism in the post-tensioned specimens

As the tested specimens represent the exterior beam-column joint, the load transfer mechanism is visually presented in the retrofitted joints via post-tension. The equation of equilibrium for the retrofitted specimens through the post-tension was also presented in this section.

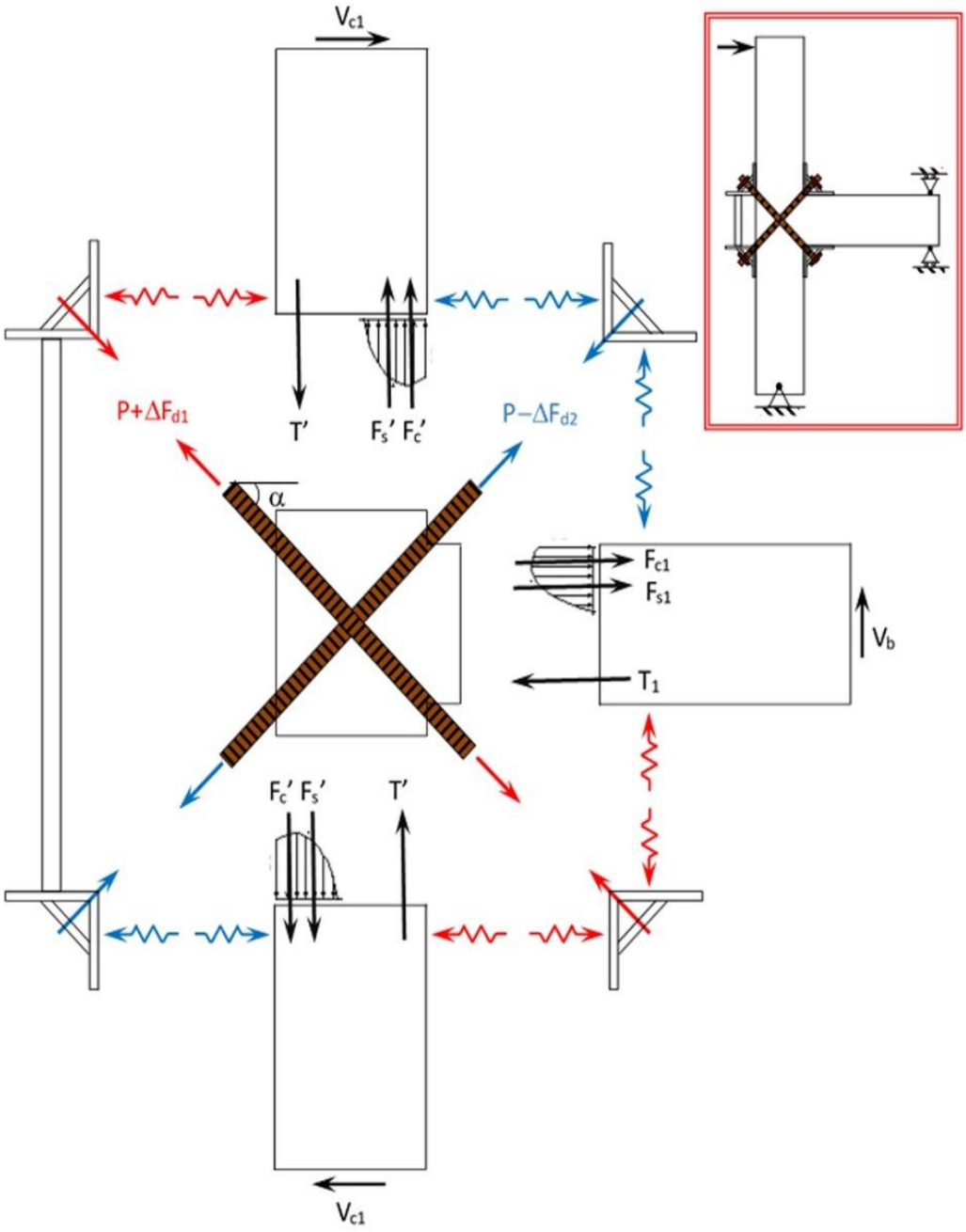

Figure 2.2. Load transfer mechanism in the retrofitted specimen

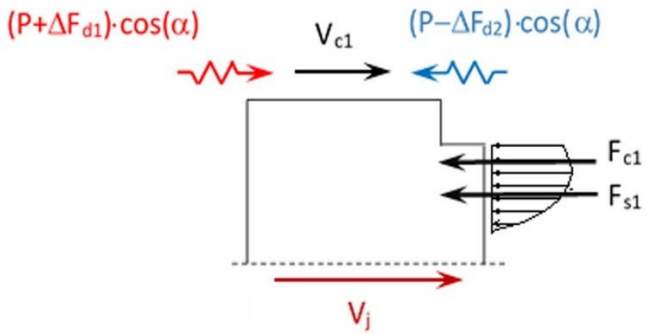

Figure 2.3. Close-up view of the retrofitted joint

The equation of equilibrium of the joint can be written as,

$$V_j = F_{c1} + F_{s1} - V_{c1} - (\Delta F_{d1} + \Delta F_{d2}) \cos \alpha \qquad 2.3$$

It is known that sum of the forces F_{s1} and F_{c1} equals to T_1 so Equation 2.3 can be rewritten as in Equation 2.4.

$$V_j = T_1 - V_{c1} - (\Delta F_{d1} + \Delta F_{d2}) \cos \alpha \qquad 2.4$$

Where the ΔF_{d1} and ΔF_{d2} are the change in the axial force of rods due to the deformation imposed in the rods during the tests.

2.3. Joint Failures in the Past Earthquakes

Non-seismically designed RC frames suffer from brittle type of failure at local level such as shear failure of beam-column joint. This can result in moderate to severe structural damage or even the total collapse of moment-resisting frame buildings. The reconnaissance reports for the recent earthquakes on the substandard RC joints show the damage level in the existing buildings [1,11,12]. Figure 2.4-Figure 2.8 visually present the severity of damages in the past earthquakes. Examples including joint failures are Erzincan-Turkey Earthquake (1992), Adapazarı-Turkey Earthquake (1999), L'Aquila-Italy Earthquake (2009), Simav-Turkey Earthquake (2011).

Figure 2.4. Erzincan-Turkey Earthquake (1992), Photo credit: Güney ÖZCEBE [8]

Figure 2.5. Collapsed building in Adapazarı-Turkey Earthquake (1999) [13]

Figure 2.6. L'Aquila-Italy Earthquake (2009), Photo credit: Özgür AVŞAR [14]

Figure 2.7. Simav-Turkey Earthquake (2011), Photo credit: Özgür AVŞAR [14]

Figure 2.8. Adapazarı-Turkey Earthquake (1999), Photo credit: NISEE [15]

CHAPTER 3

3. LITERATURE REVIEW

The knowledge about behavior of the beam-column joint, repair and retrofit of the deficient joint is presented in this section. Therefore, numerous up-to-date literature surveys belonging the response of the as-built, repaired and strengthened joints are included. Laboratory test techniques for both deficient and well-designed joints are also discussed.

In Section 3.1, the response of as built specimens was investigated deeply. Two rehabilitation techniques, which are repair and retrofit of the beam-column joints, are within the content of this study. Therefore, an extensive literature survey on either repair or retrofit of the joint was also included. Those related to the repair and retrofit of the joints were summarized in Section 3.2 and 3.3, respectively.

Among the limited number of recent studies on joints, papers described in the following sections are the most extensive.

3.1. Performance of the Joint

Hassan [15] reports the assessment of seismic performance of the unconfined corner beam-column joints in existing buildings (Figure 3.1a and b). Four full-scale tests of corner joints were tested under the unidirectional and bidirectional displacement-controlled quasi-static loading. To simulate the overturning seismic moment effects, the axial load was applied regarding to the lateral load. It varied about 50% during the experiments.

The test variables were loading procedure, beam reinforcement and joint aspect ratio. While the deformation in the joint was decreased by high axial load, there was an enhancement in the joint shear strength.

The role of joint aspect ratio is much certain. The deeper the joint, the lower the shear strength is found. The lower strength with respect to unidirectional loading was also observed in the joints loaded in bidirectional axis.

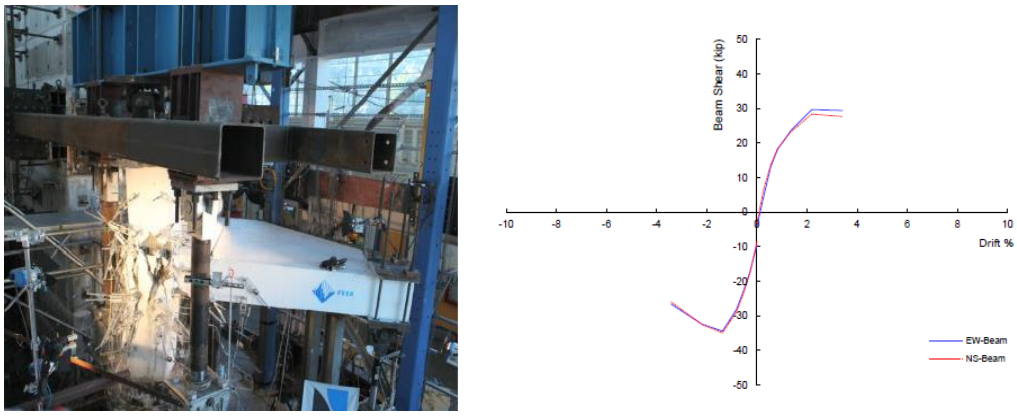

(a) (b)

Figure 3.1. (a) Axial failure of B-J-1 (b) backbone curve of hysteresis loops [15]

Pantelides et al. [16] performed six full-scale tests of exterior beam-column joints. All the specimens were constructed without shear reinforcement in the joint and transverse beam. The effect of anchorage detail and axial load was investigated in this study. The tested anchorage details were (i) short embedment of the beam bottom bars (ii) embedment up to far side of the joint (iii) bent up beam bottom bars (Figure 3.2). Three different anchorage types preceded the response of the tested specimens, which were bond-slip failure in the specimen with short embedded beam bottom bars, beam-joint failure and joint shear failure in rest of the anchorage details. Two different axial load were applied which are $0.1f_cA_c$ and $0.25f_cA_c$. Depending on the anchorage detail, there was 15-35% strength enhancement in the specimens.

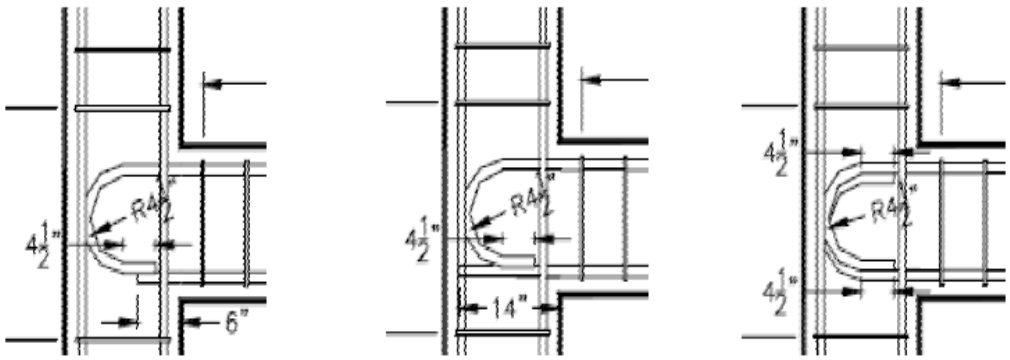

Figure 3.2. Anchorage detail of tested specimens [16]

Wong [17] presents the tests of eleven full-scale exterior beam-column joints (Figure 3.3). The variables of the tests are axial load, joint aspect ratio, and reinforcement detail in the column longitudinal bars and hooks of beam longitudinal bars. All specimens displayed brittle type of failure with concentration of the damage in the joint (joint shear failure) or joint shear failure shortly after beam yielding (beam-joint failure). The applied axial load was in the range between $0.03f_cA_c$-$0.15f_cA_c$. An improvement was observed in the strength of the specimens that were constructed with intermediate column reinforcement. The increase in the beam height resulted in a decrement in the joint shear strength.

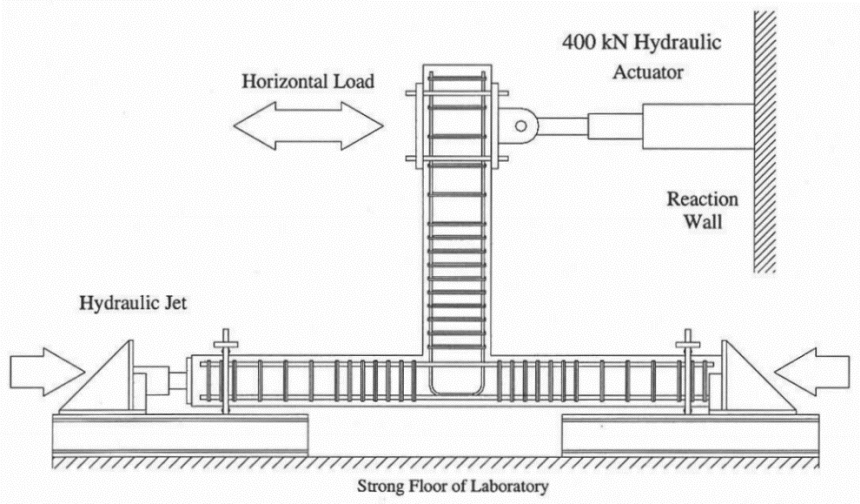

Figure 3.3. Test set up for reversed loading [17]

Bedirhanoglu et al. [18] reports the effect of welding of the beam bottom and top hooks to each other. The test parameters were the hook detail, the joint shear reinforcement, the axial load and the displacement history. Depending on the axial load and anchorage detail, there were two major failure modes in the specimens. The bond slip failure preceded the overall response in the specimens constructed with bent up anchorage detail. On the other hand, the combination of bond slip and joint shear failure was observed in the specimen whose beam top and bottom longitudinal bars' hooks were welded. There were nine test specimens built with low strength concrete and plain round bars. Some of the tested specimens were also constructed with transverse beam and slab (Figure 3.4). There different levels of axial load, which were zero axial load, $0.125f_cA_c$ and $0.50f_cA_c$, were tested. A 20%

of strength enhancement was found between specimens with and without axial load. Maximum load observed in the specimen without transverse beam and slab was 30% less. The difference in the capacity can be attributed to the presence of the transverse beam and slab. Two of the specimens were tested under different displacement history. No notable difference was monitored in the lateral load carrying capacities of the specimens.

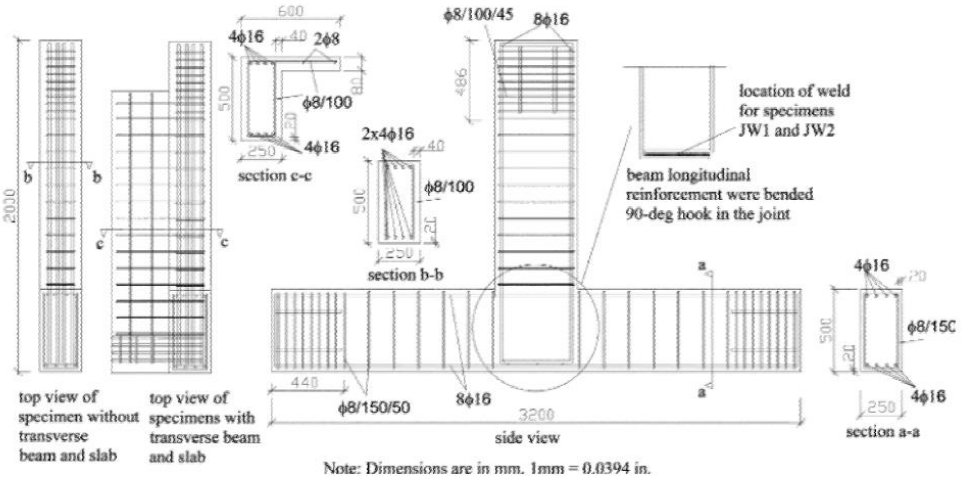

Figure 3.4. Reinforcement detail of the specimens [18]

Park and Mosallam [19] present the test of four full-scale RC joints which were constructed according to pre-1970s construction practices. Therefore, there was no joint shear reinforcement, which leads to non-ductile behavior. The specimens were built with transverse beam and slab and tested under quasi-static cyclic loading. The joint aspect ratio, which is the ratio of beam to column cross-section heights, and the beam longitudinal reinforcement ratio are the test parameters in this study. After testing the specimens, it is found that the lateral load capacities were covered by joint shear strength. Therefore, the damage was mostly concentrated in the joint due to lack of the transverse reinforcement. Then, a poor seismic performance was observed during experiments. One of the parameters effecting the joint shear strength is the joint aspect ratio, which is inversely proportional to joint shear strength. The increase in the joint aspect ratio decreases the joint shear strength. Joints without shear reinforcement underwent shear failure either prior to or after beam yielding. Therefore, overall response could not be

affected by the beam longitudinal reinforcement. It only limited the beam yielding so the failure could be either joint shear failure or beam-joint failure (Figure 3.5).

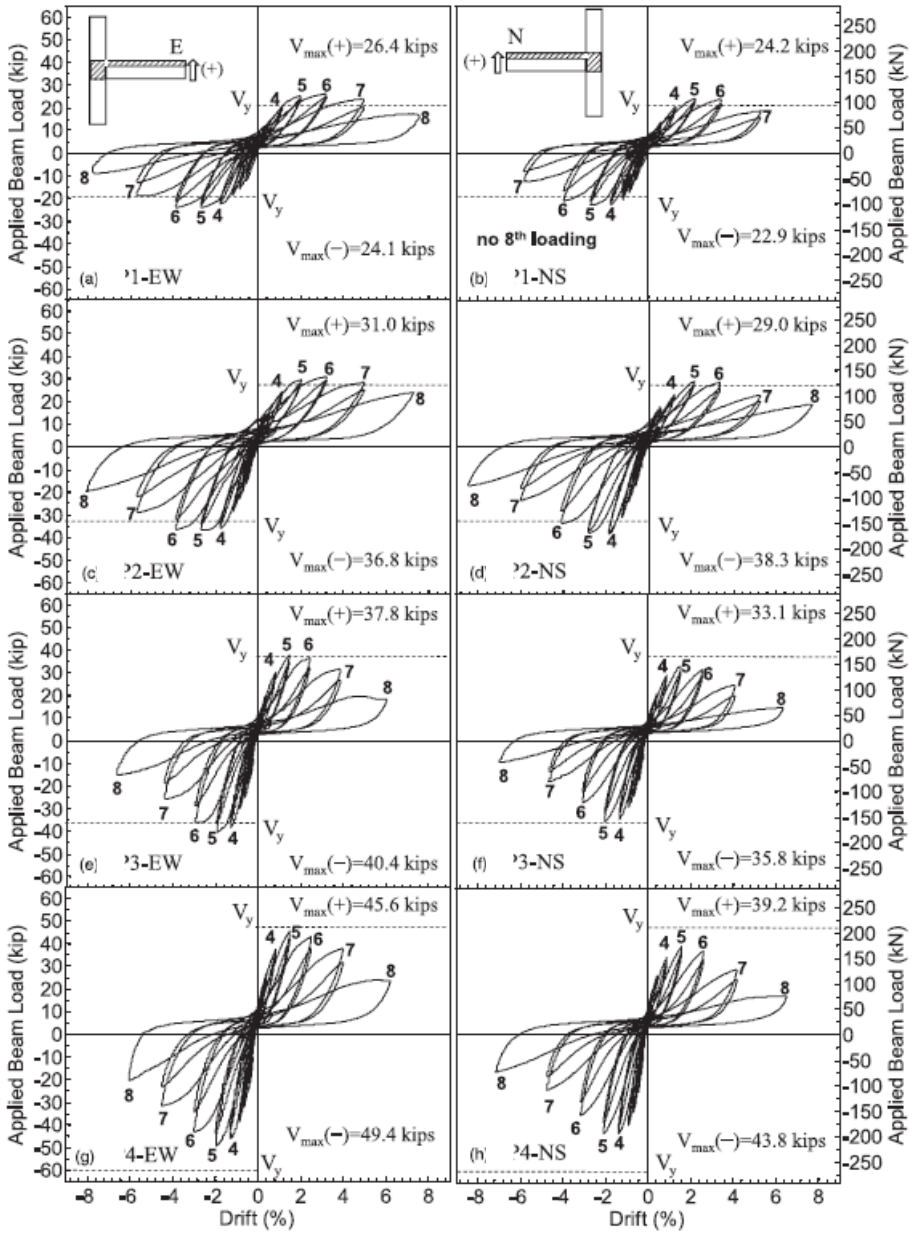

Figure 3.5. Hysteresis responses of the four test specimens [19]

Kotsovou and Mouzakis [20] report the test series of six full-scale beam-column joints. All of the well-detailed specimens were subjected to cyclic loading. The lateral displacement was applied at the top of the upper storey column level. The beam end detailed such that they become zero-moment and movement-free joint like roller support (Figure 3.6). Effect of inclined reinforcement in the joint

and welding of the beam longitudinal reinforcement to a plate mounted at joint back were investigated. All specimens displayed a ductile behavior with beam yielding. A relatively less shear deformation with respect to specimen without additional reinforcement is monitored in the specimens with inclined reinforcement in the joint. The shear deformation was also less in the specimen built with joint back plate.

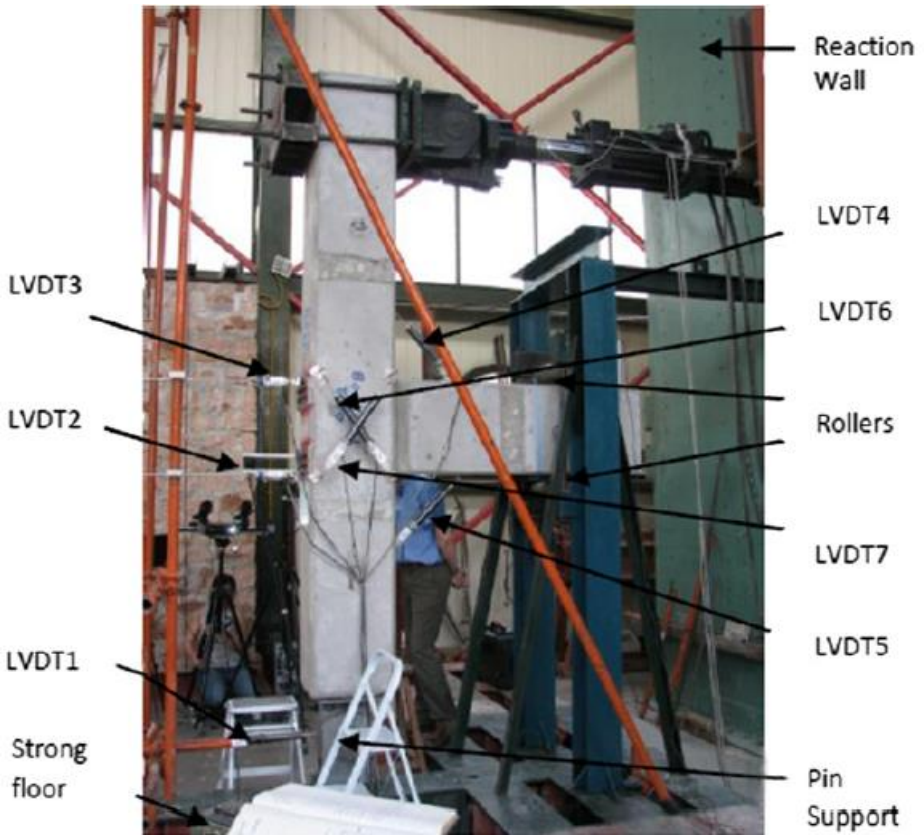

Figure 3.6. Test set up [20]

Burak and Wight [21] investigated the effect of eccentricity on the response of exterior joints. The test parameters were beam width, column section aspect ratio and the eccentricity of the spandrel beam with respect to the centroidal axis of the column. Three 3/4 scale specimens were tested under the combined effect of bidirectional loading. However, loading history was applied to the specimens separately in each direction (Figure 3.7a and b). In other words, the specimen was first loaded in the spandrel beam direction. After that, the specimen was rotated 90 degrees. Finally, the second test was performed in the normal beam direction. The

built up specimen, which was constructed with a square column, regular-sized beams, and lower eccentricity, complied with the ACI code requirements. On the other hand, a higher eccentricity and a rectangular column with wide beam existed in the second specimen. A wide-normal beam and a rectangular column were carried out in the third specimen. The level of joint stress was also increased in this specimen. In spite of the high eccentricity levels, the spandrel beams reached its plastic flexural capacity in all test specimens. The monitored moment capacity of the normal beam and its design values matched closely in two specimens. Diagonal shear cracks were observed at joint core in the highly eccentric specimens. It was also emphasized that the softening of members due to prior loading did not affect the joint strength.

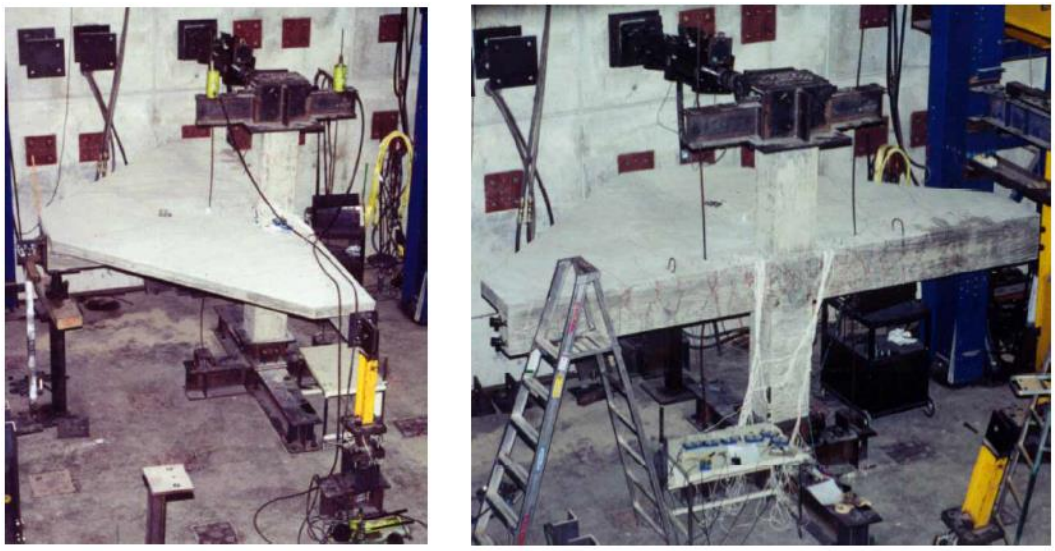

(a) (b)

Figure 3.7. Loading of the specimens (a) spandrel (b) normal beam directions [21]

Unal and Burak [22] present the response of one exterior and one interior joint of a 1:2 scale three storey frame. Pseudo-dynamic testing method was carried out the seismically designed frame to represent the earthquake excitations with different intensities (Figure 3.8a). Even though the design parameters of the joint comply with the TEC 2007 [4] and ACI 352-2002 [3], failure type was partially joint mechanism for the high intensity earthquake loading (Figure 3.8b). Nevertheless, the frame continued to carry the applied gravity load without significant lost in its lateral load-carrying capacity [22].

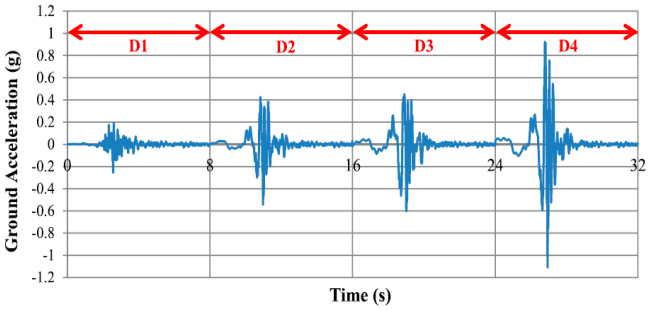

(a)

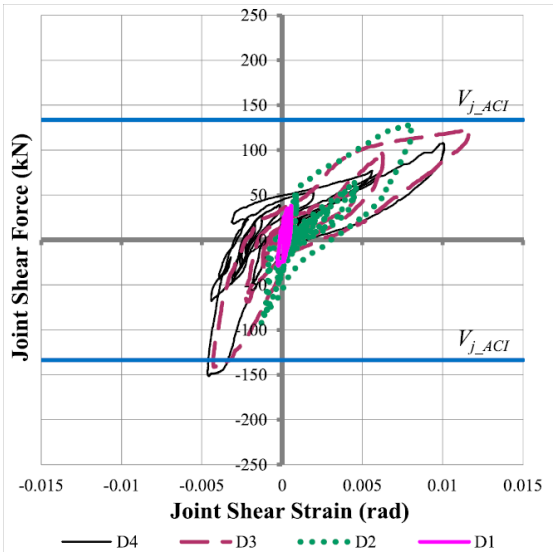

(b)

Figure 3.8. (a) Ground motion data (b) response of exterior joint [22]

3.2. Joint Repairing

Karayannis et al. [23] report the evaluation of specimens' performance in both before and after repair process. Therefore, seventeen specimens with different reinforcement detail in the joint were used in this study. The specimens were initially subjected to the cyclic loading until maximum lateral load was decreased to 40% of the yield load. Then, initially damaged specimens were repaired by epoxy injection (Figure 3.9). Based on the progress of damage and the hysteretic response, the equal or higher response quantities such as strength, energy were found in the repaired specimens. There was 8% to 40% and 53% to 139% enhancement in the lateral load and energy respectively. While the failure mode (joint shear failure)

could not be transformed by the proposed method in most of the specimens, a relatively ductile behavior was observed in the specimens of test series 2 and 3.

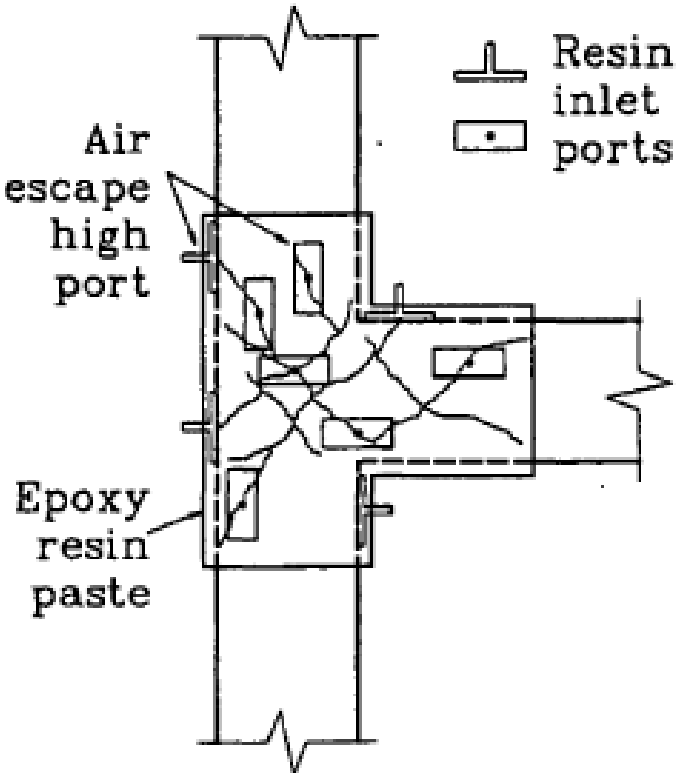

Figure 3.9. Repair process [23]

Sezen [24] deals with the repair of the specimens which have certain damage in the joint region. Three exterior joint specimens were tested under the reverse cyclic loading first, followed by the repair of the damaged member. The spalled concrete was removed and a high strength repair mortar was replaced (Figure 3.10a and b). Then, FRP layers were wrapped diagonally (Figure 3.10c). FRP strips, which were anchored to the beam, were also applied along the beam longitudinal axis. After testing the repaired specimens under the same loading history, the former capacities of the specimens were recovered. In addition, an enhancement in the deformation capacities with respect to original state was observed in the repaired specimens. This, of course, shows the efficiency of proposed repairing technique.

(a) (b)

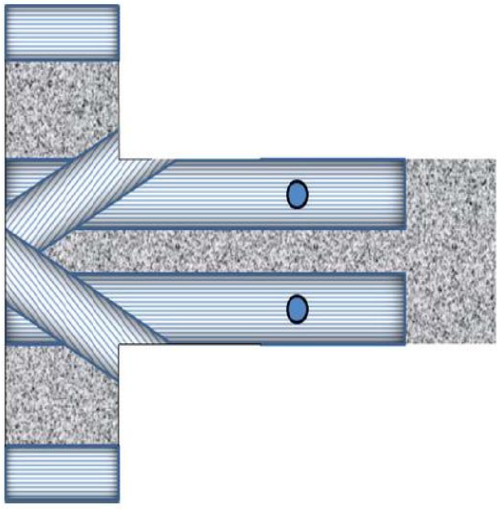

(c)

Figure 3.10. (a) Damaged specimen (b) application of mortar (c) FRP repair scheme [24]

Engindeniz et al. [25] present the response of a 1:1 scale RC joints constructed with transverse beam and slab (Figure 3.11a). The specimen were first tested under bidirectional quasi-static loading, then repaired and retested. Severe damage was observed in the joint region as the specimen was constructed according to the pre-1970s construction practices like absence of shear reinforcement in the joint. The pre-damaged specimen was first repaired by pressure-injection of a high-strength, high-modulus, low-viscosity epoxy that filled all cracks larger than 0.3 mm. Then, CFPRs were wrapped to the damaged members. The experiment result indicated that application of the CFRPs was efficient to achieve ductile beam failure. The specimens could sustain the lateral load capacity up to 3.7% drift ratio without any loss in the applied axial load (Figure 3.11 b and c).

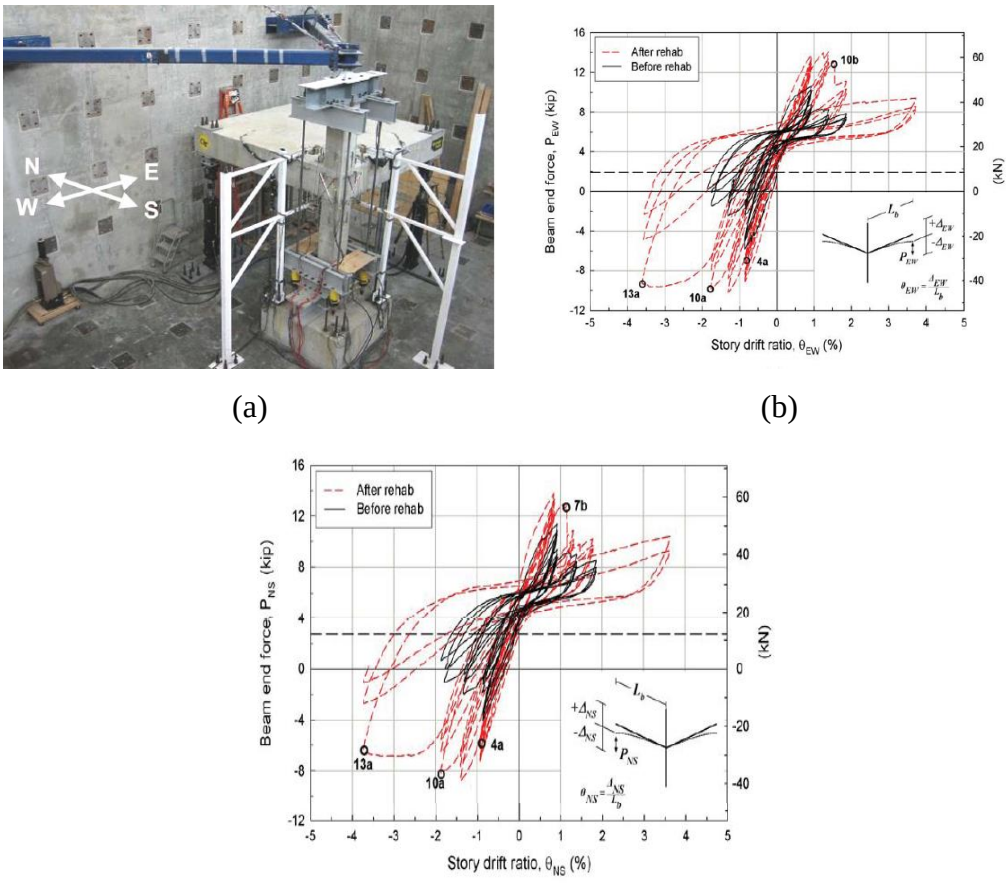

Figure 3.11. (a) Bidirectional loading (b) EW direction (c) NS direction [25]

Ghobarah and Said [26] present the repair of the exterior beam-column joint specimens by means of glass fiber-reinforced polymer (GFRPs). Four joint specimens representing the existing pre-1970s buildings were tested. While two of the specimens repaired after testing, the remaining specimens retrofitted before any damage was done (Figure 3.12). Two different levels of axial load were applied (300 and 600 kN). Four different FRPs wrapping technique was used. The FRP sheets were applied in U pattern to the joints in the repaired specimens. The FRP was not extended to the upper and lower storey column in the first specimen. The case was opposite to the presented case of the first specimen. The joint shear mode could be either eliminated or delayed with the proposed repair technique. This, of course, meets the main objective of repair.

(a) (b)

Figure 3.12. Specimen TR1 (a) before (b) after repair [26]

Tsonos [27] reports the repair and retrofit of four exterior beam-column joints built with transverse beam and slab. Four non-seismically designed joint specimens were tested under cyclic loading. All specimens were constructed with several structural deficiencies such as absence of shear reinforcement in the joint, inadequate column shear reinforcement, non-optimal flexural strength ratio and joint shear strength. One of the specimens (F_1) was repaired by epoxy jacketing/CFRPs, (Figure 3.13). On the other hand, another conventional method, which is RC jacketing, was applied in the remaining specimen, O_2 (Figure 3.13). A brittle joint shear failure was observed in the built up specimens. After repairing the specimens, the brittle failure was transformed to the ductile behavior with flexural beam hinging.

Reference Specimens

Repaired Specimens

Figure 3.13. Damaged photos of reference and repaired specimen [27]

3.3. Joint Strengthening Techniques

Alcoher and Jirsa [28] report the retrofit of four interior beam-column joints by jacketing (Figure 3.14). All specimens representing a prototype structure were designed according to 1950s design principles. In addition, the specimens consisted of a joint with weak column and strong beam. After testing the all specimens, an enhancement was found in the response quantities such as strength, dissipated energy and stiffness. In the retrofitted specimens, measured joint shear strength was higher than code recommendation.

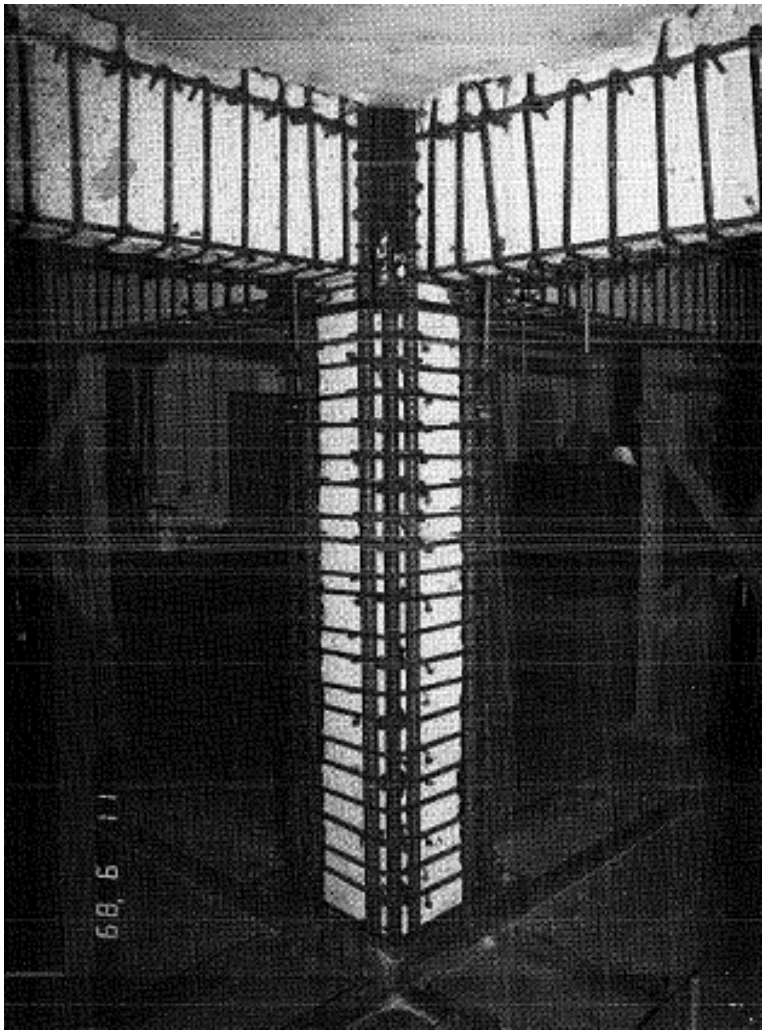

Figure 3.14. Reinforcement cage [28]

Said and Nehdi [29] present the retrofit of non-seismically designed RC exterior beam-column joints via local steel bracing. While one specimen was constructed with transverse reinforcement the joint, there was no shear reinforcement in both control and retrofitted specimen. The loading history involves two sections, which are load controlled, and displacement controlled part. A ductile behavior with beam yielding was observed in the specimen complying with code requirement. However, control specimen displayed a brittle behavior with a severe damage in the joint. The steel braced enhanced the peak load 2.6 and 1.7 times in positive and negative directions, respectively. This, of course, delayed the brittle joint shear failure and bond slip failure. Nevertheless, the cracks were concentrated mostly in the joint core (Figure 3.15).

Figure 3.15. Crack patterns in retrofitted specimen [29]

Topcu [30] deals with the strengthening of external beam-column joints via CFRPs. The effect of transverse slap was also investigated in this study. All specimens were constructed with plain round bars. The anchorage detail was designed such that the beam bottom bars were embedded shorter than required length. Therefore, the bond slip failure preceded the overall response in the reference specimen with transverse slab. Even though the peak load was enhanced, the bond slip characteristic was not affected by slab. The bond slip failure was transformed to other failure modes such as joint shear failure and ductile beam hinging by retrofitting with CFRPs. A ductile beam failure was observed in one of the retrofitted specimens. Even though the joint shear failure was fully prevented in this specimen, the bond slip failure was only delayed to the subsequent drift ratios

(Figure 3.16). This study yet again proved that the bond slip failure could not be easily prevented by CFRPs wrapped in different orientations.

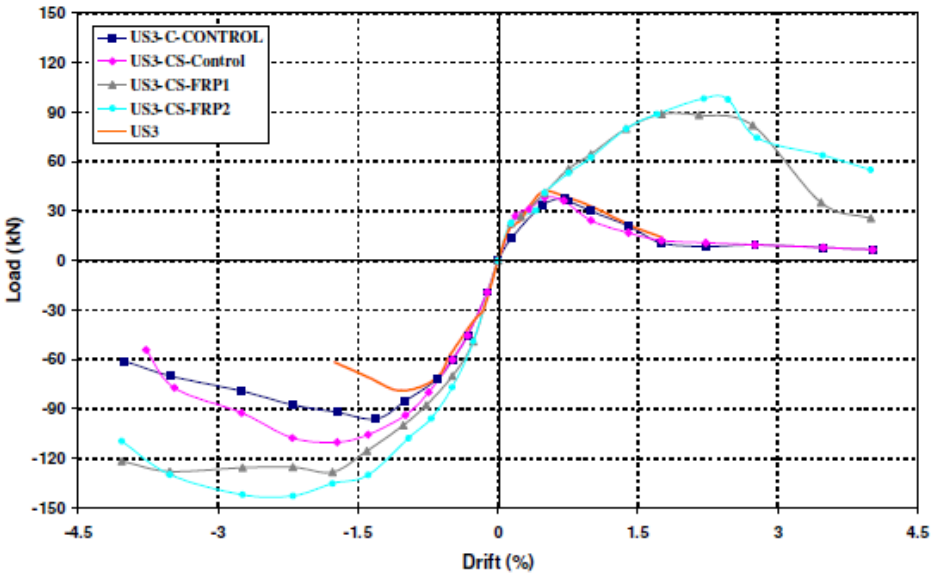

Figure 3.16. Backbone curves of hysteresis loops [30]

Coskun et al. [31] tested two full-scale three-dimensional reinforced concrete frames under reversed cyclic quasi-static load up to 8% drift ratio. The loading pattern was obtained from the time history analysis of an actual structure hit by Düzce Earthquake. The specimens represented the most common characteristics of Turkish building stocks, which has low strength concrete and poor reinforcement detail such as absence of shear reinforcement in the joint and use of plain round bar. One of the tested specimen was retrofitted by CFRPs which were applied in X pattern to the joint (Figure 3.17). The combination of bond slip and joint shear failure preceded the overall response in the reference specimen. On the other hand, the retrofitted specimen could sustain the 95% of lateral load capacity at 8% drift ratio, which indicates the efficiency of retrofit technique. In addition, outcome of this study highlighted the applicability of CFRPs wrapping technique in X pattern to the joint.

Figure 3.17. CFRPs retrofitted specimen [31]

Del Vecchio et al. [32] investigated the response of specimens retrofitted with CFRPs under cyclic loading. There was no shear reinforcement in the joint region of six specimens. While three of them were tested in as-built configuration, remaining specimens were strengthened by CFPRs wrapped in different configuration for each specimen. The joint shear failure was observed in the reference specimen. On the other hand, the joint shear failure was transformed to the column flexural or CFRPs failure in two of the retrofitted specimens.

Akguzel and Pampanin [33] present the seismic behavior of 2D and 3D deficient exterior joints before and after retrofit with GFRP. Depending on the transversal direction beam, a total of ten specimens were tested under uni- or bidirectional loading regime (Figure 3.18). The tested parameters were the effect of bidirectional loading, variable axial load, reinforcement detail in the joint and retrofit by GFRPs. The axial load was varied in proportion to lateral force. The observed damage in the specimens tested in bidirectional loading regime was more severe than 2D specimen. Therefore, one important outcome of this study is that

neglecting the multi-directional load demand was an unconservative solution for the test of joint specimens.

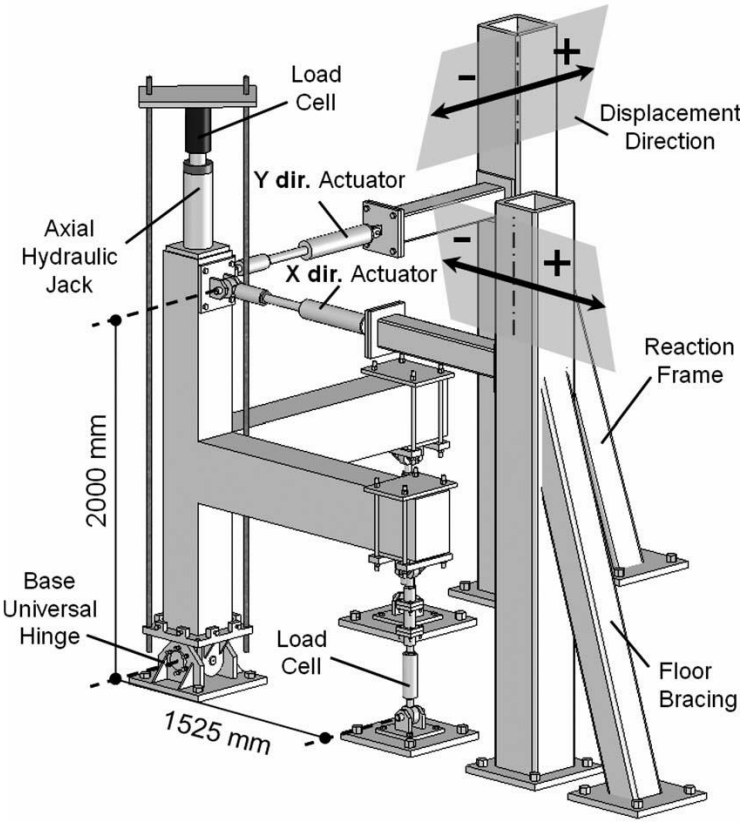

Figure 3.18. Test set up for uni- or bidirectional loading [33]

Bedirhanoglu et al. [34] investigate the response of the deficient reinforced concrete exterior joints built with low strength concrete and plain round bars before and after retrofit through high-performance fiber-reinforced cementitious composite (HPFRCC). The epoxy resin was first applied to the surface and then HPFRCC panels were anchored to the joint by steel rods (Figure 3.19a and b). There were four-tested specimens -two reference and two retrofitted- in this study. The effect of welding of beam bottom and top hooks to each other was also investigated in both control and retrofitted specimens. The bond slip failure preceded the overall response in the specimens constructed with bent up anchorage detail. On the other hand, the combination of bond slip and joint shear failure was observed in the specimen whose beam top and bottom hooks were welded. The shear deformations in the joint core were limited by HPFRCC panels and plastic hinges took a place in

the beam. This enhancement resulted in a higher level of displacement without any loss in the lateral load carrying capacity.

(a)

(b)

Figure 3.19. (a) Application of epoxy resin (b) anchoring HPFRCC panel [34]

Shafaei et al. [35] studied on the joint enlargement by using pre-stressed steel angles (Figure 3.20). The presented retrofit method in this study relocated the plastic hinges away from the joint panel by enlarging the joint with pre-stressed steel angles. In addition, the slippage of the beam longitudinal bar was restricted by this method. Seven half-scale external joint specimens -three control and four retrofitted- were subjected to cyclic loading up to 10% of drift ratio. Relatively less joint deformation was found in the retrofitted specimens. Unlike the control

specimens, the retrofitted specimens could sustain the lateral load carrying capacities with low stiffness degradation.

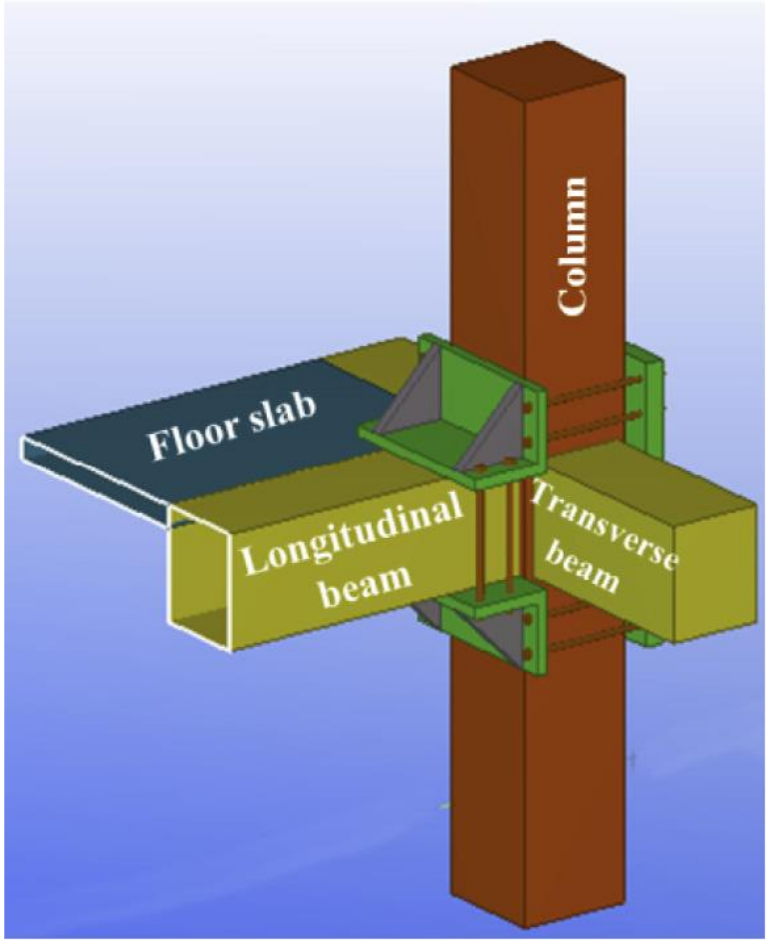

Figure 3.20. Retrofit by pre-stressed steel angles [35]

Kam and Pampanin [36] proposed a member retrofit technique called as selective weakening. In this method, the joint and the beam were retrofitted by post-tension wires. However, the beam flexure capacity can be increased by additional axial force provided by post-tension. Therefore, other members can fail before plastic hinge takes a place in the beam for certain cases. Hence, beam flexure capacity is weakened by severing beam longitudinal reinforcements (Figure 3.21). If the column capacity is greater than the beam and joint capacity, post-tension force is enough to prevent damage in the joint. There were four-tested specimens in this study. A joint shear failure was observed in the benchmark specimen. In the specimen retrofitted with only post-tension, the failure mode was beam and column

hinging. The specimens whose beam were weakened and retrofitted with post-tension displayed a ductile behavior with beam hinging. Post-tension with selective weakening increases the energy dissipation capacity of the joint.

Figure 3.21. Beam weakening and application of post-tension [36]

Several researchers have performed experimental studies on the response of as-built and rehabilitated specimens. Parvin et al. [37], Chaimahawan and Pimanmas [38], Lee et al. [39], Biddah et al. [40], Hadi and Tran [41], Le-Trung et al. [42], Bindhu et al. [43], Elsouri and Harajli [44], Fisher and Sezen [45], Garcia et al. [46], Lee et al. [47], Li and Kai [48], Karayannis et al. [49], Kim and LaFave [50], Antonopoulos and Triantafillou [51] and Haach et al. [52] are among these studies.

CHAPTER 4

4. EXPERIMENTAL PROGRAM

The experimental program is reported in this chapter. A brief information about the specimens, structural repair and retrofit design is presented first, followed by the description of the test set up and procedure. Each step was investigated in depth to find out required labor work, viability and application details.

4.1. Introduction

Experimental program consists of two groups with four test series. There were seven specimens in these groups. Each group is identical in itself in terms of mechanical properties of the specimens.

The first group of beam-column assembly is designed according to the current earthquake code. On the other hand, the second group represents the deficient beam-column joint, which is very common in most of the existing buildings constructed before 1999 in Turkey. In other words, any of the specimens of the second group do not comply with the design principles of both current and former earthquake codes.

The first group involves one test series while three test series exist in the group 2. Even though the mechanical properties of the specimens in the group 2 are identical, they are classified into three different series. The only difference among the test series is material used in the retrofit scheme.

A total of seven full-scale test specimens, which are taken from the theoretical infection point of the RC frame where the moments are zero under lateral load, were tested (Figure 4.1).

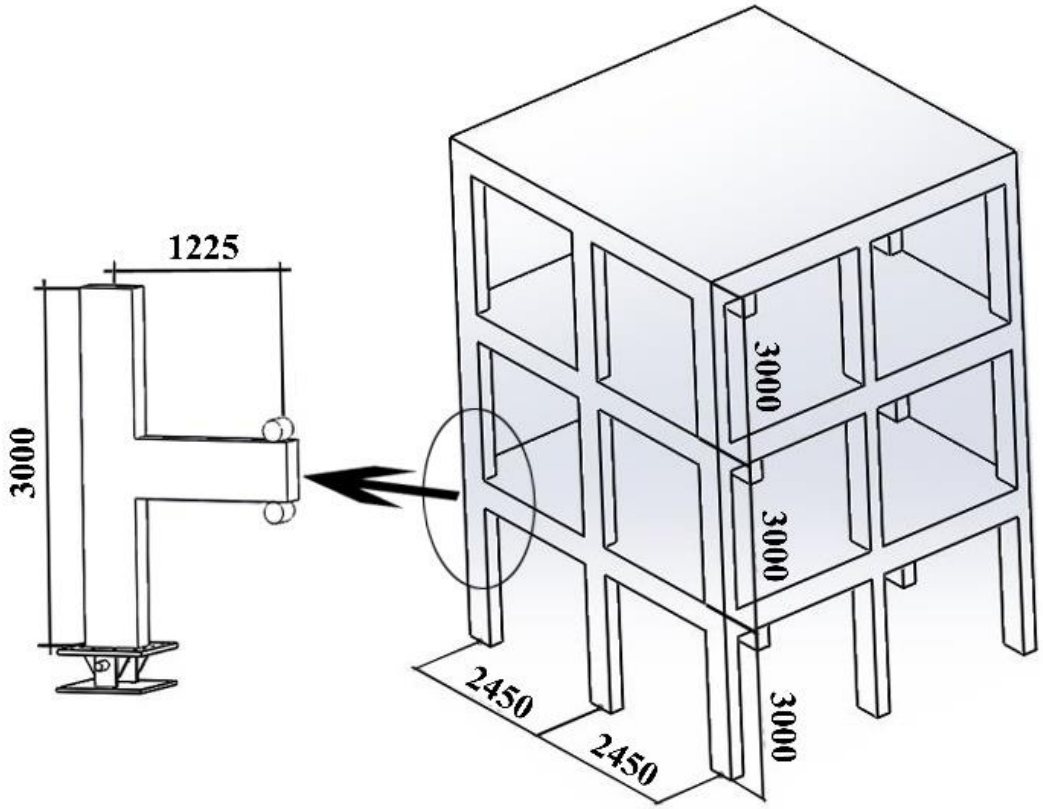

Figure 4.1. Test specimen in the model building

4.2. Test Specimens

The first group contains one test series with one specimen. However, there are two experiment in the test series 1. After testing EJ-1, there was a certain level of damage, which corresponds to moderate damage. Then, EJ-1 was structurally repaired by CFRPs and it was entitled as "EJ-1-R".

The group 1 was designed according to the current earthquake code, as discussed before. The column dimension was 250x500x3000 mm in all tested specimens. The beam was connected to the column at mid span with a cross section of 250x500 mm and a half-length of 1500 mm (Figure 4.2). The longitudinal reinforcement ratio of the column and beam were 1.22% and 1.61%, respectively. 16 mm and 18 mm diameter deformed bars were used in the column and beam. Diameter of 8 mm, deformed bar with 135-degree hooks was used as transverse reinforcement in the beam as well as the column. They were placed with a spacing of 75 mm and 50 mm at the confinement regions of the column and beam,

respectively. However, in the unconfined regions, the transverse reinforcement spacing was selected as 150 mm and 95 mm for the column and beam, respectively. Since the first test group was designed according to the earthquake code in action, transverse reinforcements are placed in the beam-column joint. Minimum concrete compressive strength is 20 MPa according to TEC 2007 [4], so it was selected as a target compressive strength for the test specimen, EJ-1.

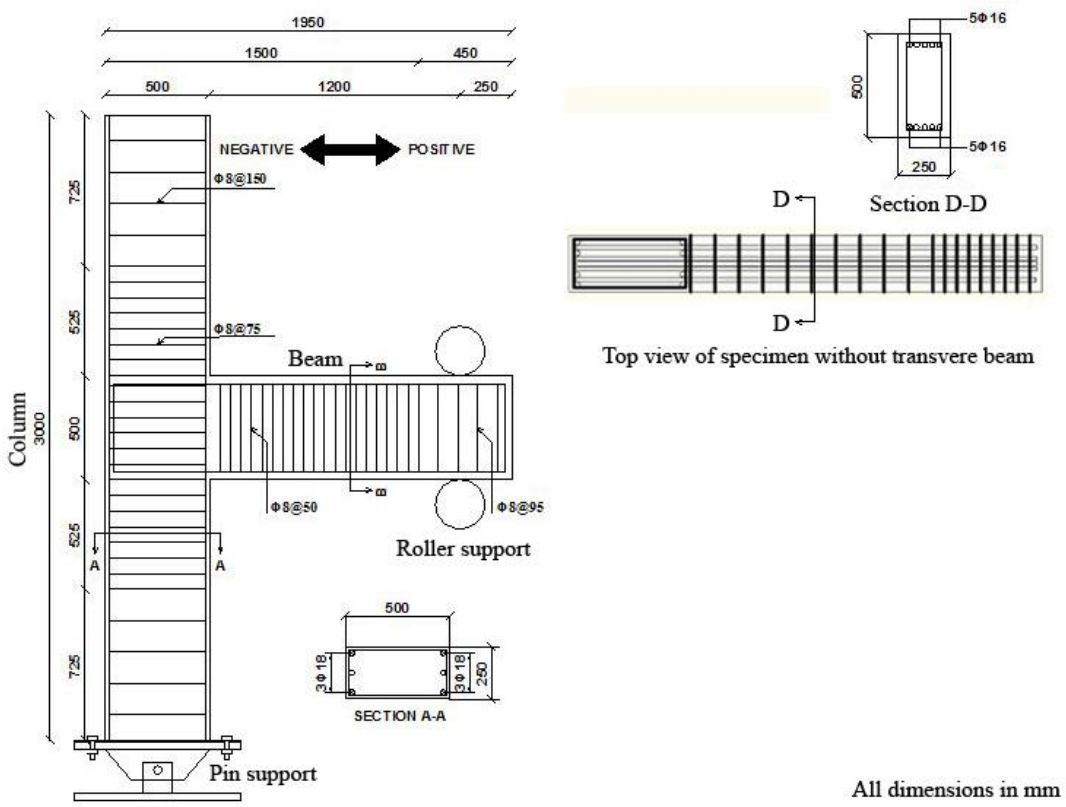

Figure 4.2. Dimensions and reinforcement details of the specimen of group 1

The specimens of the group 2 differ from the group 1 in number of important ways such as; use of low concrete compressive strength and plain round reinforcement bar. The second test group represents the substandard beam-column assembly. None of the tested specimens complied with the design principles of both current and former earthquake codes. The same dimensions with the first group were also selected; on the other hand, the reinforcement scheme was not identical with the group 1. The longitudinal reinforcement ratio of column and beam were 1.63% and 2.04 %, respectively. 18 mm diameter plain round bar was used in the

column and beam. 10 mm diameter undeformed bar with 90-degree hooks was used as a transverse reinforcement (Figure 4.3). Moreover, there was no shear reinforcement in the beam-column joint region. The concrete compressive strength was expected around 8-10 MPa.

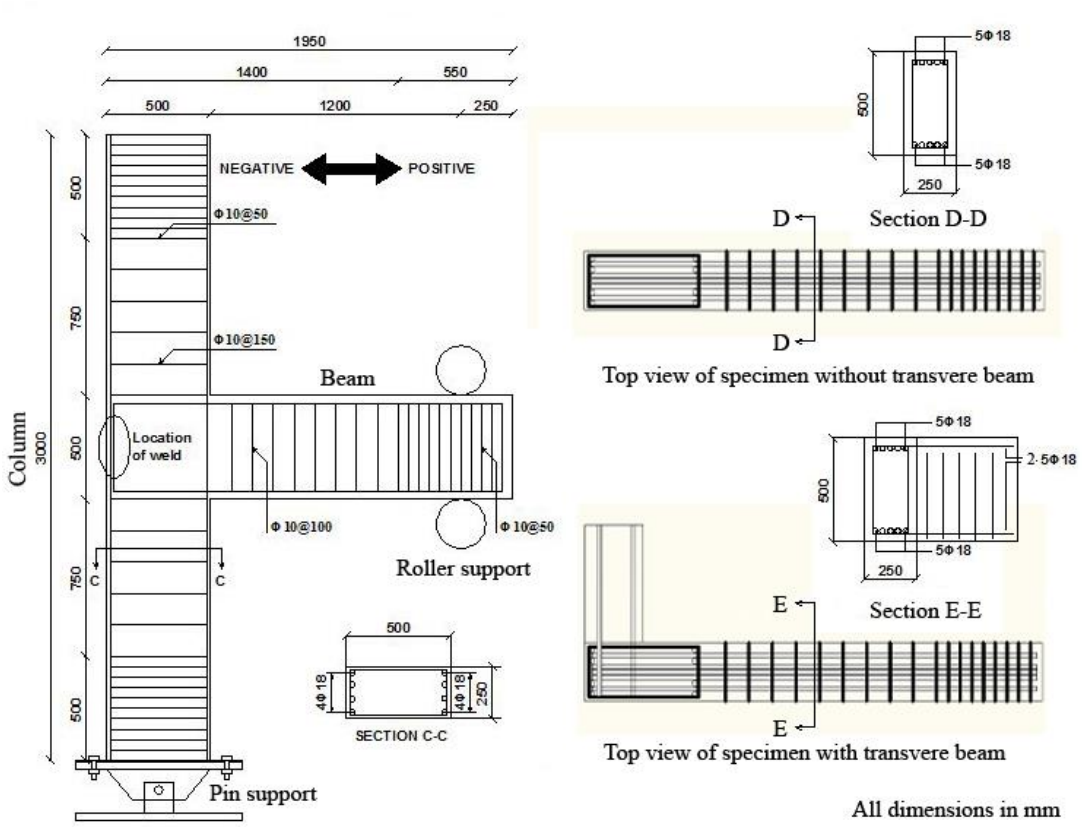

Figure 4.3. Dimensions and reinforcement details of the group 2

There are three different test series in the group 2. The first test series of the group 2 (test series 2) contains one test specimen with two experiments. After testing EJ-2, there was severe damage penetrated in its the critical components. Then, the damaged member of the specimen was repaired by CFRPs. The repaired specimen of test series 2 was entitled as "EJ-2-R".

The specimens of test series 2 and 3 were identical in terms of material used in the retrofit, amount of CFRPs and the retrofit scheme. However, the specimen in the test series 2 (EJ-2-R) was repaired after severe damage whereas EJ-C-1, which is the specimen of the test series 3, was strengthened before damage. The efficiency

of either repair or retrofit was thus investigated in depth. Table 4.1 summarized the properties of the test specimens.

Table 4.1. Test specimen summary

Group	Test series	Specimen	Description	f_c (MPa)	Joint rebar	Transverse Beam
Group 1	Series 1	EJ-1	Reference complying with code	19.14	Present	N/A
		EJ-1-R	Repair of EJ-1			
Group 2	Series 2	EJ-2	Reference substandard joint	8.05	N/A	N/A
		EJ-2-R	Repair of EJ-2			
	Series 3	EJ-C-1	Retrofit via CFRPs	9.39	N/A	N/A
	Series 4	EJ-P-1	Without post-tension	9.10	N/A	N/A
		EJ-P-2	Post-tensioned	9.47	N/A	N/A
		EJ-BP-1	Post-tensioned, back plate	9.92	N/A	N/A
		EJB-P-3	Post-tensioned with transverse beam	10.41	N/A	Present

An original method of the retrofit was employed in the last test series that involves four specimens. They were retrofitted by external post-tension rods.

The viability of the proposed method should be ensured. Therefore, aside from four specimens in this test series, one of the tested specimens consists of transverse beam with dimensions of 250x500x500 mm to demonstrate the applicability of the presented retrofit technique.

The shear failure of the joint is intended to investigate in the non-seismically designed specimens. Kim and LaFave [50] and Haach et al. [52] investigated the effect of the column axial load on the behavior of the joint. These studies showed that the high axial load in the column improves the joint shear strength. Therefore, the minimum value of the axial load for columns, which is 0.1Acfc according the TEC 2007 [4], was selected in all specimens. Even though the axial load ratio in the existing structures could be higher than the ratio discussed in the study, the worst situation, which was the minimum axial load for the columns to get a lower joint strength, must be considered.

4.3. Material Properties

This section briefly describes the materials utilized in the construction of the test specimens. While the mechanical properties of the concrete and steel were found by the laboratory tests, those related to CFRPs were presented as provided by the manufacturer.

4.3.1. Reinforcement steel

The reinforcement steel was supplied in 12 m long batches. Four sample specimens taken from these batches were tested under tension. Then, the resulting average values were found.

The test results in terms of yield strength, ultimate strength and elastic modulus of the specimen were introduced in Table 4.2.

Table 4.2. The mechanical properties of the reinforcement steel

Type of Bar	Sample No	Yield Strength, f_y (MPa)	Ultimate Strength, f_u (MPa)	Young's Modulus, E (MPa)
Deformed bar	1	541.32	798.05	184467.24
	2	516.99	783.45	202193.91
	3	533.86	789.02	186331.14
	4	498.05	766.58	180464.76
	Average	*522.56*	*784.28*	*188364.26*
Plain round bar	1	290.02	430.06	192546.23
	2	285.45	428.32	200584.41
	3	295.25	440.92	187954.69
	4	300.48	450.80	198578.45
	Average	*292.80*	*437.53*	*194915.95*

As mentioned in Section 4.2, the longitudinal and transverse reinforcement in the specimen of the group 1 (EJ-1) was ϕ16 and ϕ8 bar, respectively. The bar diameter was selected to be the most extensive in existing buildings. Since it was designed according the earthquake code in action, this specimen was constructed with S420 deformed type reinforcement steel. In contrast, a plain round bar was carried out as the longitudinal and transverse reinforcement in all specimens of the group 2. The diameter of longitudinal and lateral bar in these specimens was 18 mm and 10 mm, respectively.

4.3.2. Concrete

Normal weight conventional concrete, which was manufactured in the laboratory, was used in the specimen of the group 1. The minimum concrete strength was 20 MPa in the current earthquake code that was selected as a target strength in the specimen agreed with code requirements.

It is aimed to eliminate the change in the concrete strength due to pouring of concrete in different times for the specimens of the group 2. All of the specimens in this group were therefore constructed at the same time. However, manufacturing such massive concrete in the laboratory becomes an issue due to capacity restriction on facility.

A local contractor, SELKA BETON, supplied the concrete of the group 2 specimens. In order to simulate the prevailing strength in existing buildings, an approximate concrete strength of 8-10 MPa was desired with proper weight proportion.

The cube concrete specimens with dimensions of 15x15x15 cm were cured under the same conditions with the tested specimen. Peterson's relationship was used to investigate the shape and size effect on the compressive strength of concrete specimens as the tested specimens were in cube shape [53].

Table 4.3 presents the concrete strength of the specimens at different ages.

Table 4.3. Concrete strength of the test specimens

Experiment number	Concrete compressive strength, cube (MPa)				Concrete compressive strength according to Peterson's relation, cylindrical (MPa) [53]			
	S1	S2	S3	*Ave*	S1	S2	S3	*Ave*
EJ-1	22.62	23.13	22.19	*22.65*	19.11	19.54	18.75	*19.14*
EJ-2	9.50	9.67	9.38	*9.52*	8.05	8.18	7.94	*8.07*
EJ-C-1	11.25	11.62	10.38	*11.08*	9.53	9.84	8.80	*9.39*
EJ-P-1	10.65	11.09	10.47	*10.74*	9.02	9.40	8.88	*9.10*
EJ-P-2	11.55	11.04	10.94	*11.18*	9.78	9.36	9.27	*9.47*
EJ-BP-1	10.89	12.45	11.78	*11.71*	9.23	10.55	9.98	*9.92*
EJB-P-3	11.48	12.78	12.62	*12.29*	9.73	10.82	10.69	*10.41*

Curing of concrete was another factor affecting the strength so a special interest was also given on it. Curing of concrete is achieved by use of wet burlaps covering. After testing the specimens, the core samples were taken from the non-damaged part of the members (Figure 4.4). The strength of concrete core samples was presented in Table 4.4.

Figure 4.4. Core sampling

Table 4.4. Strength of concrete core sample

Experiment number	Properties of core sample		
	Diameter (mm)	Height (mm)	Strength (MPa)
EJ-1	94.00	113.10	20.39
EJ-2	94.00	114.00	10.71
EJ-C-1	94.10	114.00	11.17
EJ-P-1	94.00	116.00	12.54
EJ-P-2	92.00	100.00	13.75
EJ-BP-1	94.00	113.20	12.74
EJB-P-3	94.00	114.00	13.46

4.3.3. Repair and retrofit material

Primarily used material in the repair of EJ-2 was repair mortar. When the crushed concrete was removed, Sika Repair Mortar 640 had been replaced. The mechanical properties of repair mortar, as provided by the manufacturer, were summarized in Table 4.5.

Table 4.5. The mechanical properties of Sika Repair Mortar 640

Properties	Age	Strength (MPa)
Compresive strength	7	25–45
	28	40–60
Flexural strength	7	3.5
	28	6
Bonding strength	N/A	>1.5

A unidirectional composite material, CFRP, was used for retrofit and repair of the specimens of the test series 1, 2 and 3. The mechanical properties of CFRP layers were presented in Table 4.6. Then, their chemical components used for preparation of surface and bonding were introduced in Table 4.6 and Table 4.7.

Table 4.6. The mechanical properties of CFRP

Properties	
Young’s modulus (MPa)	230000
Ultimate tensile strain (%)	2.10
Tensile strength (MPa)	4900
Weight per unit area (gr/m^2)	210
Effective thickness (mm)	0.111
Fiber orientation	Unidirectional

Table 4.7. The mechanical properties of Concressive® 1406 and MBT-MBrace®

Properties		Concressive® 1406	MBT-MBrace® Adesivo Saturant
Mixing proportion	Component A	3.75	3.73
	Component B	1.25	1.27
Young's modulus (MPa)	Tensile	>700	>1800
	Flexure	>580	>900
Compresive strength (MPa)	-	>75	>80
Tensile strength (MPa)	Tensile	>12	>12
	Flexure	>24	>26
Ultimate tensile strain (%)	-	N/A	>1.6

4.4. Construction of the Specimens

4.4.1. Formwork, reinforcement work and concrete casting

The T-shape RC beam-column joint specimens were constructed at Structural Mechanics Laboratory, Department of Civil Engineering, Anadolu University. The forms of the specimens were prepared first, followed by the tying up of stirrups to the bent bars which were formed the required shape (Figure 4.5 and Figure 4.6). Then, the manufactured bars were installed to the form. Finally, the concrete was poured straight into the forms, which were manufactured in the horizontal position (Figure 4.7). Curing of concrete is achieved by use of wet burlaps covering. It should be noted that the specimens of each group were manufactured concurrently to eliminate the effect of concrete strength on the response.

(a) (b)

Figure 4.5. (a) Assembling of the form (b) final shape of the form

(a) (b)

Figure 4.6. (a) Handling of bars (b) installation of the bars

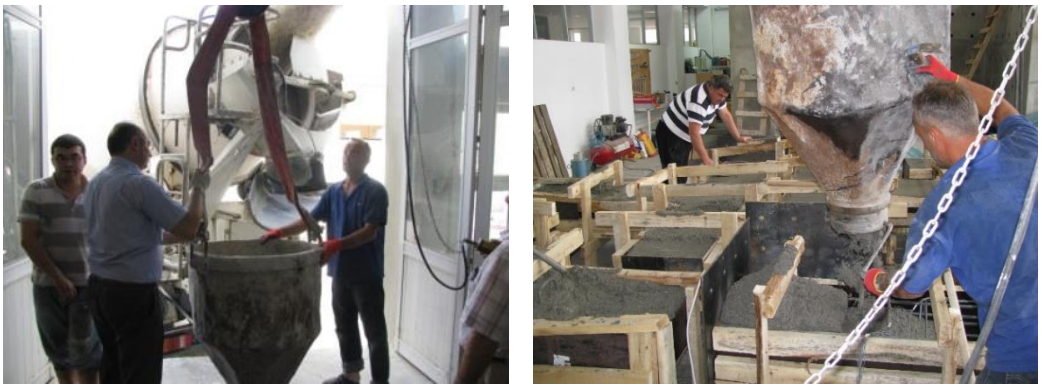

(a) (b)

Figure 4.7. (a) Ready mix concrete (b) pouring concrete

4.4.2. Prevention of bond-slip failure

Previous researches have revealed that if the plain round bars are used in the RC members, bond slip failure precedes the other types of failure for such specimens [18,54]. In addition, slippage of beam longitudinal reinforcement can result in the anchorage push out failure [36]. In this failure mode, the cover concrete at joint back is cracked due to push out forces created by movement of beam longitudinal bars. When the longitudinal bars are in tension, it is pulled from the joint and reinforcement hooks deform such that the tip of the hooks forced to split the cover concrete causing vertical cracks in the back of the joint.

Bond slip failure can be partially prevented even in the existing buildings by removing the concrete cover at joint back, welding the the hooks of beam bottom and top reinforcement bars to each other and repairing with mortar [54]. The slippage failure modes therefore can be switched to the other failure modes. Proposed retrofit methods -use of CFRPs in X pattern and externally applied post-tension rods- are not effective in reducing the bar slip deformations of the plain bars. For this reason, occurrence of the slippage problem is intended to be minimized through welding of beam bottom and top hooks to each other before pouring of concrete (Figure 4.8).

Figure 4.8. Welding of beam hooks

4.4.3. Repair and retrofit procedures

In the test series 1, application of CFRPs started with rounding the section corners to prevent the tearing of CFRP sheets due to sharp corners of the RC

sections. Then, a thin layer of undercoat (MBT-MBrace® Primer) was applied on the corresponding RC component (Figure 4.9).

Figure 4.9. Application of MBT-MBrace® Primer

Once the undercoat dries, a thin layer of epoxy based, repair and anchorage mortar (Concressive® 1406) was applied to obtain smooth surface (Figure 4.10).

Figure 4.10. Application of Concressive® 1406

Finally, CFRP sheets were saturated with epoxy (MBT-MBrace® Adesivo Saturant) and applied to the corresponding member surface (Figure 4.11a and b). The chemicals were processed by mixing two components called as A and B in their appropriate ratios. Then, CFRP layers were wrapped to the corresponding surface (Figure 4.11c). In order to get a good bonding between CFRP sheets and surfaces, a hand roller was used to remove air and stick them properly.

(a) (b)

(c)

Figure 4.11. Application of saturant to (a) surface (b) CFRP (c) wrapping of CFRPs

A ductile performance was observed in the specimen EJ-1 and plastic hinges took place in the beam. For this reason, a one layer CFRP with 200 mm width was applied to the top and bottom surfaces of the beam. Then, it anchored by three CFRP sheets with a width of 200 mm, length of 1700 mm (Figure 4.12). Those related with anchoring were placed at 100 mm in transverse direction. CFRP sheets wrapped in transverse direction also increased the shear resistance of the beam. For a ductile behavior of the specimen, plastic hinges are expected to take a place in the beam. Since the beam was repaired, strong beam weak column case could occur. Then, the flexural capacity of the column could be exceeded before the beam reached to its flexural capacity. For this reason, once the beam was repaired, the column was repaired as well. A one layer CFRP with a width of 200 mm was applied at the front and back surfaces of upper and lower story columns. Six CFRP sheets with dimensions of 100x1700mm were placed in the transverse direction with a spacing of 100 mm to anchor longitudinal CFRPs. They also increased the shear capacity of the column. It was known from the experiment of EJ-1 that, the

member capacities could not exceed the beam-column joint capacity. Therefore, no repairing action was taken for the beam-column joint.

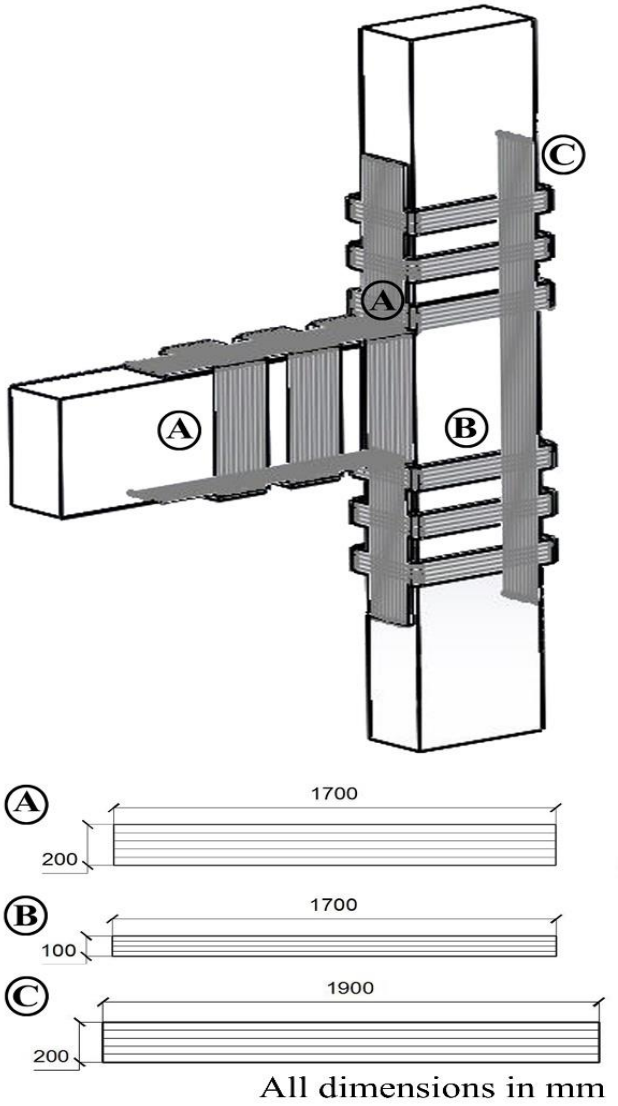

Figure 4.12. Schematic representations of CRFP repairing in the specimen EJ-1-R

The repair process of the specimen EJ-1-R is also presented in Figure 4.13.

Figure 4.13. The repair process of EJ-1-R as shown in Figure 4.12

In the test series 2, the failure mechanism was brittle joint shear failure for the specimen EJ-2. Therefore, joint region was repaired to attain the initial shear capacity of the joint. The repair process started with removing of the spalled concrete at the joint after testing EJ-2. Then, repair mortar was poured in place of removed concrete in the joint. Finally, the CFRP layers were wrapped as presented in Section **Error! Reference source not found.**. Two layers of CFRP sheets with a width of 200 mm and length of 4500 mm were orientated $\pm 45^0$ with respect to beam axis. These diagonal sheets were anchored to the beam and column at upper and lower story level via three 200x1700 mm CFRP sheets by wrapping the RC components with a single layer of CFRP (Figure 4.14).

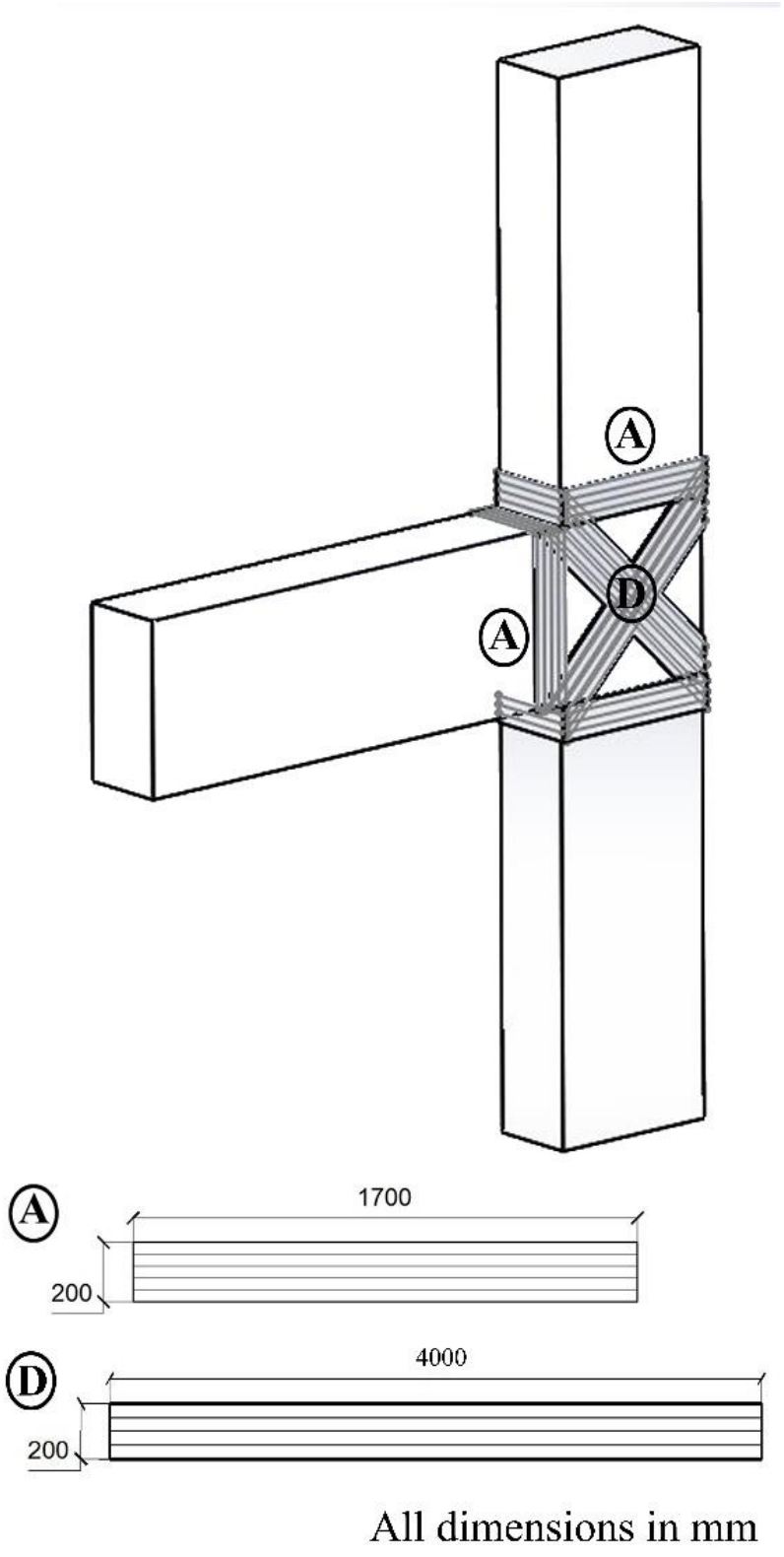

Figure 4.14. Schematic representations of CRFP repairing in the specimen EJ-2-R

Figure 4.15 presents the repair process of the specimen EJ-2-R.

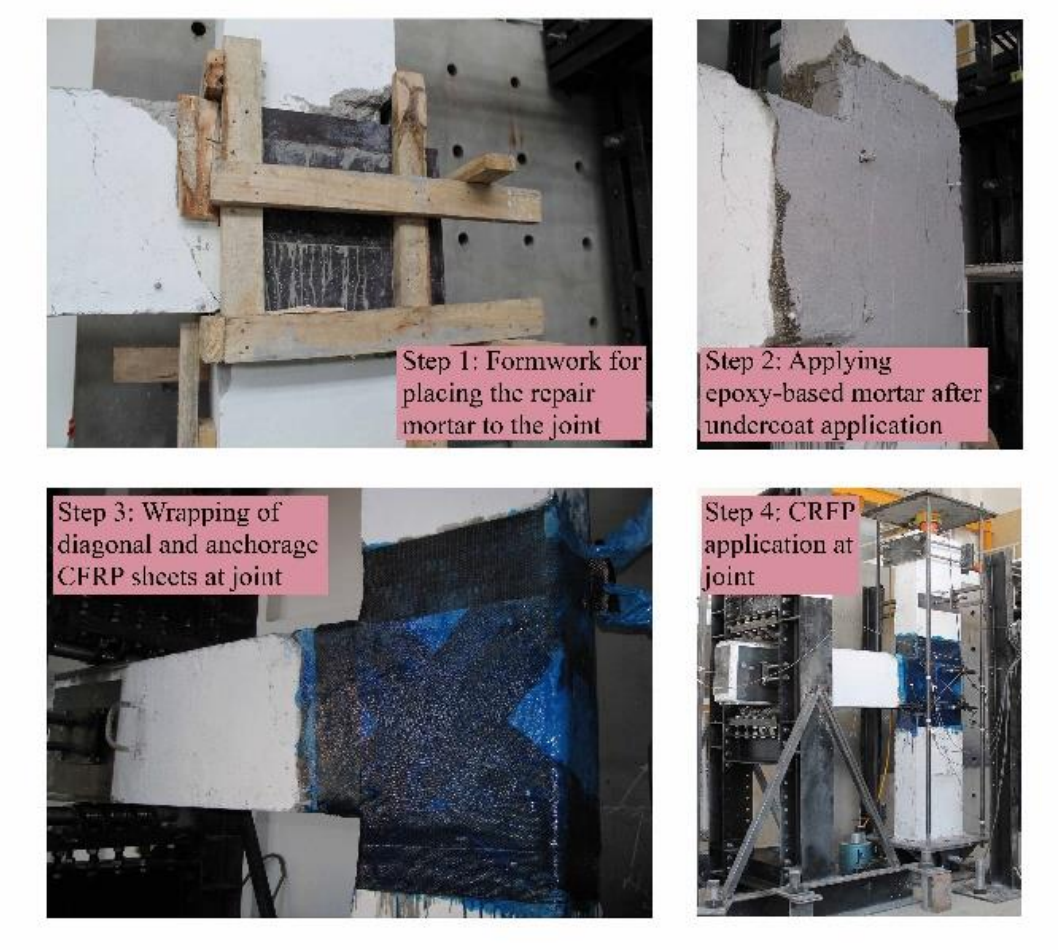

Figure 4.15. The repair process of EJ-2-R as shown in Figure 4.14

The procedure described in the repair of the specimen EJ-2 was completely followed in retrofitting of the specimen of test series 3 (EJ-C-1). In other words, the retrofit scheme in the specimen EJ-C-1 was identical with the specimen EJ-2 in terms of amount of CFRPs and its pattern. On the other hand, the process of repair mortar placement was not applied in the specimen EJ-C-1 as there was no damage in its members.

The post-tension was applied to four 24 mm diameter rods with a length of 1000 mm, in the test series 4. In order to fix the rods to the joint region, four 225x15 mm equal angle built-up sections, which had two 25 mm diameter holes at corners, were used (Figure 4.16a and c). Two of the angles were placed to the beam-joint interface without using anchor bolts, whereby rest of them were doweled to the back side of the column by three steel anchor bolts apiece. The rods were mounted diagonally and fastened to the angles by nuts. Post-tension was applied to the nuts

by torque wrench from the upper story column level while the nuts of the lower story column level were fixed (Figure 4.17a). The torque was exerted one by one to the rods to limit the eccentricity between two sides of the joint. Otherwise, concrete in the joint core could be crushed due to unbalanced force in the rods. In addition, the value of the axial load was measured by either torque wrench or load cell. One of the tested specimens was retrofitted by rods without post-tension so as to determine the contribution of rods to the response. The axial force in each rod was calculated to be 100 kN in the rest of the specimens which was the required axial force to compensate the joint shear force. Computing the axial force in the one post-tension rod is investigated in Section 4.6.2 in depth. The effect of two extreme levels of axial load in the post-tension rods on the behavior was also compared.

Push out forces due to tension force in the beam longitudinal bars can buckle the column longitudinal bars since the beam hooks were welded and fixed to the column reinforcement. It should be also emphasized that due to lack of joint's stirrups there was no confinement for the column longitudinal bars at joint region. When the tension force in the beam longitudinal bars reaches such a critical value that makes moderate to severe damage can be observed at joint back. For this reason, a plate with dimensions of 250x950x30 mm was implemented in the post-tension detail such that the joint backside will be under compression in one of the test specimens. It therefore limited the anchorage push out failure (Figure 4.16b). In addition, more confined joint was achieved with column back plate since the load provided by post-tension can be distributed uniformly at the joint back.

In order to investigate the feasibility of the proposed retrofit technique, one of the tested specimens was built with transverse beam, as discussed before. The application steps of proposed retrofit technique were (i) drilling two 45-degree holes through the transverse beam diagonally, (ii) holing the rods and (iii) fastening the rods to the steel angles. In this way, a viable solution is suggested for the structures with floor slab and transverse beam (Figure 4.16d and Figure 4.17d).

Table 4.8. Retrofit scheme summary

Specimen	Axial force in one rod, P (kN)	Application	Column back plate
EJ-P-1	0	Figure 4.16a	N/A
EJ-P-2	100	Figure 4.16a	N/A
EJ-BP-1	100	Figure 4.16b	Present
EJB-P-3	100	Figure 4.16d	N/A

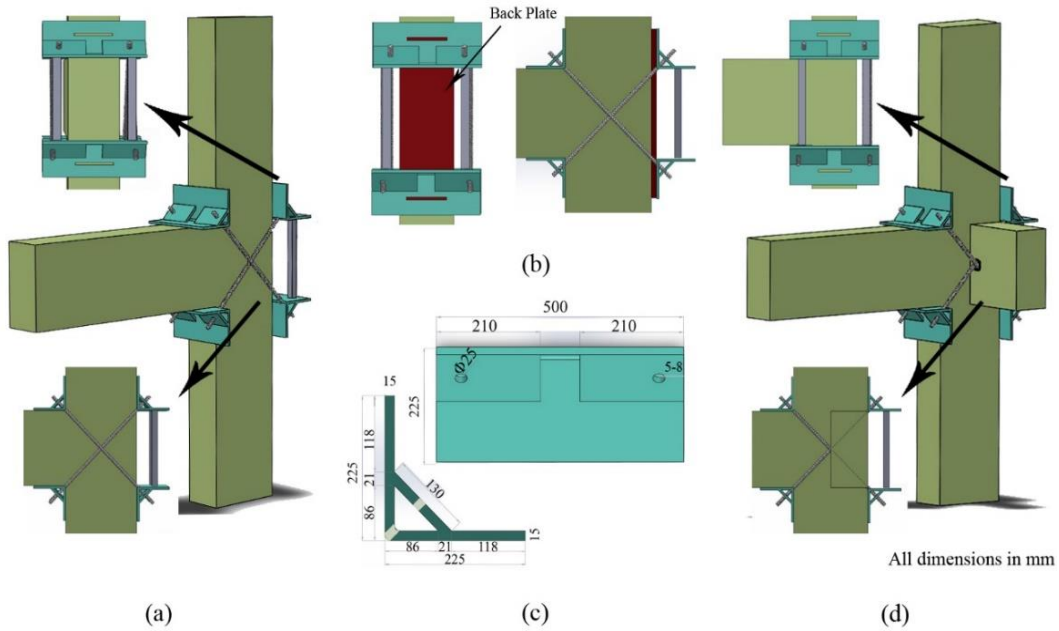

Figure 4.16. (a) EJ-P-1 and EJ-P-2 (b) EJ-BP-1 (c) detail of equal angle (d) EJB-P-3

Application of post-tension presented schematically in the Figure 4.16a to Figure 4.16d. It was also introduced on the tested specimens as shown in Figure 4.17a to Figure 4.17d.

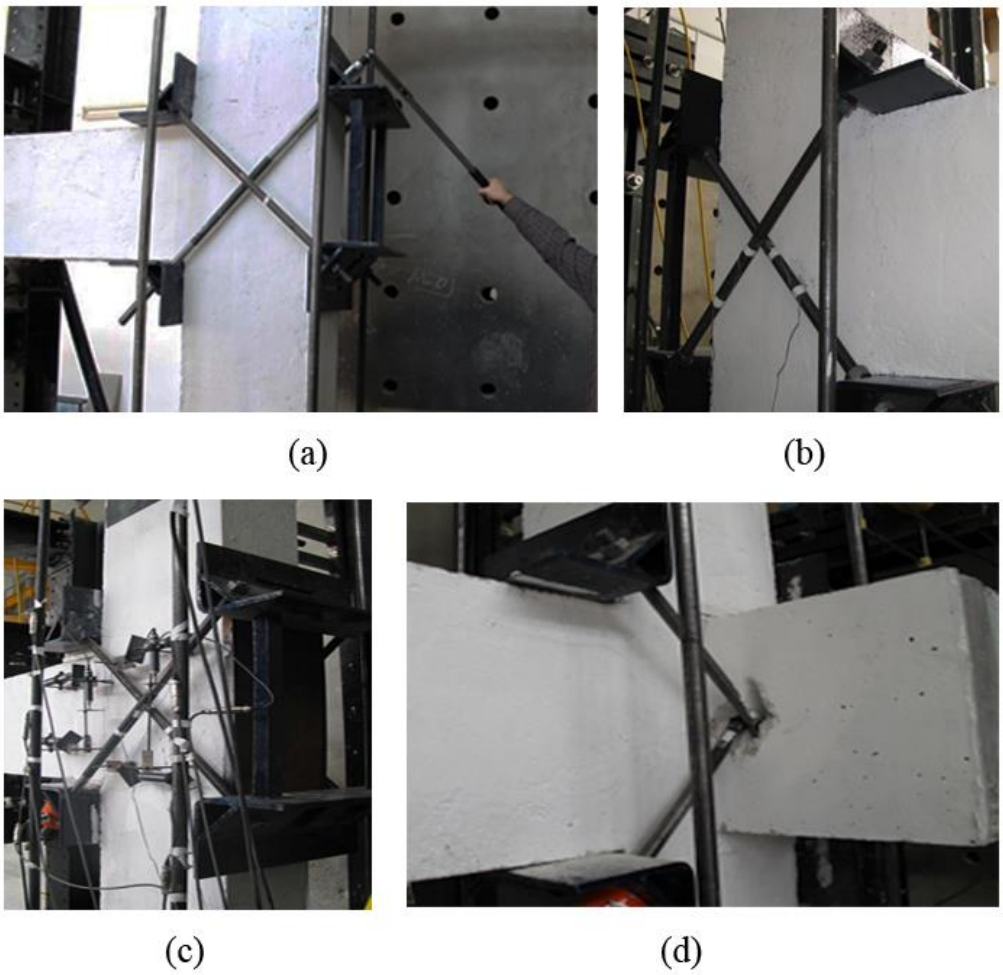

Figure 4.17. (a) Application of post-tension (b) EJ-P-1/EJ-P-2 (c) EJ-BP-1 (d) EJB-P-3

4.5. Structural Repair Design

The design philosophy of repair for initially damaged specimens is to attain the initial capacity, upgrading the seismic performance of damaged components, delaying or eliminating brittle failure modes and initiating the formation of flexural plastic hinges in the beam to attain a ductile behavior [55]. After testing the reference specimens, the deficiency of the members were realized and two different types of repairing techniques were considered. In the first specimen (EJ-1) beam and column members and in the second specimen (EJ-2) beam-column joint were repaired by CFRP wrapping. In designing the dimensions of CFRP sheets, it is assumed that the corresponding CFRP sheets will carry the entire lateral load exerted on the damaged test specimen.

While making the structural repair design of the damaged members of the first test assembly (EJ-1), it is assumed that the force acting on the beam longitudinal reinforcement bars due to flexural moment was resisted by only CFRP sheet. In the second test assembly (EJ-2), the amount of diagonal CFRP sheet was determined such that the diagonal component of the shear demand in the beam-column joint should be less than the tensile capacity of the diagonal CFRP sheet.

The axial load carried by the CFRP can be calculated by equation given below.

$$F_{CRFP} = E_{CFRP} \times \varepsilon_{CFRP} \times A_{CFRP} \quad 4.1$$

Where the E_{CFRP} is the modulus of elasticity of CFRP, A_{CFRP} is the cross sectional area and ε_{CFRP} is the effective strain of the FRP which was the minimum of 0.004 or $0.50\varepsilon_{ulf}$ according to TEC 2007 [4].

4.6. Retrofit Design

The main philosophy in the retrofit design is to eliminate the brittle type of joint failure by diverting the failure mode of the assembly to ductile beam failure by forming flexural plastic hinges at the beam-ends. On the other hand, formation of plastic hinges at the column-ends should be avoided. For this purpose joint shear capacity is intended to be improved, which is expected to prevent damage localization at the joint.

As there is no shear reinforcement in the specimens of the group 2, shear capacity of the joint is limited by the tensile strength of concrete only. The joint shear capacity is enhanced in the retrofitted specimen with the implementation of either CFRPs or external post-tension rods.

4.6.1. Retrofit by CFRPs

The strengthening principle described in Section 4.6 was not followed in retrofitting of EJ-C-1. The response of two different rehabilitation techniques - repair before damage and retrofit after damage- was intended to investigate. Therefore, same amount of CFRPs layer in the initially damaged specimen (EJ-2-

R) was carried out in the specimen retrofitted before damage (EJ-C-1). As mentioned before, the only difference is damage level in the specimen. While the specimen EJ-2-R was repaired after certain level of damage, there was no initial damage in EJ-C-1 before retrofit process.

4.6.2. Retrofit by externally applied post-tension rod

The joint shear capacity is enhanced in the retrofitted specimen with the implementation of post-tension rods. Then, the joint shear capacity is the sum of the contribution of the concrete tensile strength and the strength provided by post-tension rods [56]. In order to achieve a ductile behavior for a beam-column assembly, the beam has to reach its flexural capacity before the joint exposed to shear failure. Therefore, joint shear capacity of the retrofitted specimen is considered to be the maximum joint shear force at the formation of beam flexural plastic hinge. The difference between the maximum joint shear force corresponding to beam flexure capacity and the joint shear capacity limited by the concrete tensile strength is the necessary horizontal force to be applied in the post-tension rods. Since there are two post-tension rods mounted diagonally at each side of the joint, necessary post-tension load in one of the rod is calculated by dividing two as shown in Equation 4.2.

$$P = \frac{V_{jmax} - V_j}{\sin 45°} \times \frac{1}{2} \qquad 4.2$$

P, V_{jmax}, V_j denotes the axial force in one of the post-tension rod, joint shear force corresponds to the beam plastic flexure capacity, joint shear force corresponds to the tensile strength of concrete, respectively. Apart from the result obtained from Equation 4.2, the axial load in the rods was also limited by allowable axial stress in the rod.

4.7. Test Setup

The top-end of the column was subjected to quasi-static reversed cyclic loading, which is considered to be the representative earthquake force. The column-ends of the assembly were detailed such that they become zero-moment joints like

a pin support. The right-end of the beam was supported by roller supports so that beam-end can freely move in the horizontal direction.

Six equal length angles with dimensions of 40x4x400 mm were welded to firstly 800x800x10 mm plate, which is called as column bottom plate, then to column longitudinal bars and its hooks for mounting the pin support to column (Figure 4.18). After that, the column bottom plate was fixed with eight 30 mm bolts to the top plate of pin support.

Figure 4.18. Detail of column bottom plate

The beam was positioned horizontally and supported by roller support at the end. The roller support was provided by seven cylindrical rolling bearing units (Figure 4.19). Two plates with dimensions of 250x500x30 mm were mounted between the bearing units and the beam top-bottom surface at the beam end to eliminate the large bearing stress concentrations and hence to prevent concrete crushing in specified area.

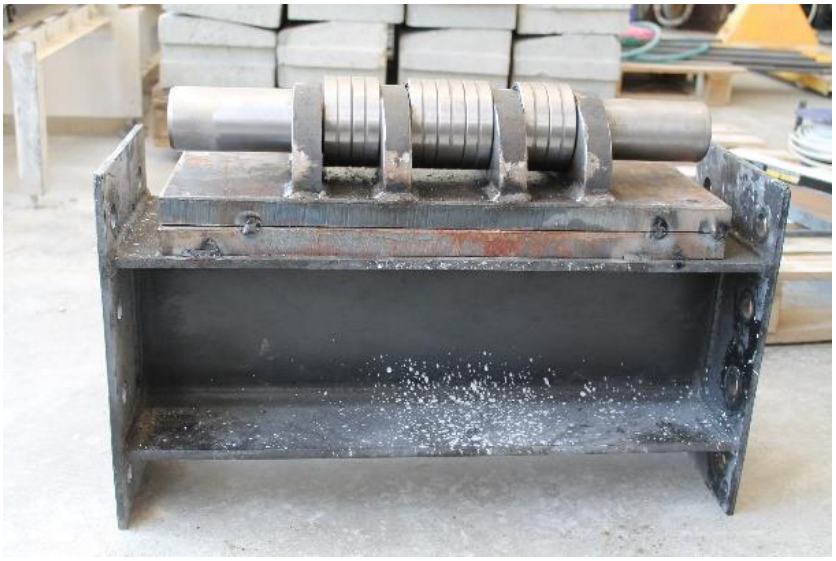

Figure 4.19. Roller support detail

The specimens were laterally supported by bearing units from beam-end and top of column to prevent out of plane movement (Figure 4.20).

Figure 4.20. Prevention of out of plane movement

Axial and lateral loads were applied by a single-acting and double-acting hydraulic cylinder, respectively. Double-acting hydraulic cylinder was placed to an adjustable steel frame that allows movement in both horizontal and vertical direction and the steel frame was fixed to reaction wall (Figure 4.21).

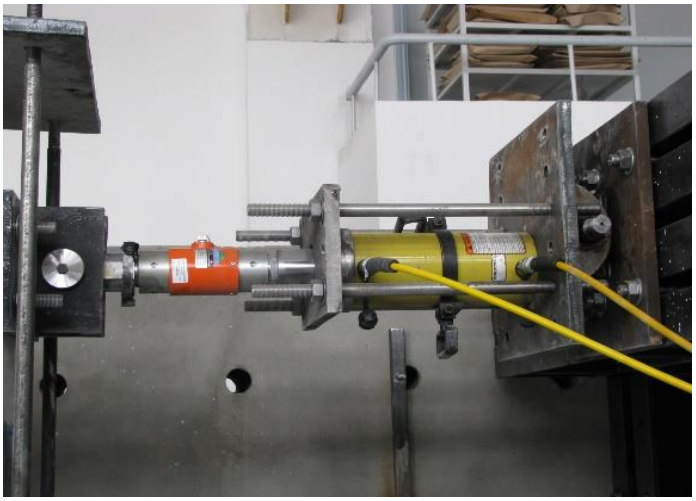

Figure 4.21. Double-acting hydraulic cylinder

The single-acting hydraulic cylinder was fixed to 800x800x30 mm plate at the top of the column. This plate was connected to top plate of pin support by four 3500 mm longitudinal rods. Axial load was applied by means of four vertical post-tension rods placed between the pin support and plate over the top of the column supporting the hydraulic cylinder acting vertically (Figure 4.22). Since axial load was always in the direction of column axis, constant axial load in push and pull cases was observed in the early stage of lateral displacement. Due to the formation of cracks and crushing of concrete, axial load was controlled to keep it constant in the subsequent drift levels.

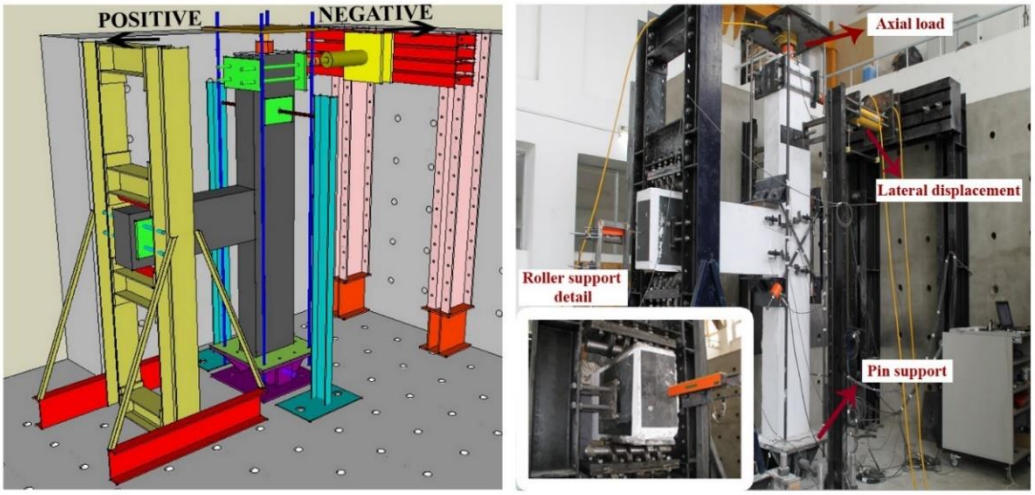

Figure 4.22. 3D view of the test setup

4.8. Instrumentations

Two different types of measuring systems were utilized for the specimens of first three test series and test series 4. The column tip and story level displacements, the diagonal and horizontal deformations of the joint, horizontal movement and rotation of the pin support were measured by thirteen strain gage-based linear variable differential transducers (LVDTs) in the specimens of the first three test series (Figure 4.23a).

The diagonal deformation in the joint could not be measured because of overlapping of diagonally placed post-tension rods and LVDTs in the retrofitted specimens via post-tension (test series 4). Therefore, twelve LVDTs were mounted on the retrofitted specimens in a different orientation (Figure 4.23b). The strain levels of reinforcement bars were measured by fifteen unidirectional strain gauges (Figure 4.23c). In addition, one tension-compression and two compression load cells were used to measure the lateral load, the axial load in the column and post-tension rod, respectively.

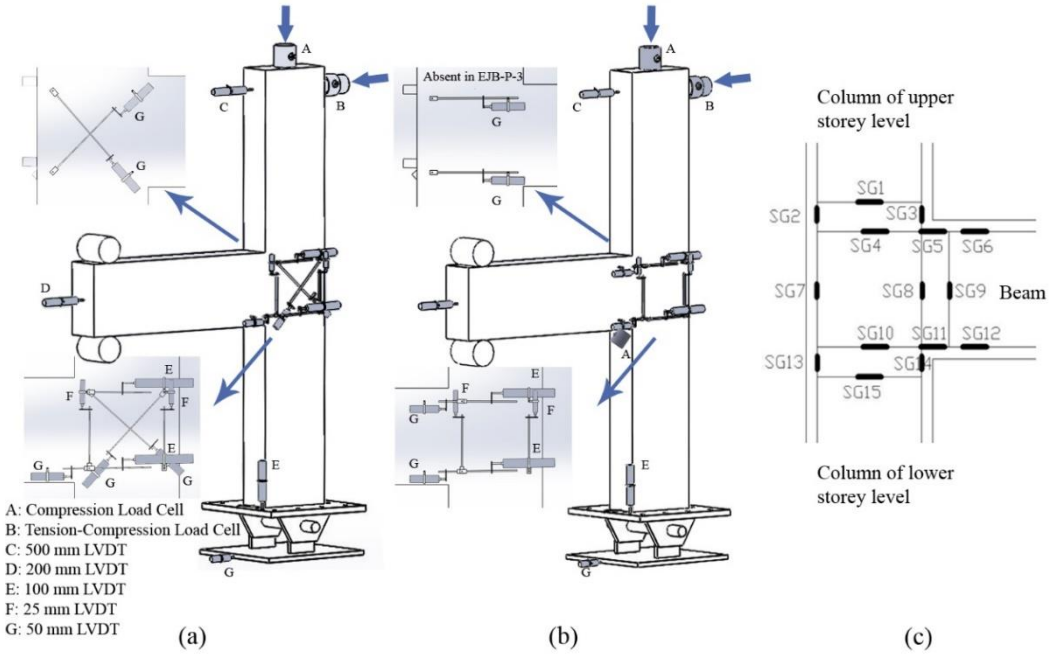

Figure 4.23. Instrumentations (a) test series 1, 2 and 3 (b) test series 4 (c) strain gauge

4.9. Loading History

Quasi-static cyclic lateral displacement was applied from top of column under the combined action of the constant column axial load so that the actual behavior of beam-column assembly can be investigated in the laboratory. Lateral displacements were carried out until the expected drift ratios. It should be emphasized that notified drift ratios are the ratio of measured lateral displacement to the distance between the point of application of lateral displacement and bottom of lower story column.

There were two different test sequences in this study. While applied drift ratio was up to 4% in the first test series, drift ratio of 8% was reached for rest of the test series. This inconsistency was due to the inadequate capacity of the test facility. The capacity of the hydraulic jack was limited up to displacement corresponding the 4% drift ratio in the experiment of test series 1 (Figure 4.24a). Then, a new hydraulic cylinder, which is capable to apply 8% drift ratio, was used in the following experiments (Figure 4.24b). This study would have been more interesting if drift ratio of 8% had been applied in the test series 1.

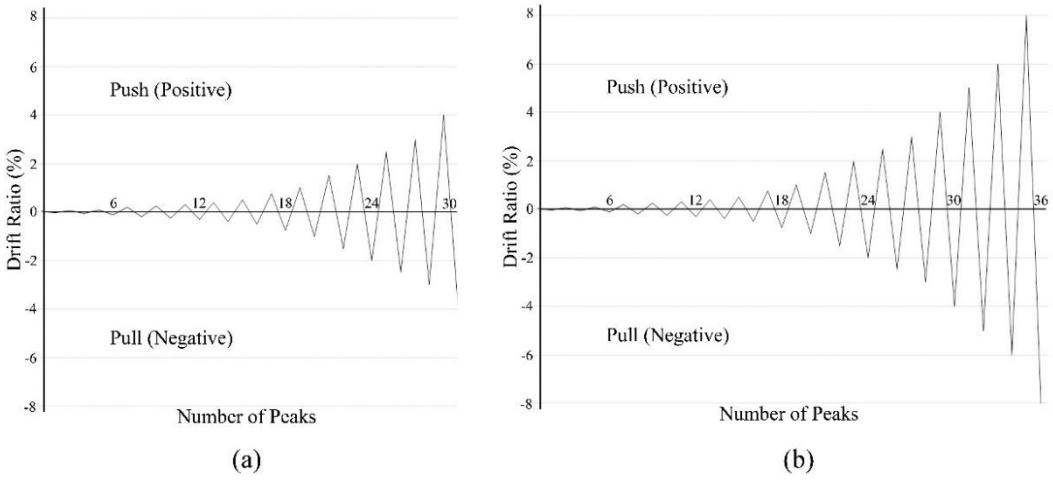

Figure 4.24. Displacement history (a) test series 1 (b) test series 2, 3 and 4

CHAPTER 5

5. RESULTS AND DISCUSSION

The response of the test specimens is summarized and the overall performance of the reference specimen is compared with the repaired and retrofitted specimens in this section.

Test results for the effectiveness of repair and retrofit schemes are compared and discussed in terms of the response quantities such as strength, stiffness, stiffness degradation, ductility and energy dissipation capacity of the specimens.

Due to the limited number of experiment studies on the response of substandard joint, several aspects have been discussed in this chapter.

5.1. Hysteretic Response of the Specimens

5.1.1. Specimen EJ-1

A ductile response was observed through the strain gauge measurements as the longitudinal reinforcement bars of the beam yielded before any type of failure, which is an expected behavior of EJ-1. The applied drift ratio was up to 4%. Therefore, the response at 8% drift ratio was not monitored due to restriction on the facility. A partial ductile failure was observed as the imposed displacement was not sufficient enough to reach the beam hinging with severe damage.

The computed plastic flexural capacity of the beam, which corresponds to the lateral force capacity of the beam-column assembly, is 110 kN and the beam member reached that value with the global yielding of the assembly (Figure 5.1). The first flexural crack at beam was observed at 0.25% drift ratio, which corresponds to 17.5% of the maximum load before yielding the beam longitudinal bars.

Due to the presence of deformed bars in accordance with the code requirements, the flexural and shear cracks were extended to almost whole beam length evenly and the plastic hinge initiated at beam joint interface due to flexure. The first observed inclined joint crack was at 0.50% drift ratio. Then, although the

flexural capacity of the beam did not exceed the joint shear capacity, hairline cracks in the joint were observed. However, these cracks did not widen. In the last loading stages of the specimen, hairline flexural cracks developed in the column that did not affect the behavior of the specimen.

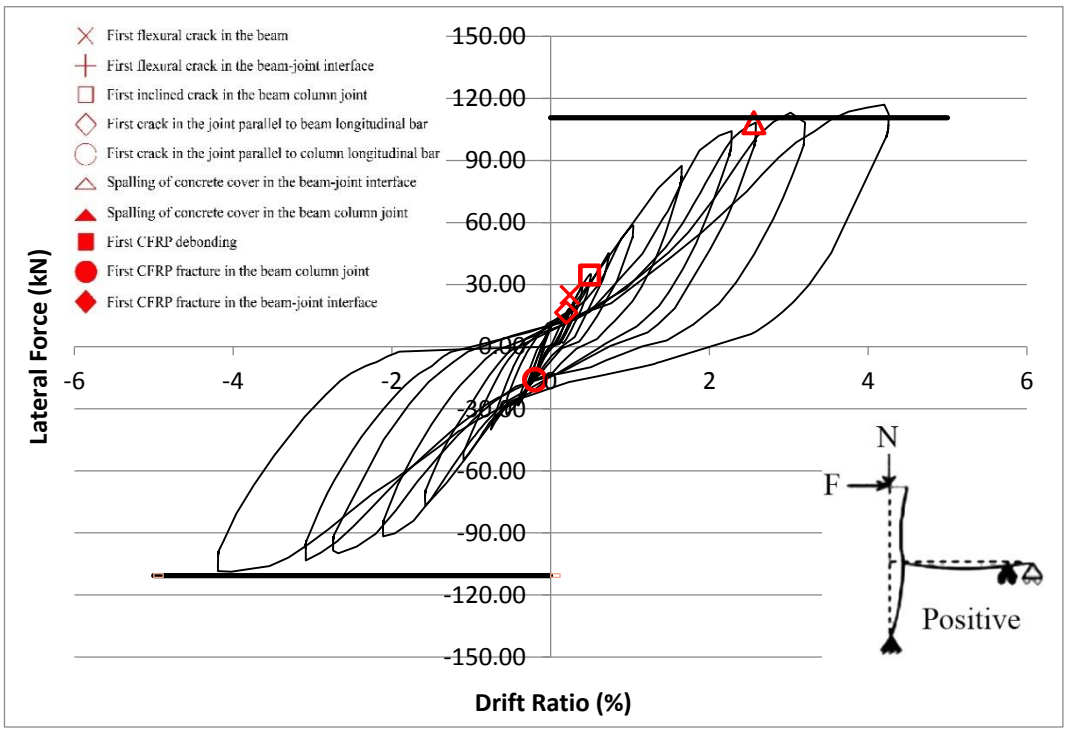

Figure 5.1. Hysteresis curve of the specimen EJ-1

Photographs of the damaged members of the specimen were presented in Figure 5.2a and c.

The pictures showing the damages member of the specimens were also presented the level of damage in the members. Even though the flexure capacity of the beam was reached, the imposed displacement was not enough to be observed full ductile behavior with severe damage in the beam.

As mentioned in Section 4.9, this study would have been more interesting if drift ratio of 8% had been applied in this specimen.

(a) (b)

(c)

Figure 5.2. Photographs of EJ-1, at (a) 1% (b) 2% (c) 4% drift ratios

5.1.2. Specimen EJ-1-R

The failure mode of EJ-1-R under cyclic loading was almost similar to EJ-1. During the first few cycles, hairline cracks at the joint and flexural cracks at the beam joint interface occurred during the experiment of the specimen EJ-1 were widened. However, no longer cracks in the column and beam from EJ-1 test could be observed due to presence of CFRP sheets. The first CFRP debonding initiated at 0.50% drift ratio which corresponds to 29.5% of maximum load at beam joint interface (Figure 5.3). A few cycle later, the first CFRP fracture started around the debonding region at 1.00% drift ratio. With the increase in the column lateral tip displacement, the CFRP ruptured and the existing flexural crack at interface and shear cracks at joint enlarged. Spalling of concrete cover also took place at the beam-column interface as observed at EJ-1 in a similar way. Figure 5.4a and c show the damaged photos of the specimens EJ-1-R.

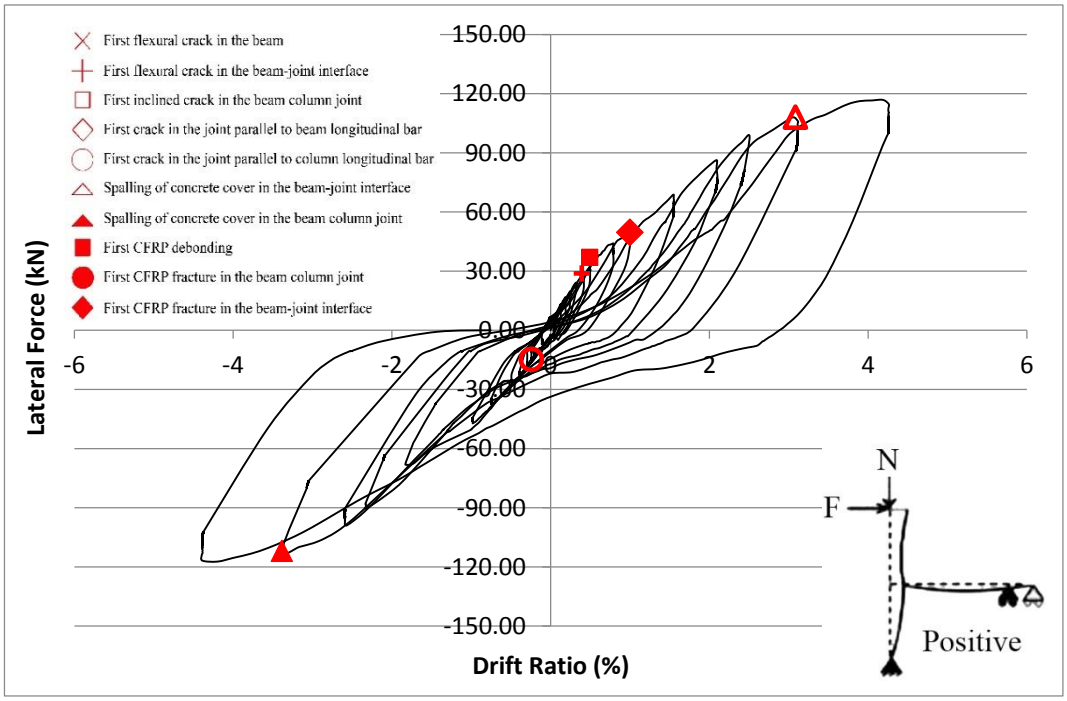

Figure 5.3. Hysteresis curve of the specimen EJ-1-R

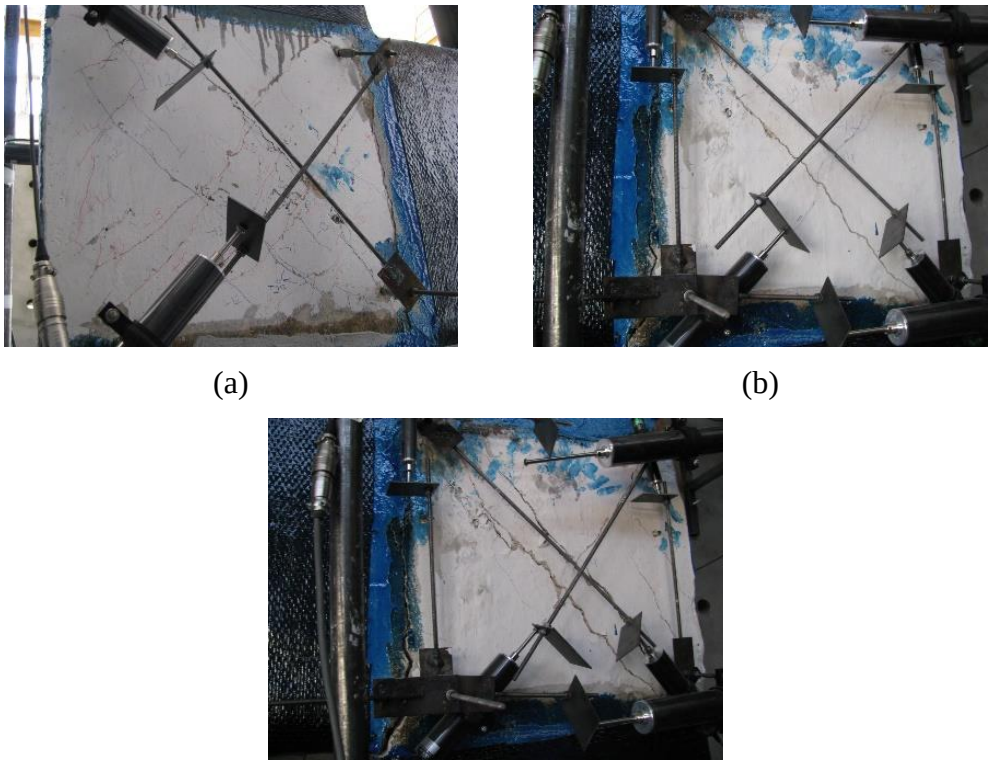

(a) (b)

(c)

Figure 5.4. Photographs of EJ-1-R, at (a) 1% (b) 2% (c) 4% drift ratios

5.1.3. Specimen EJ-2

The reference specimen of the group 2 (EJ-2) displayed a non-ductile behavior with the concentration of shear cracks mostly in the joint panel (Figure 5.6a and c). The capacity of the specimen was therefore limited by joint shear strength.

The first inclined crack in the joint, the first flexural crack in the beam and beam-joint interface were observed at 0.2% drift ratio, which corresponds the 29.5% of the ultimate load capacity of EJ-2. As the imposed displacement increased, new cracks were formed in the joint panel parallel to the beam longitudinal bar and parallel to the column reinforcement at 0.5% and 1.5% drift ratios, respectively.

In the subsequent drift levels, spalling of concrete cover in the joint was observed which corresponds to severe damage. Beam hooks forced to split the concrete cover at the joint back as a result of push out forces created by movement of beam longitudinal bars. Therefore, spalling of concrete cover at the joint back due to anchorage push out failure was observed at 3% drift ratio. This indicates that the slippage of beam longitudinal bars was not fully prevented. In addition, anchorage push out failure induced the local buckling of column reinforcement since the beam hooks were tied up the column longitudinal bars. However, both bond slip and anchorage push out failure modes did not precede the overall failure mode of the specimen. Presence of plain round bars in the beam lead to vertical splitting cracks in the beam-joint interface while the crack propagation was not uniformly distributed to the rest of the beam.

The lateral load capacity of the test specimen is calculated as 68.9 kN for the initiation of plastic hinge at the beam end. However, as shown in Figure 5.5, the experimentally obtained ultimate lateral load is less than 68.9 kN, which indicates that the joint panel reaches to its shear capacity before the beam attains its flexural capacity.

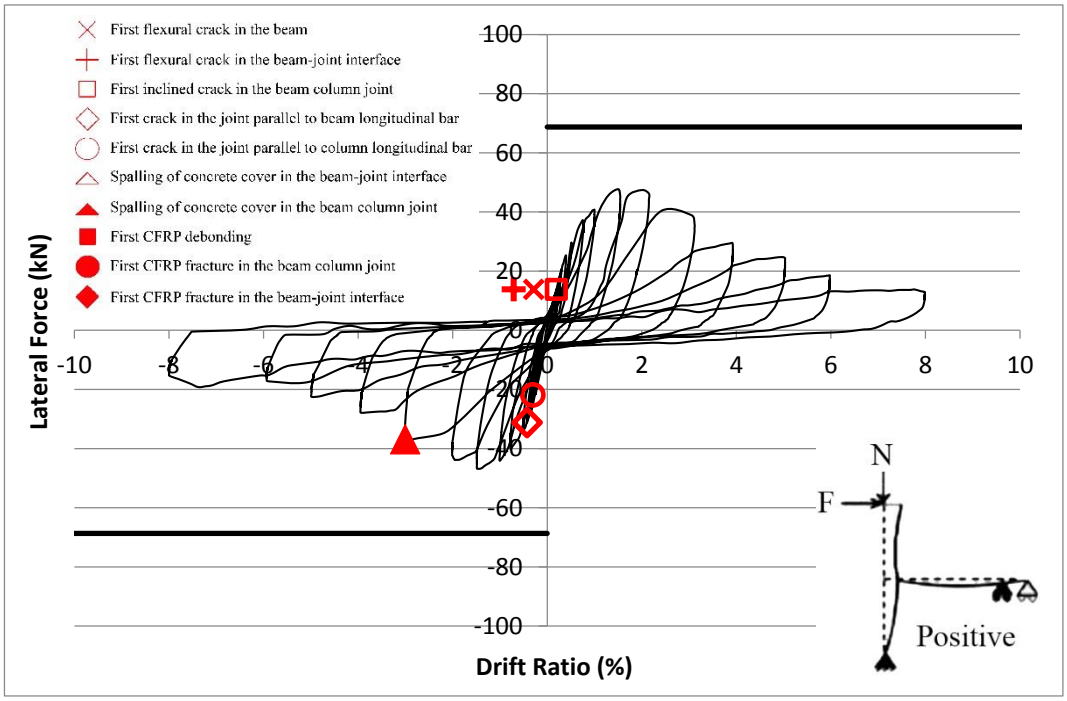

Figure 5.5. Hysteresis curve of the specimen EJ-2

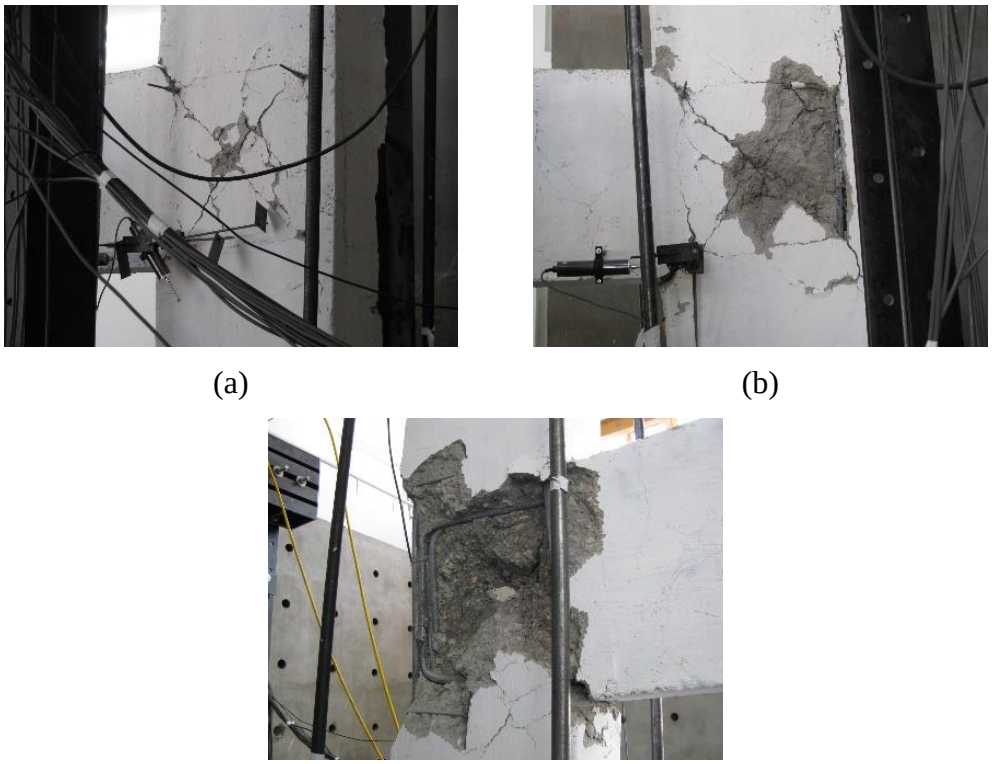

(a) (b)

(c)

Figure 5.6. Photographs of EJ-2, at (a) 2% (b) 4% (c) 8% drift ratios

5.1.4. Specimen EJ-2-R

The observed failure mode of EJ-2-R was shear failure at joint, which was also observed for the reference specimen, EJ-2. The performance of repaired specimen was quite satisfactory until debonding of the diagonal CFRP sheets on the joint surface.

The first CFRP debonding was observed at 0.40% drift ratio, which corresponds to 50% of maximum lateral load (Figure 5.7). However, the flexural crack was observed on the beam at 0.20% drift ratio which is prior to the occurrence of CFRP debonding. This implies that the application of the diagonal CFRP at the beam-column joint has changed the behavior of the beam-column assembly and flexural deformations in the beam preceded the overall response just before the fracture of CFRPs.

Beyond the several cycles of the first debonding, fracture of CFRPs was initiated. The damage in the members was visually illustrated in Figure 5.8a and c.

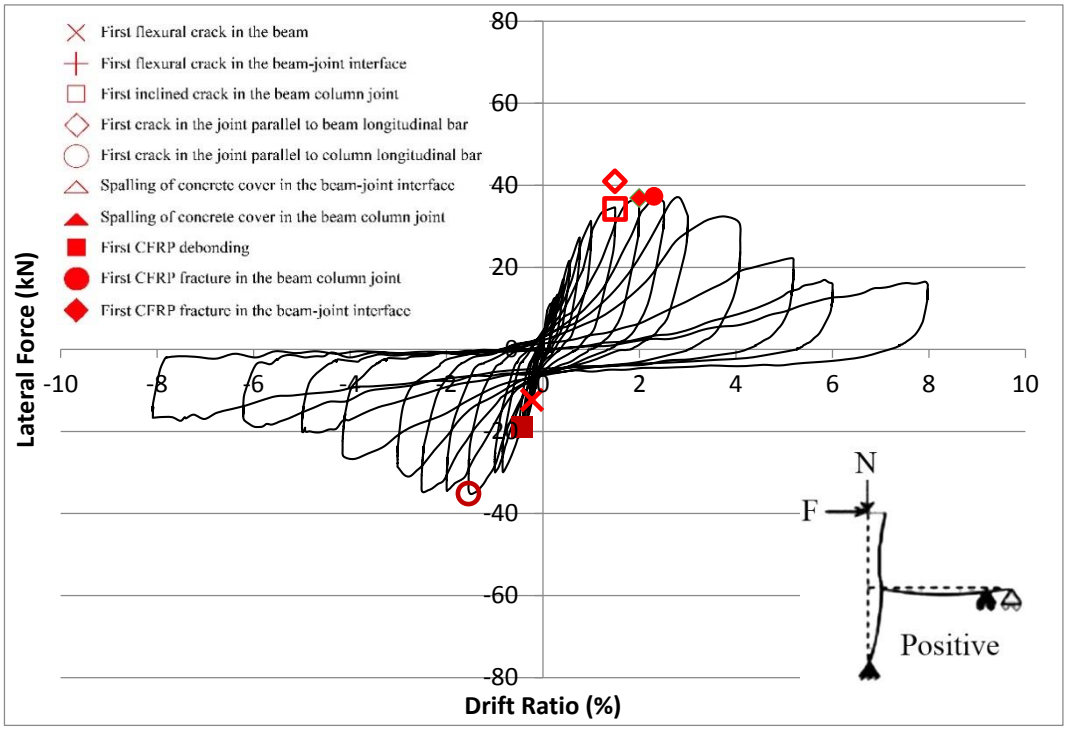

Figure 5.7. Hysteresis curve of the specimen EJ-2-R

(a) (b)

(c)

Figure 5.8. Photographs of EJ-2-R, at (a) 2% (b) 4% (c) 8% drift ratios

5.1.5. Specimen EJ-C-1

A shear failure due to CFRPs fracture was monitored in the specimen EJ-C-1. Because of brittle failure, a rapid strength deterioration together with non-ductile behavior was observed. The plastic flexural capacity of the beam was computed as 76.16 kN, which has not been reached during the test. The first beam flexural crack was observed at 0.3% drift ratio, which corresponds the 55.12% of the ultimate load (Figure 5.9). Then, new hairline cracks spread over the whole beam length. The formation of the beam flexural cracks stopped soon after debonding of the CFRP (2.5% drift ratio). CFRPs fracture occurred in the subsequent drift levels, which corresponds the severe damage in both RC members and CFRPs. Finally, the concrete split at joint core as it was no longer being wrapped by CFRPs. The different damage levels were presented in Figure 5.10a and c.

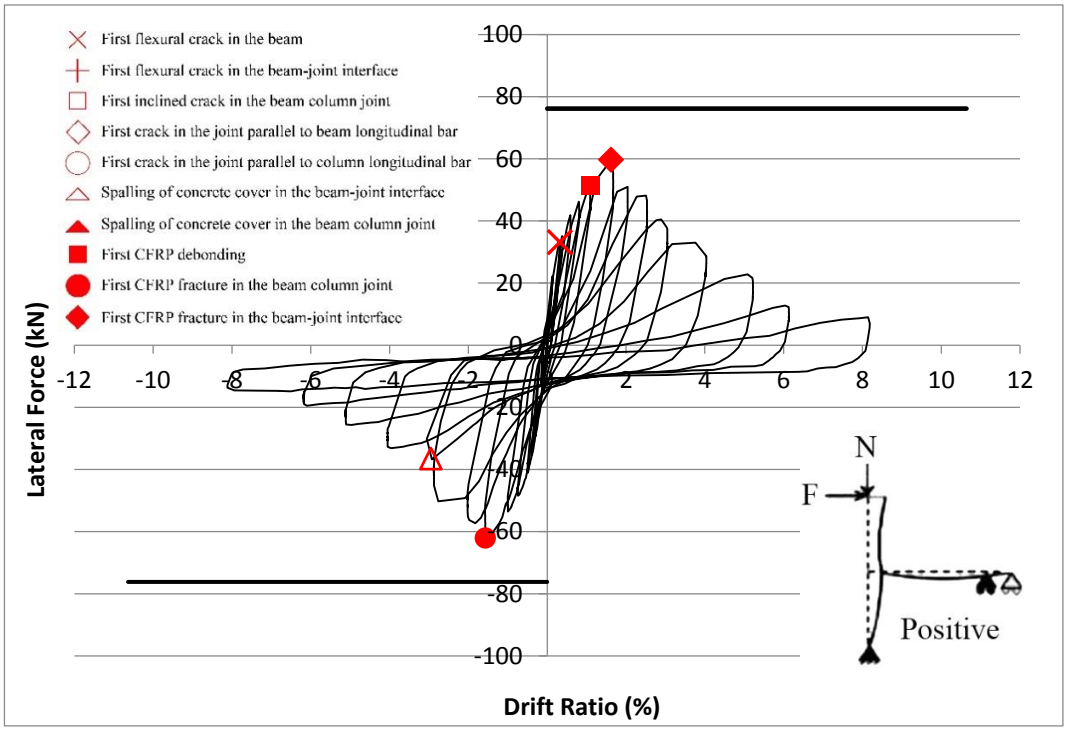

Figure 5.9. Hysteresis curve of the specimen EJ-C-1

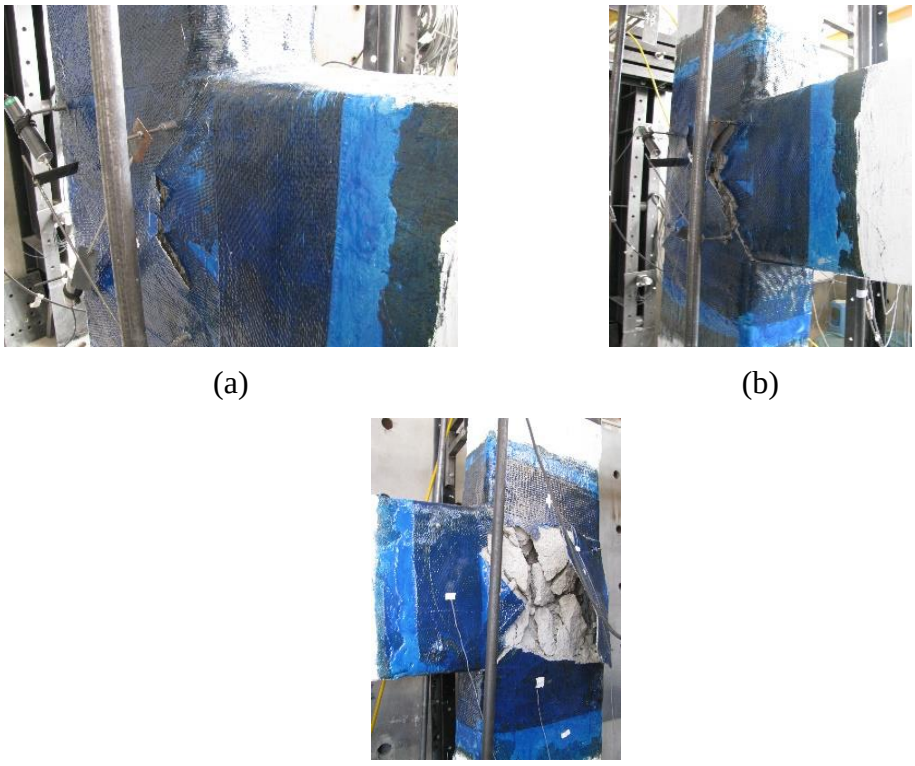

(a) (b)

(c)

Figure 5.10. Photographs of EJ-C-1, at (a) 2% (b) 4% (c) 8% drift ratios

5.1.6. Specimen EJ-P-1

Shear failure of the joint panel preceded the hysteric response of EJ-P-1 (Figure 5.12a and c). The first joint inclined crack was observed at 0.5% drift ratio which corresponds to 62% of maximum lateral load (Figure 5.11).

The diagonal cracks in the joint developed in the form of X-pattern and spread all over the joint panel in the subsequent drift levels. The first crack due to splitting at the joint back initiated at 0.5% drift level. As the drift ratio increases, enlargement in the existing cracks and deterioration in concrete were monitored in the joint panel. As a consequence of such severe damage, spalling of concrete cover was observed at the joint back and at the joint panel at 3% drift ratio.

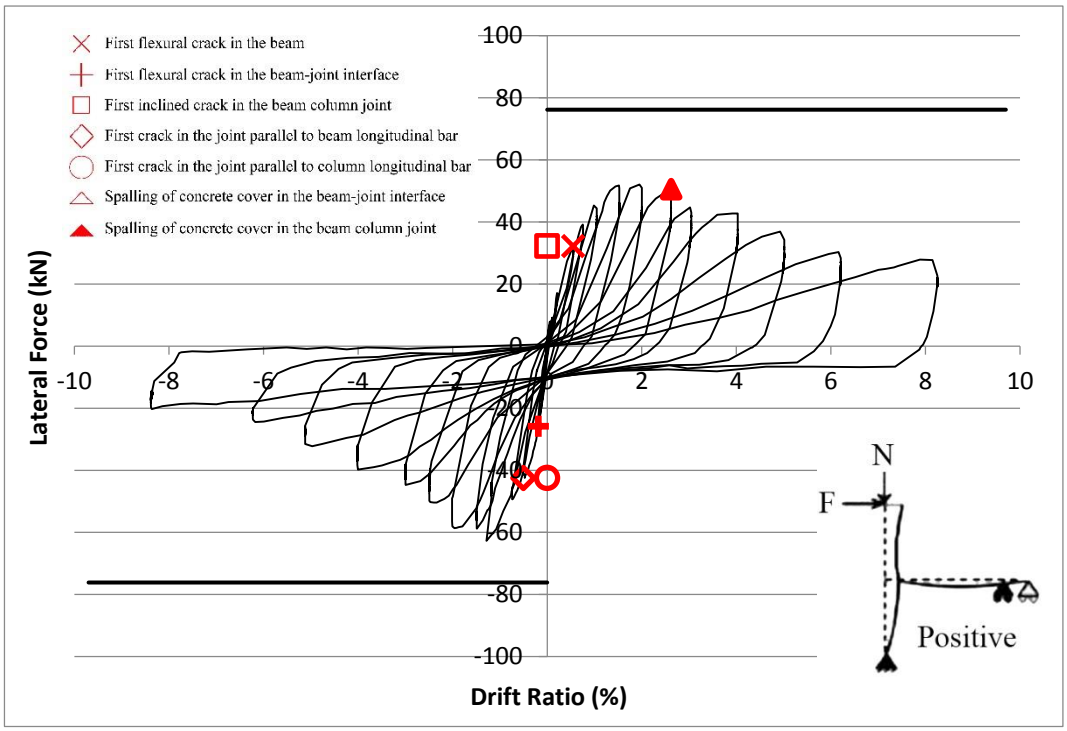

Figure 5.11. Hysteresis curve of the specimen EJ-P-1

The calculated flexure capacity of beam was 76.19 kN, which has not been reached during the experiment. The first flexural crack in the beam-joint interface was occurred at 0.5% drift ratio, as well. Then, the new hairline cracks spread over the beam length at which the steel angles are connected.

The formation of flexural cracks in the beam continued up to 2.5% drift ratio, after which the joint shear failure precedes the overall response. As the shear failure

took place in the joint panel, no longer damage was observed at the beam. Damage was mostly concentrated in the joint panel, while the rest of the structural members were relaxed.

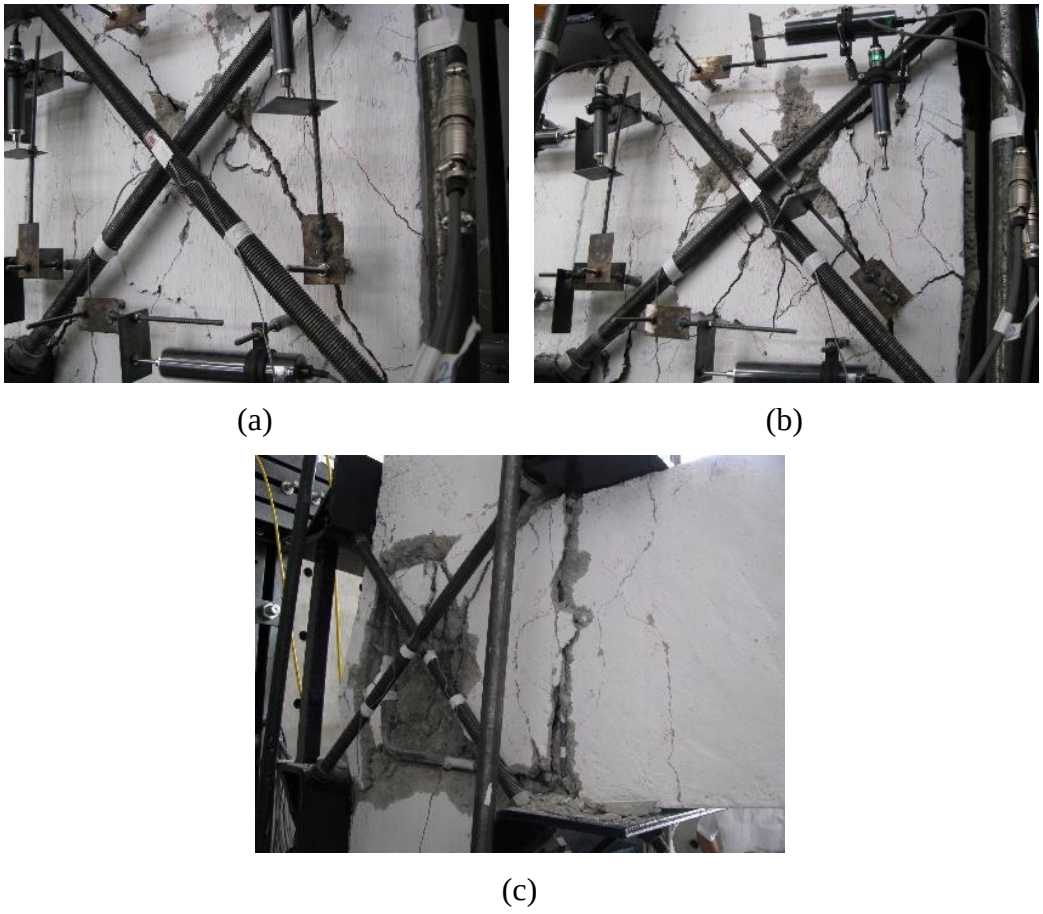

(a) (b)

(c)

Figure 5.12. Photographs of EJ-P-1, at (a) 2% (b) 4% (c) 8% drift ratios

5.1.7. Specimen EJ-P-2

The beam-joint failure and joint shear failure were observed in negative and positive direction of EJ-P-2, respectively. The beam-joint failure was begun by yielding of longitudinal beam reinforcement bar. Shortly after beam yielding, severe joint shear cracks were appeared and then joint exposed to shear failure as also indicated by Hassan [15]. Therefore, it can be assumed that the behavior was relatively satisfactory once compared with the first two specimens in terms of strength (Figure 5.13).

The first beam flexural cracks initiated at 0.25 % drift ratio. Formation of new cracks and widening of existing cracks in the beam stabilized after 3% drift ratio when the joint shear failure preceded the overall response. While, the beam flexural capacity (76.3 kN) was almost reached in negative direction of EJ-P-2, the beam did not attain its flexure capacity in positive direction. Up to 1.5% loading level, no significant crack was formed in the joint region of specimen EJ-P-2. As the drift ratio increases, damage concentrates mostly in the joint panel (Figure 5.14a and c).

Vertical cracks in the joint were observed parallel to the column reinforcement near the beam-joint interface at 0.3% drift level. The first inclined crack in the joint panel and the first crack at the joint back were developed at 0.4% and 0.75% drift ratio, respectively.

Concrete cover in the joint was partially spalled at 2.5% drift ratio, which corresponds to severe damage. At 1.5% drift ratio, some hairline cracks occurred in the lower story column under the steel angle. Such column cracks have not been observed in the previous test specimens. Nevertheless, crack widths in the lower story column were not so critical that they appeared to be constant in further loading steps.

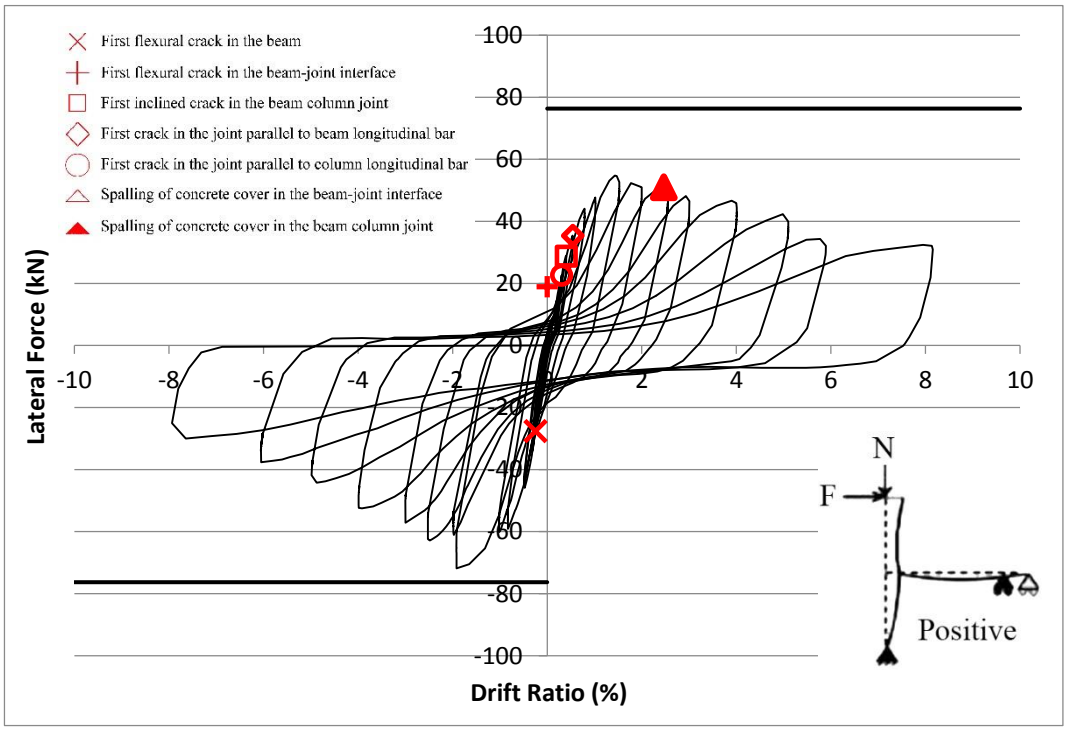

Figure 5.13. Hysteresis curve of the specimen EJ-P-2

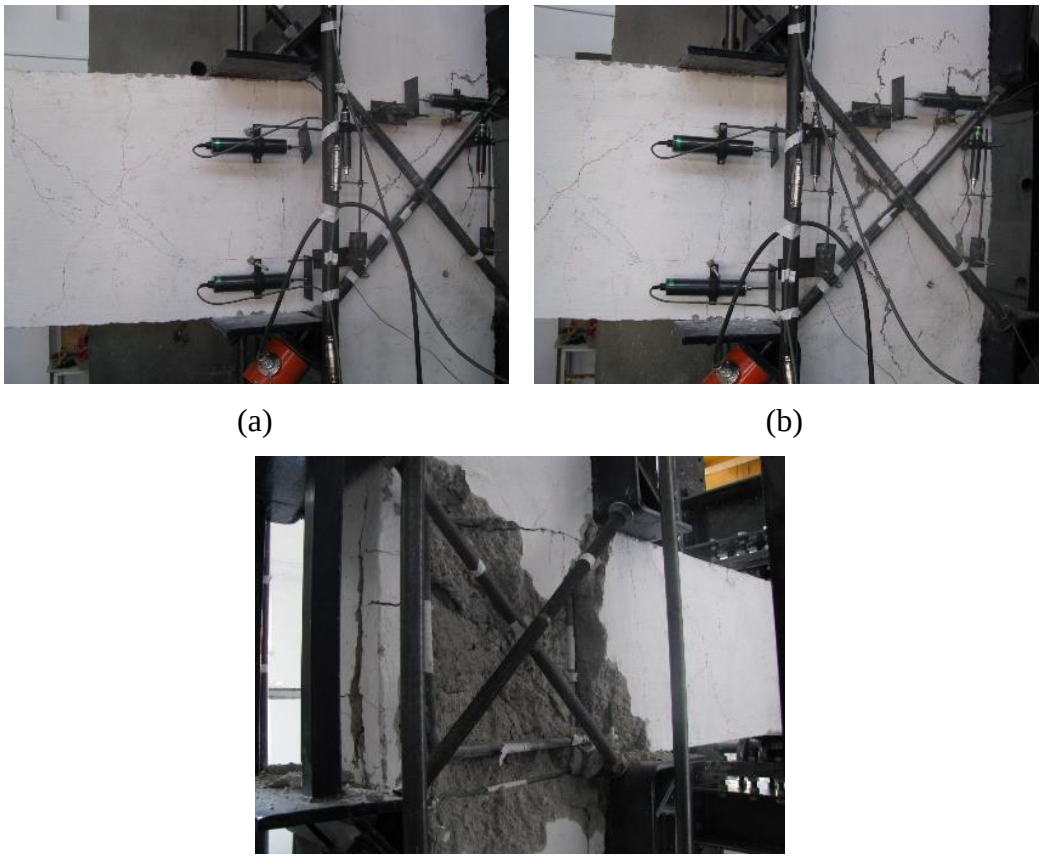

(a) (b)

(c)

Figure 5.14. Photographs of EJ-P-2, at (a) 2% (b) 4% (c) 8% drift ratios

5.1.8. Specimen EJ-BP-1

A combination of beam-joint failure was monitored in the specimen EJ-BP-1. Therefore, a rapid strength deterioration and partially ductile behavior were observed (Figure 5.15).

The first flexural cracks in the beam appeared between the steel angles at 0.2% drift ratio. Formation of hairline flexural cracks in the beam continued up to 3% drift ratio. Then, no additional cracks were developed when the crushing of concrete took place in the joint panel.

It was also found that vertical splitting cracks were formed in the beam-joint interface. Nevertheless, the cracks were mostly concentrated in the joint after yielding of longitudinal reinforcement of the beam.

The back plate restricted the splitting of concrete cover at joint back due to anchorage push out failure (Figure 5.16a and c). More confined joint panel was thus achieved. However, crack propagation from the joint panel to the column was observed. Therefore, more cracks formed in the column which differed from the previous specimens.

The first diagonal crack in the joint panel appeared at 0.3% and then, it continued to develop until merging the cracks in the beam-joint interface. After 3% drift ratio, joint shear failure became more critical and severe damage was monitored in the joint panel.

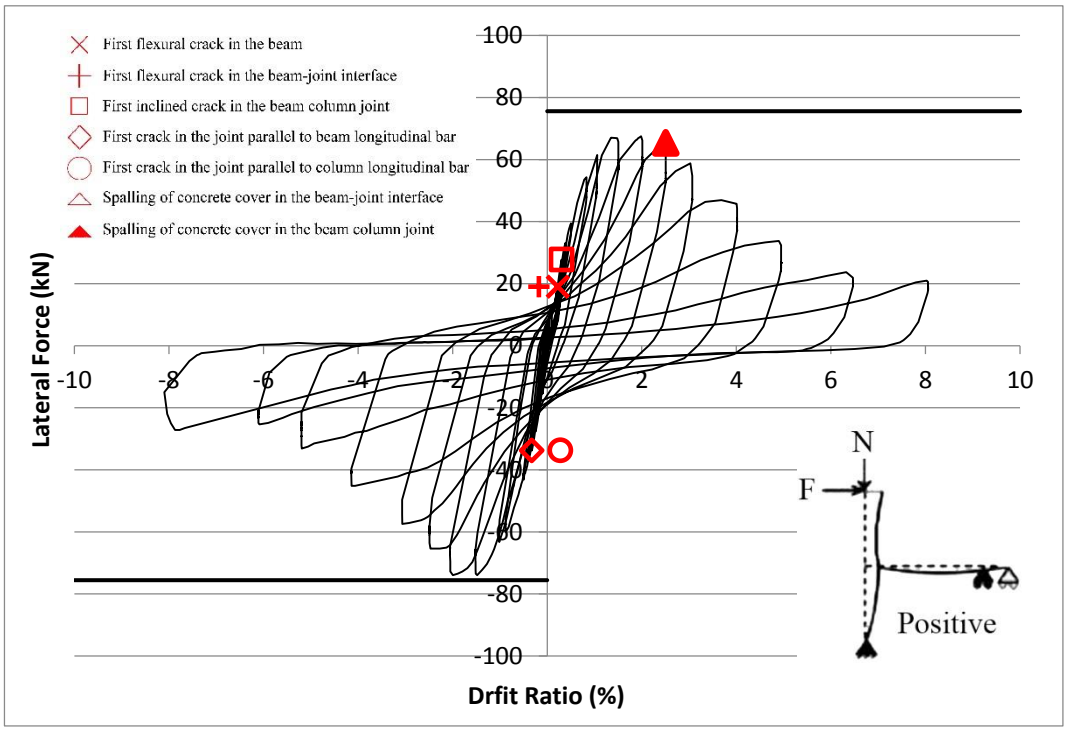

Figure 5.15. Hysteresis curve of the specimen EJ-BP-1

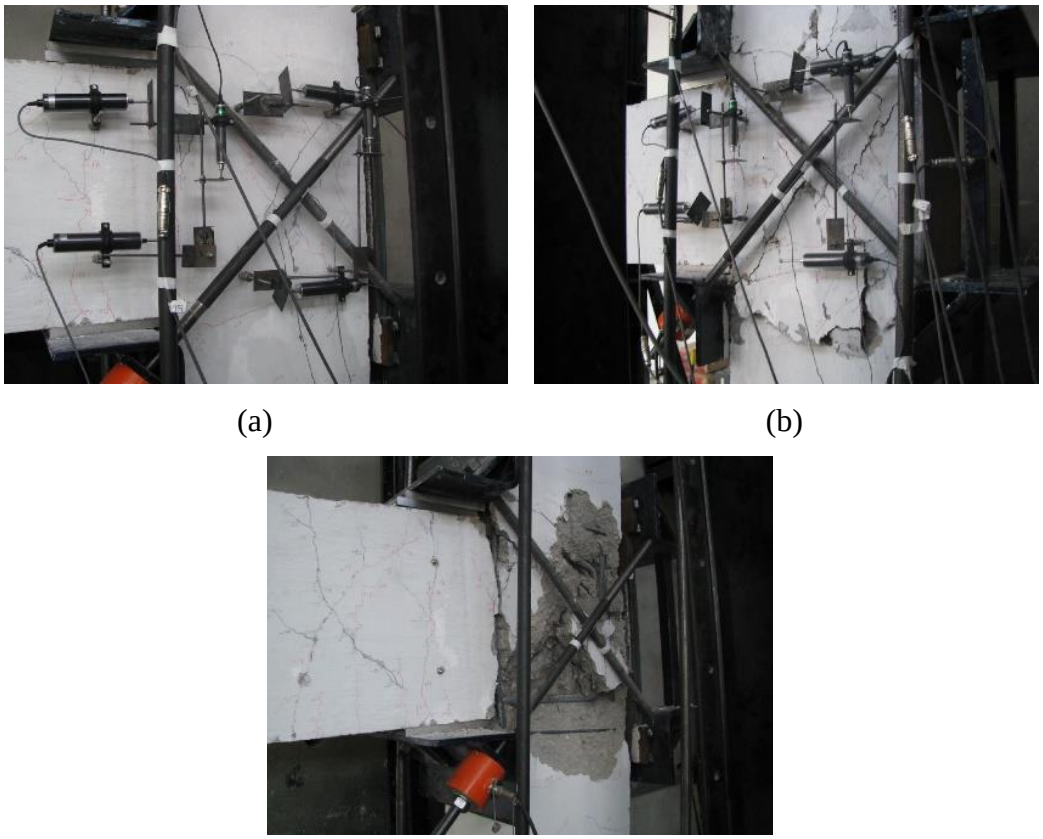

(a) (b)

(c)

Figure 5.16. Photographs of EJ-BP-1, at (a) 2% (b) 4% (c) 8% drift ratios

5.1.9. Specimen EJB-P-3

The overall response of the last specimen (EJB-P-3), which has a transverse beam connecting at the joint, was quite satisfactory compared to other specimens. A ductile behavior was monitored by the strain gauge measurements as the longitudinal reinforcement bars of the beam yielded before any type of failure. The computed plastic flexural capacity of the beam corresponding to the lateral force capacity of the specimen is 75.9 kN.

The beam reached that value with the global yielding of the assembly (Figure 5.17). The first flexural crack in the beam occurred at 0.20% drift ratio that corresponds to 18.7% of maximum lateral load. Most of the propagated cracks in the beam occurred in the plastic hinge zone and did not extend the rest of the beam (Figure 5.18a and c). Formation of cracks stabilized in the beams and diagonal

cracks continued to widen in the joint after 5% drift level. The first observed inclined joint crack was formed during the 1% drift ratio.

During the 0.3% drift ratio, the first column crack, which was parallel to the beam and nearly perpendicular to the steel angles, was formed. As the drift ratio increases, some hairline cracks developed in the column between the steel angles but the behavior of the specimen has not been affected considerably.

Torsional stiffness of the transverse beam provides additional strength while the transverse beam restricted the movement of the post-tension rods in the direction of column. Shear cracks thus occurred in the transverse beam. The first shear crack was observed at 1.5% drift and new cracks continued to develop and spread over the whole length of transverse beam as the imposed displacement increased.

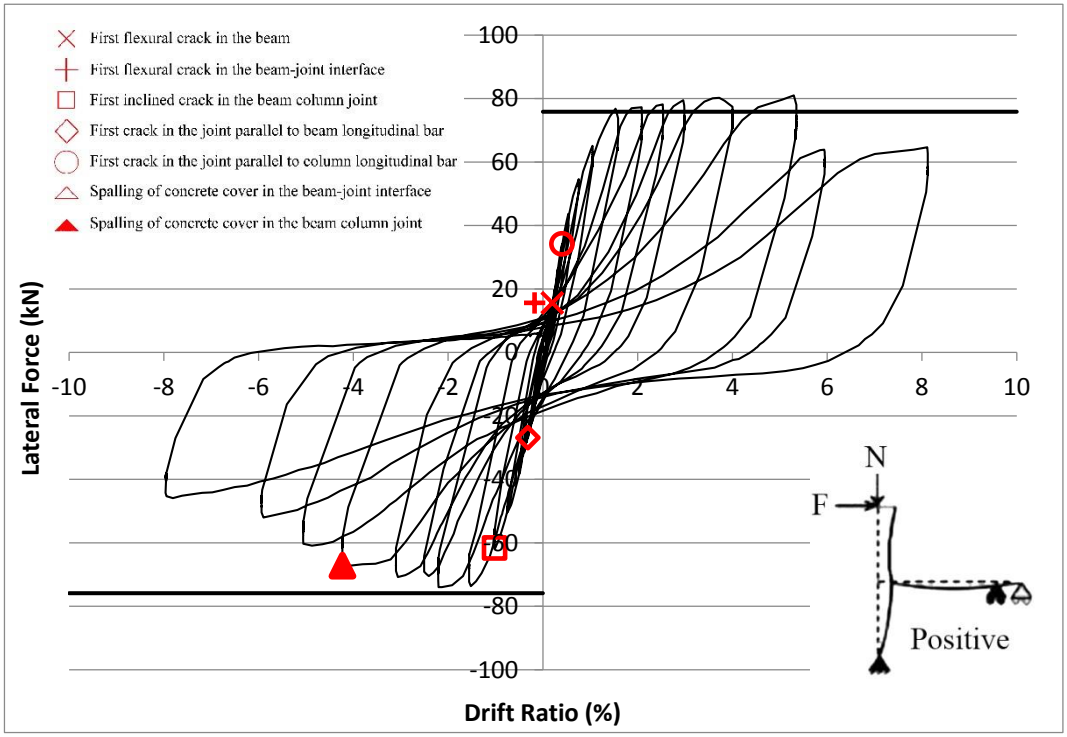

Figure 5.17. Hysteresis curve of the specimen EJB-P-3

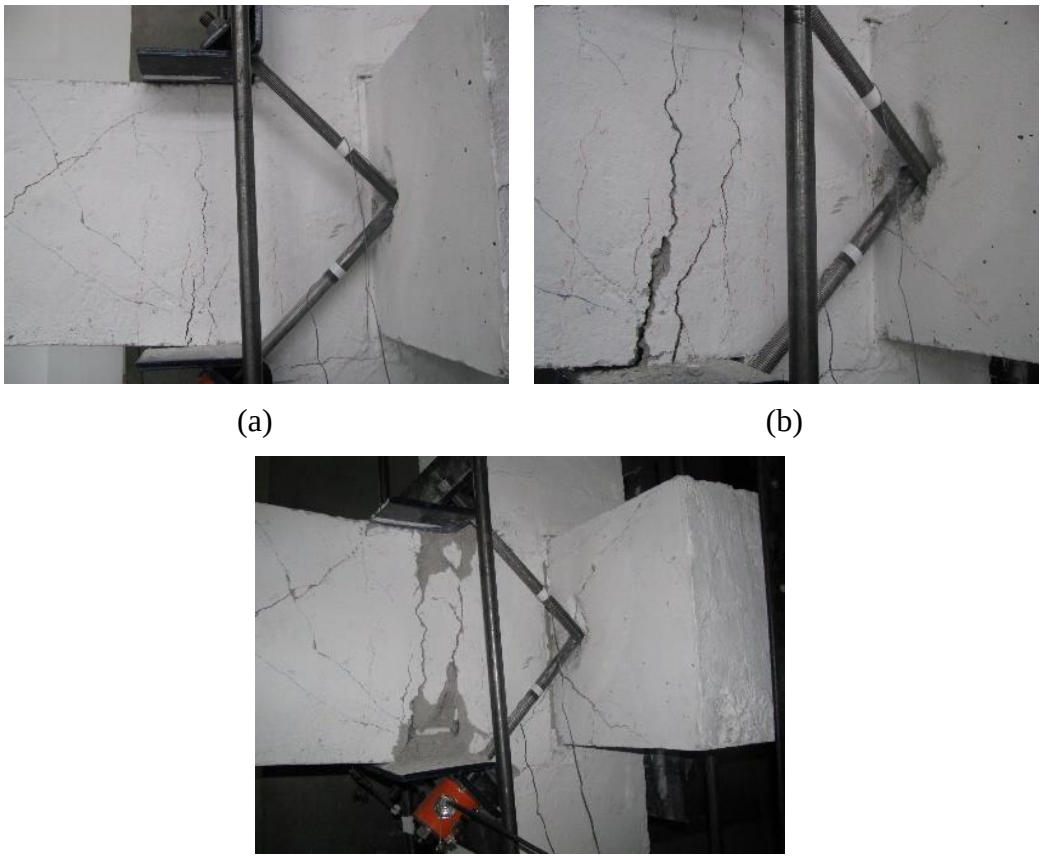

(a) (b)

(c)

Figure 5.18. Photographs of EJB-P-3, at (a) 2% (b) 4% (c) 8% drift ratios

5.2. Envelope Curves of Hysteretic Loops

The envelope curve is obtained by joining the peak value of each cycle with a linear line (Figure 5.19). The envelope curves of hysteretic loops can be useful for comparison purposes. While the envelope curves of each specimen were presented, the envelope curve of its reference specimen was also included to the graph for comparison purposes.

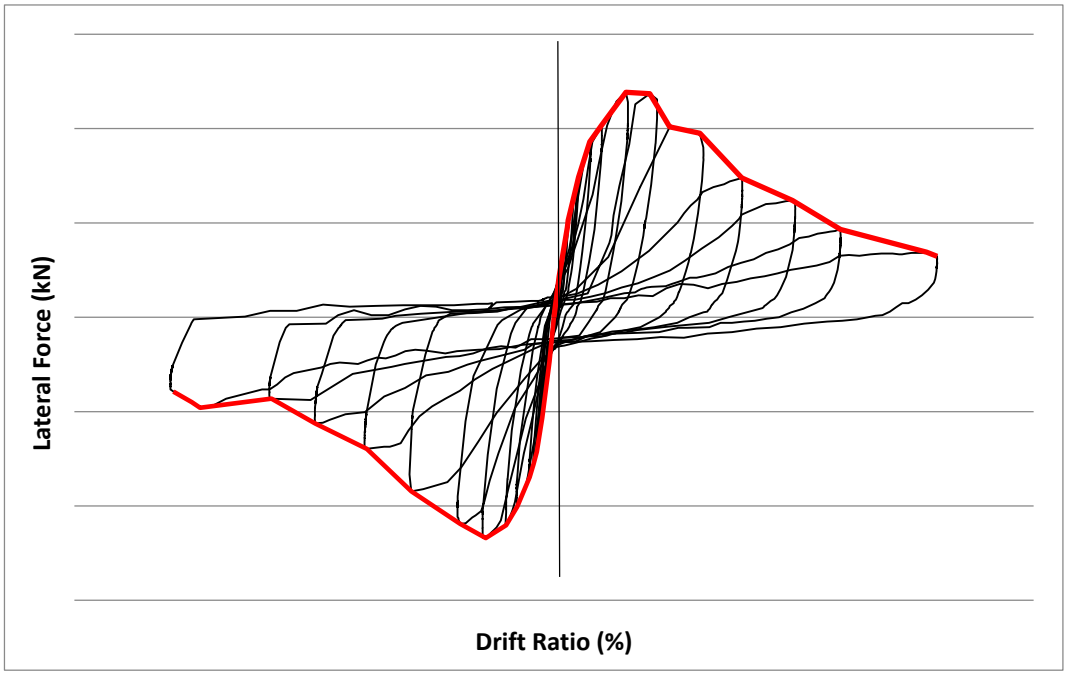

Figure 5.19. Illustration of obtaining envelope curve

The envelope curve of each test series were presented in Figure 5.20-Figure 5.23.

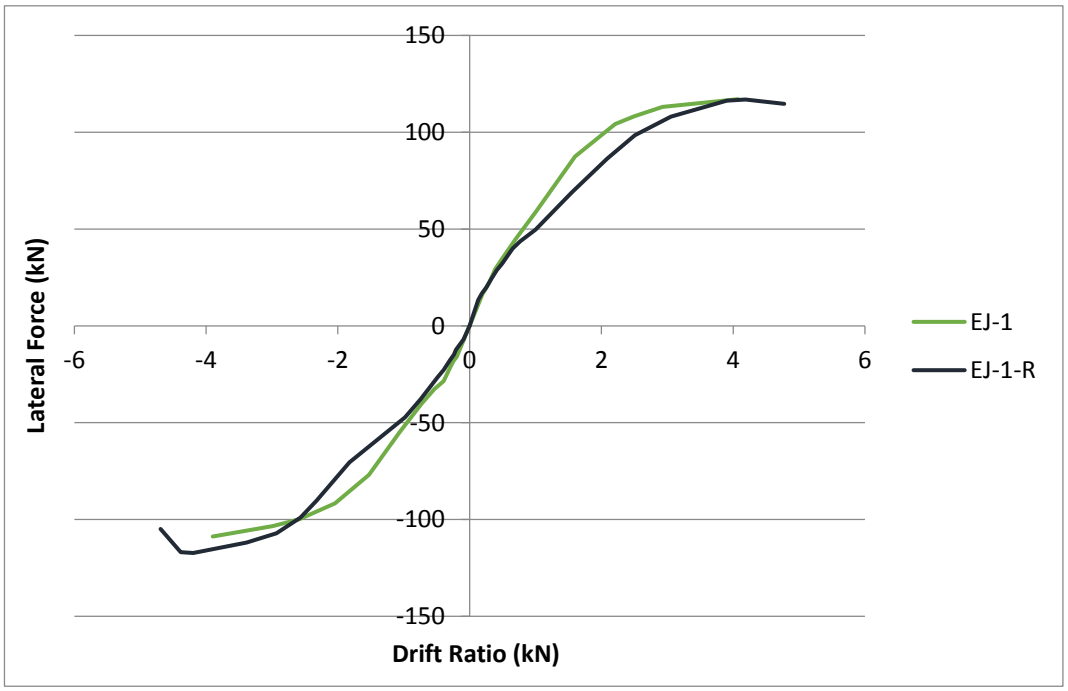

Figure 5.20. Envelope curves of hysteretic loops, test series 1

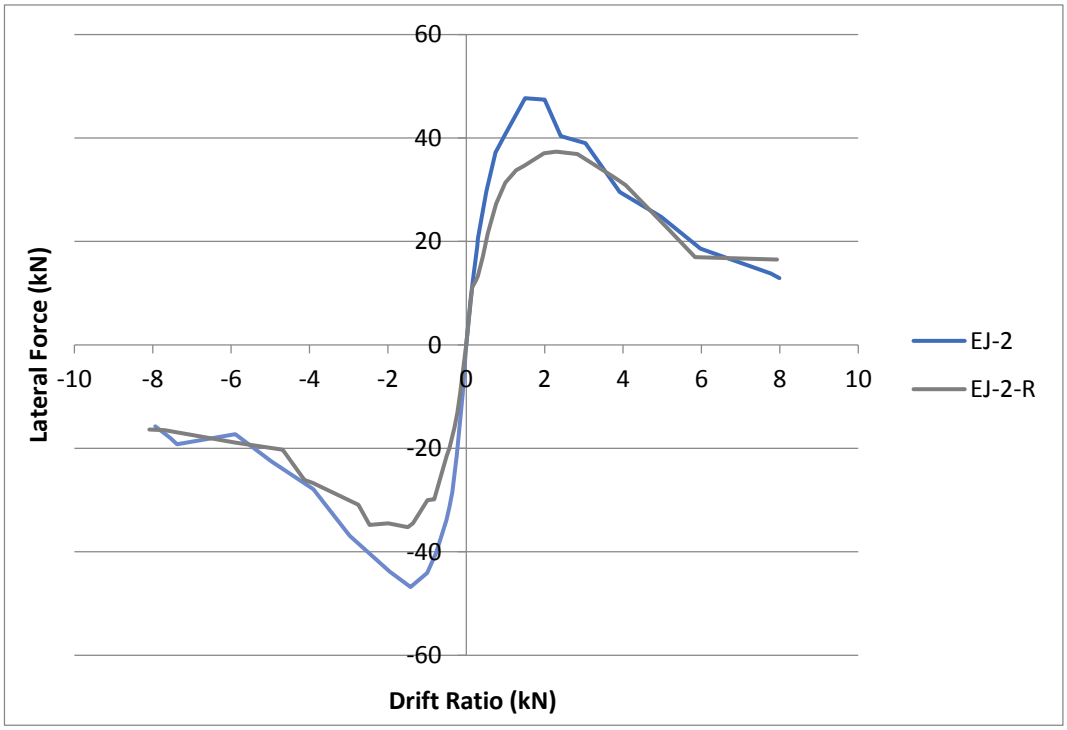

Figure 5.21. Envelope curves of hysteretic loops, test series 2

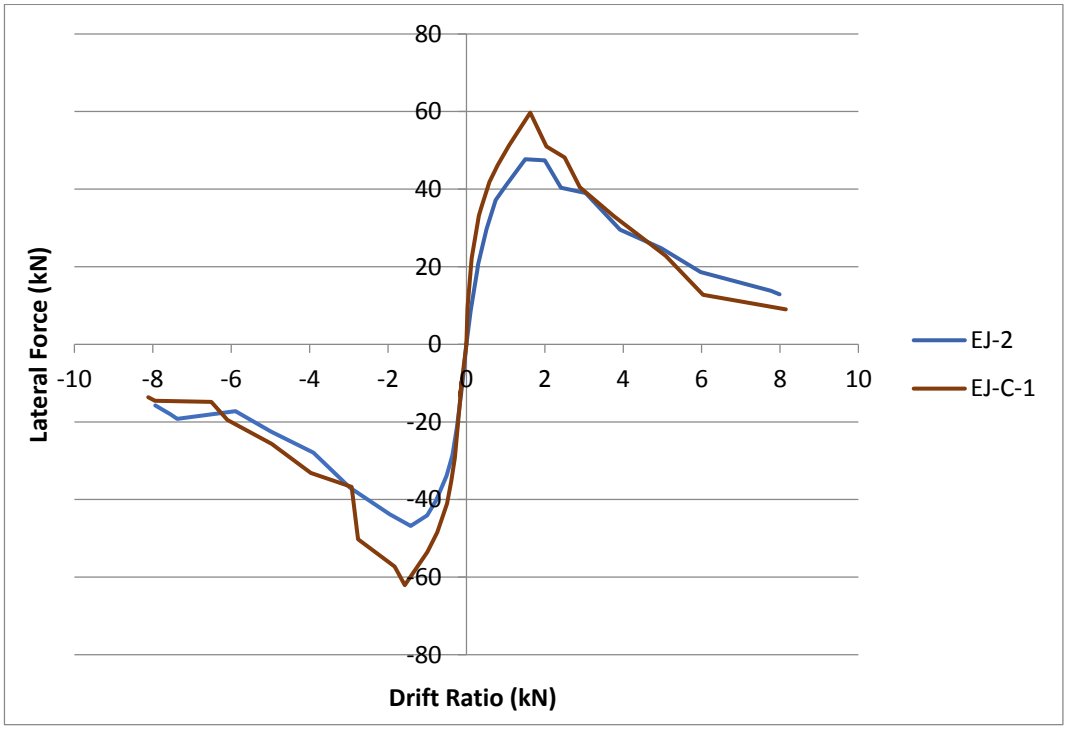

Figure 5.22. Envelope curves of hysteretic loops, test series 3

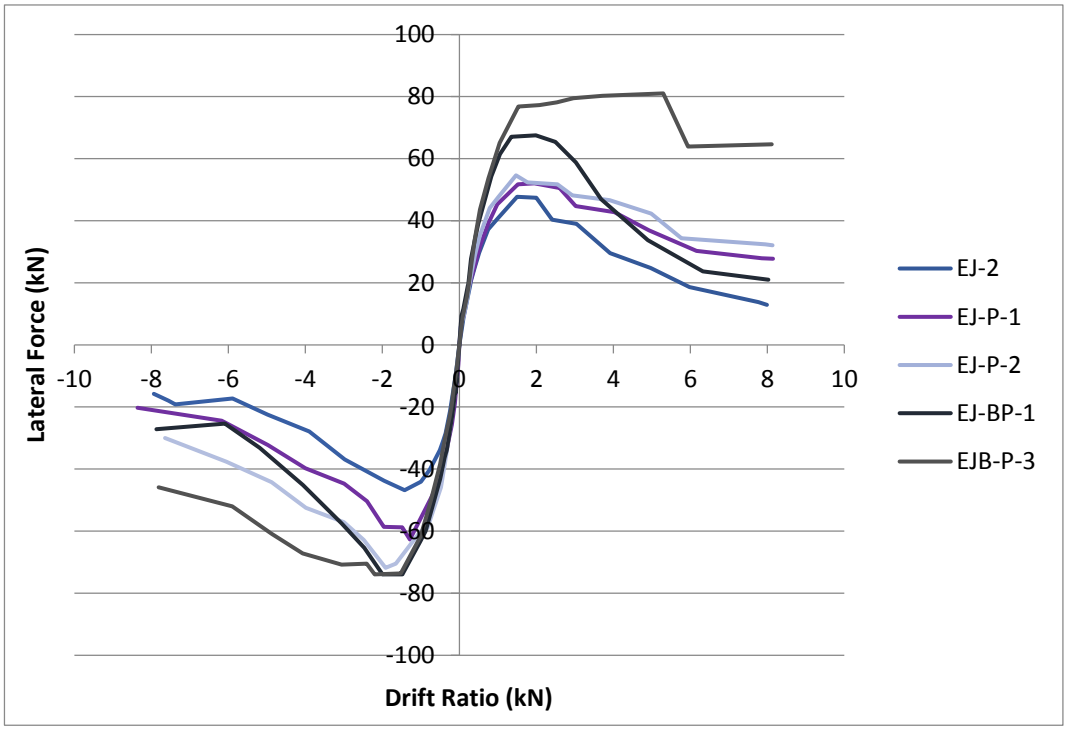

Figure 5.23. Envelope curves of hysteretic loops, test series 4

5.3. Strength

Maximum horizontal load and joint shear force are the important parameters that indicate the effectiveness of the proposed technique applied for the specimens. The strength parameters were discussed in terms of maximum horizontal load applied at the assembly and the joint shear force that computed from experimental results. The improvement in the peak load (strength), which verifies the efficiency of proposed member retrofit technique, can be compared by the backbone curves.

The joint shear force directly depends on the column tip force and the force in beam reinforcement. Therefore, the joint shear force is limited by the beam plastic flexural capacity, which is based on the capacity design philosophy for the beam-column joints. If the joint has sufficient capacity, the maximum joint shear force is expected to be observed when the beam reaches its plastic flexural capacity. The joint shear force is calculated from the experimental results by using Equation 5.1.

$$V_j = T_1 - V_{c1} \quad (5.1)$$

V_j, T_1, V_{c1} denotes the joint shear force obtained from experimental results, the forces in the longitudinal reinforcement of beam obtained from either measured data in strain gauges that located in the beam longitudinal bars or section analysis and the horizontal load applied at the beam-column assembly, respectively. The joint shear forces could not be determined in the repaired specimens (EJ-1-R and EJ-2-R) of both test series 1 and 2. After testing the reference specimens up 8% drift ratio, the strain gauges were not functional anymore due to rupture or separation from the reinforcement surfaces to which they were attached. Therefore, no data could be collected from strain gauges after testing the reference specimens.

Experimental joint shear stress was obtained by dividing the shear force to the joint area as given in Equation 5.2. However, the failure mechanism of joint was due to diagonal cracks. Therefore, principal normal stresses at joint should be calculated by using Mohr Theorem to obtain maximum and minimum stresses which are normal and parallel to the diagonal cracks and represent the compression (σ_c) and tensile (σ_t) joint stresses.

$$\tau_j = \frac{V_j}{A_c} \quad (5.2)$$

5.3.1. Test series 1

The applied maximum horizontal forces are quite similar with the reference (EJ-1) and repaired (EJ-1-R) specimens of test series one. The backbone curve of the repaired specimen is very close to the reference specimen, which verifies the effectiveness of the applied repairing scheme for the damaged specimen (EJ-1) according to main philosophy of repair [55].

5.3.2. Test series 2

Once the results were compared for the second reference specimen (EJ-2), the repaired specimen of the second test series had a 22% and 25% lower value of

strength in positive and negative directions, respectively. As discussed before, the maximum horizontal load capacity of the repaired specimen (EJ-2-R) did not attain the corresponding capacity for the reference specimen due to the fracture of diagonal CFRP sheets.

One can conclude that the repairing technique applied for the damaged EJ-2 sample is not effective enough in terms of the horizontal load capacity of the beam-column assembly. However, it should be noted that depending on the number of diagonal CFRP sheet layers, the fracture of the CFRP sheets is expected to take place in higher drift ratios with the attainment of greater horizontal load capacities.

5.3.3. Test series 3

The average strength enhancement in the specimen of the third test series (EJ-C-1) was 28.92% with respect to reference specimen (EJ-2). However, this improvement was not sufficient enough to be reached the beam flexure capacity. The response of two different rehabilitation techniques -repair after damage and retrofit before damage- was investigated, as mentioned in Section 4.6.1. Therefore, the same amount of CFRPs used in EJ-2-R was applied to EJ-C-1.

A ductile performance with the yielding of the beam reinforcement was not expected in this specimen.

5.3.4. Test series 4

Once the results were investigated in detail in terms of strengths in positive and negative direction, considerable amount of strength improvement with respect to reference specimen was achieved in the specimen EJB-P-3 (64%). It is certain that transverse beam provides additional confinement to the joint which increases its capacity. Therefore, observed ultimate lateral load is the maximum in the EJB-P-3 with respect to the other retrofitted specimens.

Sufficient amount of strength enhancement in EJ-BP-1 and EJ-P-2 was also observed, which are 50% and 34%, respectively. Even though the strength improvement was almost similar in negative direction of EJ-P-2 and EJ-BP-1, significant difference was found in positive direction of EJ-P-2, which decreases the mean value of strength improvement in EJ-P-2. A possible explanation for the

difference in the results may be the confinement provided by the column back plate. It kept the strength in both directions almost the same. Increase in the peak load of EJ-P-1 (21%) is relatively less. It is due to the absence of additional confinement in the joint by post-tension rods.

One can conclude that the retrofit technique for specimens strengthened via post-tension was efficient enough in terms of strength. It, of course, depends on the axial load in the post-tension rods, confinement provided by transverse beam and column back plate.

The joint shear force of EJB-P-3 with respect to reference specimen is the maximum (49%) among the retrofitted specimens. EJ-BP-1, EJ-P-2 and EJ-P-1 followed the EJB-P-3 with a decreasing trend, which were 43%, 27%, 16%, respectively.

5.4. Initial Stiffness

Initial stiffness can be defined as resistance against the load in elastic region. Two different approaches exist in the literature to compute the initial stiffness. The initial stiffness, $K_{ini1,}$ of the specimens in the first approach is the slope of the tangent line in the initial elastic section [57]. The initial stiffness, K_{ini2}, of the specimens in the second approach is defined as the slope of the line that joins the origin of backbone curve and the point where 60% of the ultimate lateral strength on the ascending part of the envelope curve [57]. The calculation of initial stiffness was visually presented in Figure 5.24.

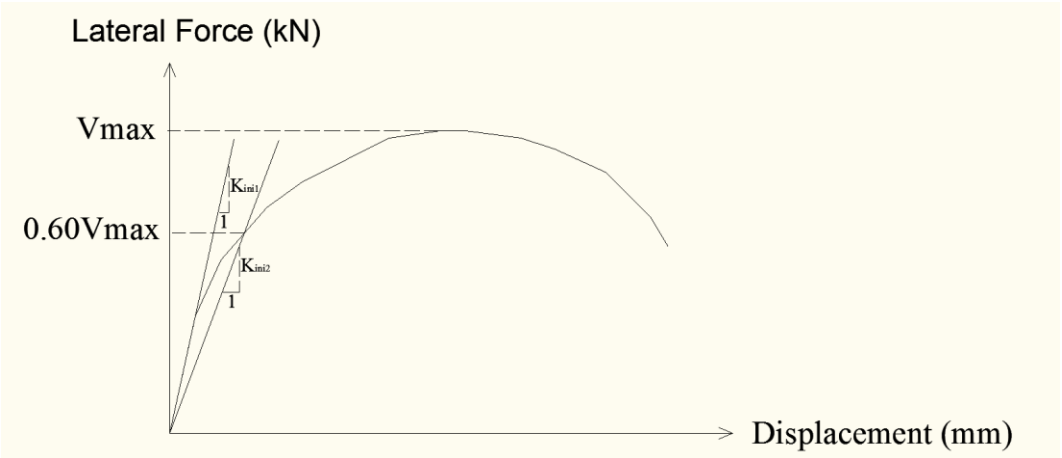

Figure 5.24. Calculation of initial stiffness

The initial stiffness values of specimens were calculated for either positive or negative direction as presented in Table 5.1. The change in the initial stiffness values was also compared.

Table 5.1. Initial stiffness of the specimens

Test No	Direction of loading	K_{ini1} (kN/mm)	Change in the initial stiffness wrt reference specimen (%)	K_{ini2} (kN/mm)	Change in the initial stiffness wrt reference specimen (%)
EJ-1	Positive	2.76	N/A	1.97	N/A
	Negative	2.64		1.77	
EJ-1-R	Positive	3.15	14.13	1.54	-21.83
	Negative	2.28	-13.64	1.35	-23.73
EJ-2	Positive	2.61	N/A	2.08	N/A
	Negative	3.18		2.84	
EJ-2-R	Positive	1.99	-23.75	1.36	-34.62
	Negative	2.02	-36.48	1.54	-45.77
EJ-C-1	Positive	3.46	32.57	3.17	52.40
	Negative	3.20	0.63	3.09	8.80
EJ-P-1	Positive	4.16	59.39	2.62	25.96
	Negative	6.39	100.94	2.83	-0.35
EJ-P-2	Positive	4.68	79.31	2.55	22.60
	Negative	4.99	56.92	3.39	19.37
EJ-BP-1	Positive	5.66	116.86	3.20	53.85
	Negative	5.19	63.21	3.46	21.83
EJB-P-3	Positive	3.39	29.89	3.52	69.23
	Negative	3.55	11.64	3.46	21.83

The initial stiffness values of repaired specimens are lower than its initial value. A possible explanation for this might be the imposed damage in the reference specimens. The initial stiffness provided by either CFRPs or post-tension rods in retrofitted specimens was higher than the reference specimen. It is believed that this enhancement was due to the additional material in the joint.

A remarkable difference in the results of two different methods was found for some specimens. The first approach (K_{ini1}) provides slightly higher results when compared with the second approach (K_{ini2}). It is initiation of moderate or severe cracks up to 60% of the ultimate capacity [57]. This, of course, decreased the initial stiffness of specimens.

5.5. Stiffness Degradation

The peak-to-peak stiffness, K^p, is the slope of the line that joins the ultimate load points in positive and negative direction of hysteresis loop at each loading cycle (Figure 5.25) [57]. The peak-to-peak stiffness at each loading cycle decreased when the applied lateral load devolved into inelastic range along with the increased level of damage. To make better comparison, the peak-to-peak stiffness was normalized with respect to the reference specimen.

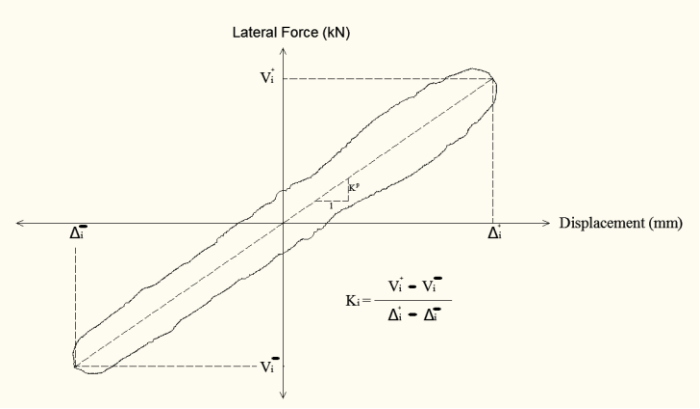

Figure 5.25. Peak-to-peak stiffness

Due to existence of pre-formed cracks in the reference specimens, the sustained stiffness in each loading cycle of the reference specimens was higher than the repaired specimens. However, for drift ratios greater than 3%, the reference specimens could sustain the same level of peak-to-peak stiffness with the repaired

specimens due to reduction in the contribution of CFRPs (Figure 5.26 and Figure 5.27).

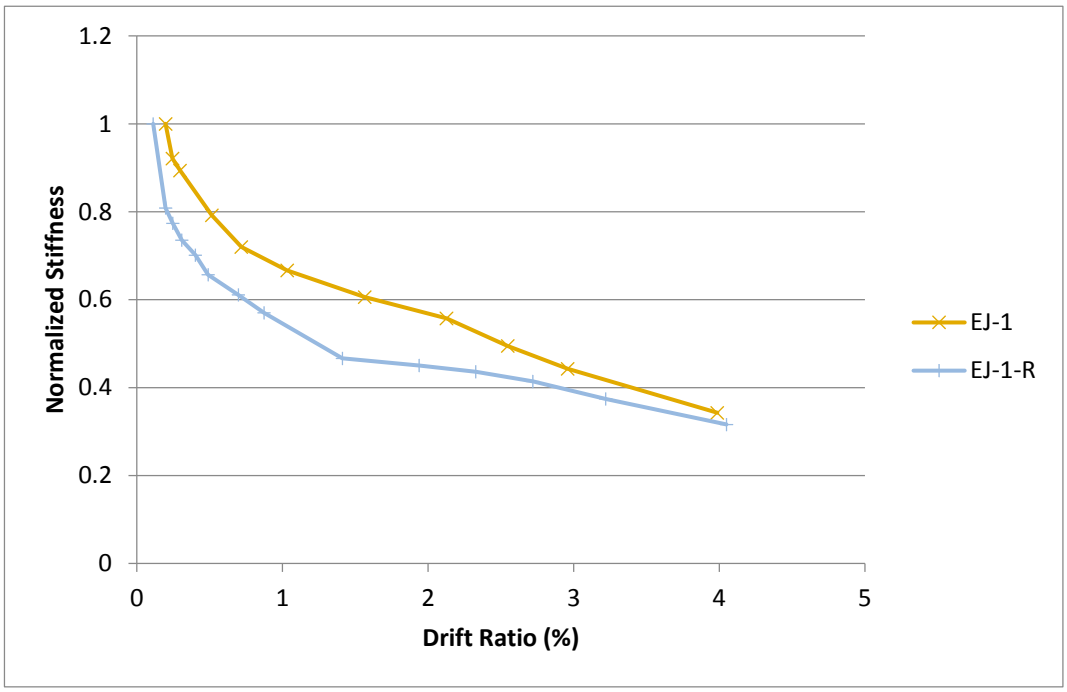

Figure 5.26. Stiffness degradation curves, test series 1

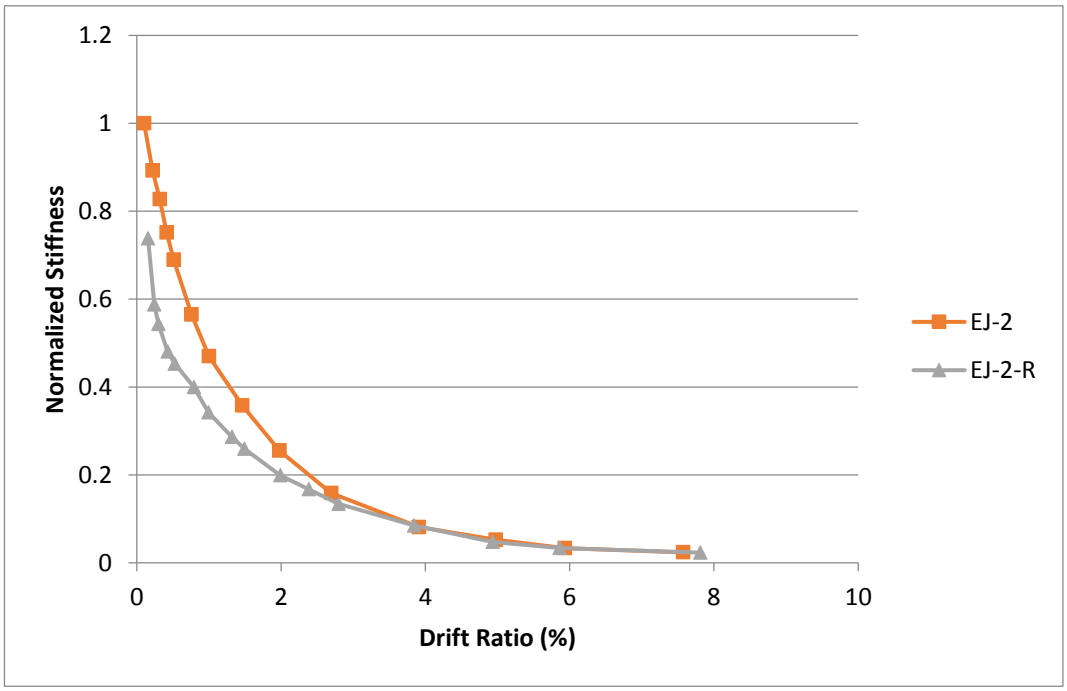

Figure 5.27. Stiffness degradation curves, test series 2

Unlike the first two test series, the existence of CFRPs provides an enhancement in the sustained stiffness up to CFRPs fracture in the test series 3 (Figure 5.28). Over 3 % drift ratios, the joint underwent critical damage level since the contribution of CFRPs decreased due to debonding and fracture of CFRPs. The same values of peak-to-peak stiffness were therefore found over 3% drift levels.

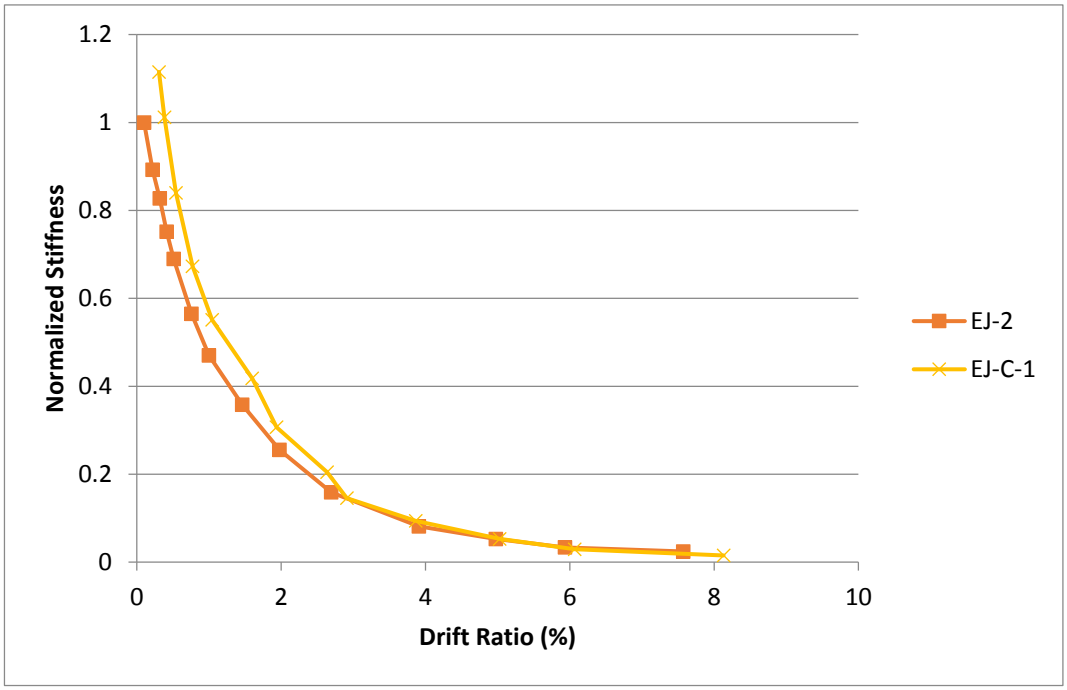

Figure 5.28. Stiffness degradation curves, test series 3

The sustained stiffness at each loading cycle of the retrofitted specimens is higher than the stiffness of the reference specimen due to existence of post-tension bars in the 4th test series. As presented in Figure 5.29, the higher the confinement in the joint through post-tensioning, the lower the rate of decrease in the peak-to-peak stiffness was calculated. Almost 50% drop in the stiffness was observed within 0.5% and 1.5% drift ratios in the specimens EJ-2, EJ-P-1, EJ-P-2 and EJ-BP-1. The recorded value that corresponds to the same amount of decrement in the EJB-P-3 was between 0.5% and 2% drift ratios. After 3% drift ratio, decrease in the stiffness was almost linear. Over the 5% drift levels, the retrofitted specimens could sustain almost the same level of peak-to-peak stiffness with the reference specimen due to reduction in the contribution of post-tension rods. The reason for such behavior is

the relaxation in the post-tension rods due to the significant deformation of the joint in the subsequent drift levels (Figure 5.29).

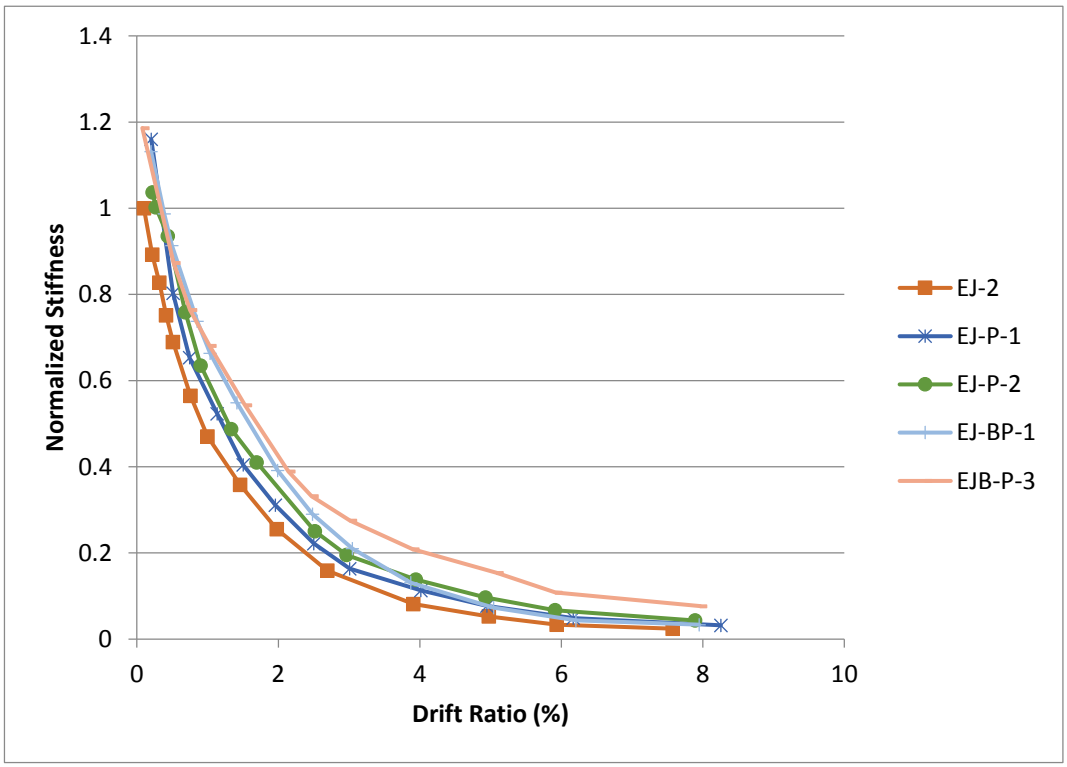

Figure 5.29. Stiffness degradation curves, test series 4

5.6. Ductility

Ductility of the test specimens can be calculated by dividing the ultimate horizontal displacement, $\Delta_{0.80}$, which corresponds to the displacement when maximum lateral load reduces 20% to the yield displacement Δ_y (Figure 5.30) [57].

The equivalent yield displacement of each specimen was determined in terms of global drift ratio as given in Table 5.2.

In order to determine the yield displacement, an equivalent elasto-plastic force-displacement relation was obtained to represent the nonlinear backbone curve such that the area under both curves in other words energy absorption capacities are the same [58]. An iterative process was implemented to achieve the equal area concept.

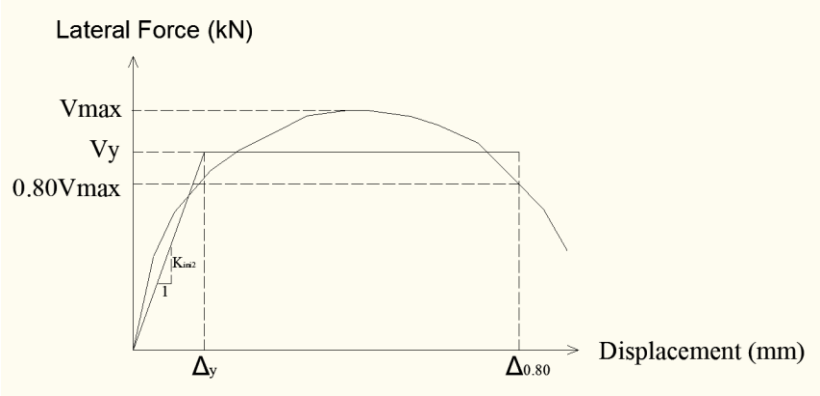

Figure 5.30. Bi-linear curve of the envelope curve

The ultimate displacement capacity of the experiments of the group 1 was not attained with the available test set-up (up to 4% drift ratio). Therefore, no comparison was made in terms of the ductility in the 1st group. Nevertheless, the values were presented in Table 5.2.

A slightly higher value of ductility with respect to reference specimen of the group 2 was found in the specimen of the test series 3 although the failure mode was brittle joint shear failure. This enhancement can be attributed to the both postponing of the crack initiation and lower damage level.

In the test series 4, even though the capacity of the EJB-P-3 reached the beam flexural capacity, the ductility still remained the most challenging part for the rest of the specimens. According to Table 5.2, the ductility of the retrofitted specimens did not improve much. Even though a ductile behavior was observed in the specimen EJB-P-3, its calculated ductility was not that much different from the other retrofitted specimens. This inconsistency might be attributed to the difference in the yield displacements of specimens calculated for the equivalent elasto-plastic force-displacement relation. In addition, it can be difficult to discuss about ductility in the shear critical members. In fact, the identification of the yielding may lead to difficulties in the discussion of the results. Discussion in terms of ultimate displacement capacity ($\Delta_{0.80}$) may be more appropriate, which was presented in Table 5.2 .

Table 5.2. Ductility

Test No	Direction of loading	$0.80V_{max}$ (kN)	$\Delta_{0.80}$ (mm)	$\Delta_{0.80}^{*}$ (%)	V_y (kN)	Δ_y (mm)	Δ_y^{*} (%)	μ
EJ-1	Positive	93.60	116.90	4.07	111.96	56.77	1.98	2.1
	Negative	87.00	111.88	3.95	97.97	49.54	1.75	2.3
EJ-1-R	Positive	93.48	120.14	4.19	112.95	73.40	2.56	1.6
	Negative	93.84	120.14	4.24	108.40	72.26	2.55	1.7
EJ-2	Positive	38.16	87.94	3.12	42.95	20.63	0.72	4.3
	Negative	37.44	81.66	2.88	42.27	14.88	0.53	5.5
EJ-2-R	Positive	29.88	118.35	4.20	34.87	25.52	0.89	4.6
	Negative	28.20	98.68	3.49	32.48	21.04	0.74	5.4
EJ-C-1	Positive	47.76	71.89	2.53	52.28	16.49	0.57	4.4
	Negative	49.68	78.79	2.78	54.58	17.64	0.62	4.5
EJ-P-1	Positive	41.64	119.22	4.20	47.48	22.68	0.79	5.3
	Negative	50.16	68.86	2.43	56.66	16.86	0.60	4.1
EJ-P-2	Positive	43.68	131.78	4.64	48.88	20.45	0.71	6.4
	Negative	57.48	84.26	2.98	63.02	18.30	0.65	4.1
EJ-BP-1	Positive	54.00	93.35	3.29	63.57	23.28	0.81	4.1
	Negative	59.16	83.26	2.94	68.40	23.03	0.81	3.6
EJB-P-3	Positive	64.80	167.14	5.90	77.47	29.07	1.01	5.7
	Negative	59.16	143.67	5.07	68.68	27.28	0.96	5.3

5.7. Energy Dissipation Capacity

The energy dissipation capacity at each loading cycle was computed to be the area enclosed within load-displacement curves. The dissipated cumulative energy in the specimens was obtained by summing the areas calculated for each loading cycle (Figure 5.31) [57].

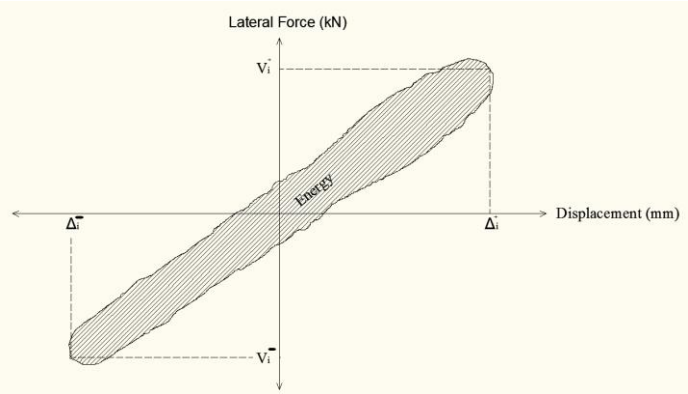

Figure 5.31. Dissipated energy in one cycle

The difference between the energy dissipation of EJ-1 and EJ-1-R is not more than 10% for each cycle (Figure 5.32). Therefore, repairing technique applied for EJ-1 is considered to be effective in terms of energy dissipation. For the second specimen, energy dissipation capacity of the repaired specimen is always less than the reference specimen. As mentioned before, fracture of diagonal CFRP sheets result in less lateral force capacity and hence less energy dissipation capacity. If the fracture of CFRPs had been prevented by employing more layers of CFRPs, energy dissipation capacity of the repaired specimen expected to be higher than the reference specimen. At preceding drift ratios (before the fracture of the CFRPs), the energy dissipation capacity of EJ-2 is larger than the repaired counterpart (EJ-2-R) (Figure 5.33). This can be explained by the imposed structural damage in the repaired assembly occurred during the tests of the reference assembly.

Dissipated energy in the retrofitted specimens was more than the reference specimen. Therefore, proposed retrofit technique is considered to be effective in terms of energy dissipation. Energy dissipation capacity of tested specimens is very similar up to 1.5% drift ratio even though the specimens were in post-yield region. However, energy dissipation in the retrofitted specimens undergo a sudden

increment after 2.5% drift ratio which corresponds to the drift level when concrete crushing at the joint was potentially critical in the benchmark specimen (Figure 5.34 and Figure 5.35).

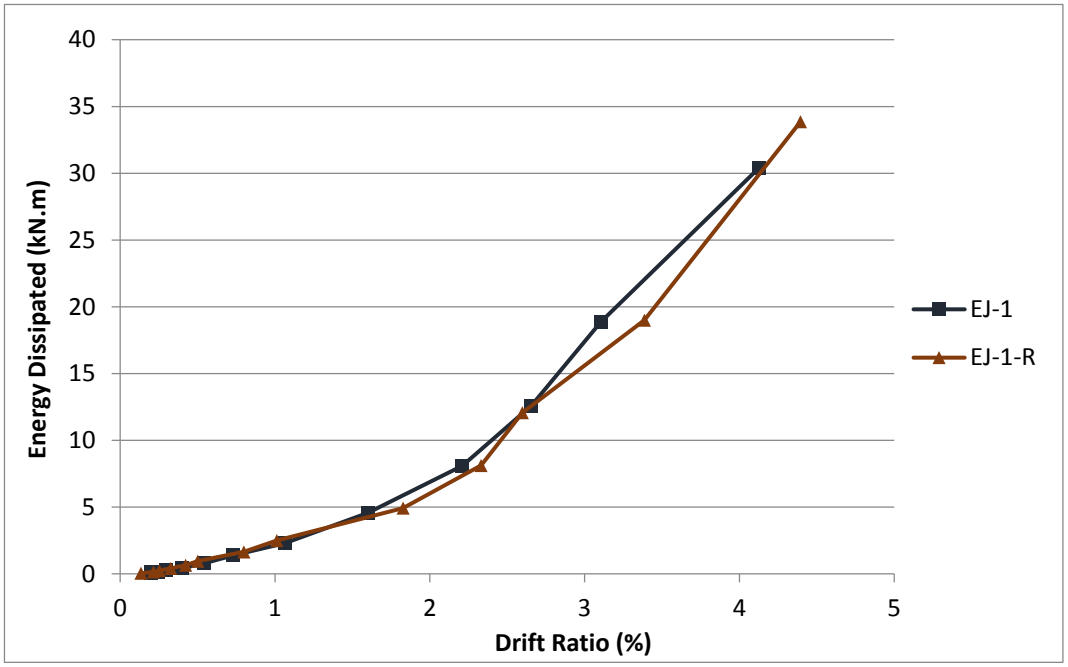

Figure 5.32. Cumulative dissipated energy curves, test series 1

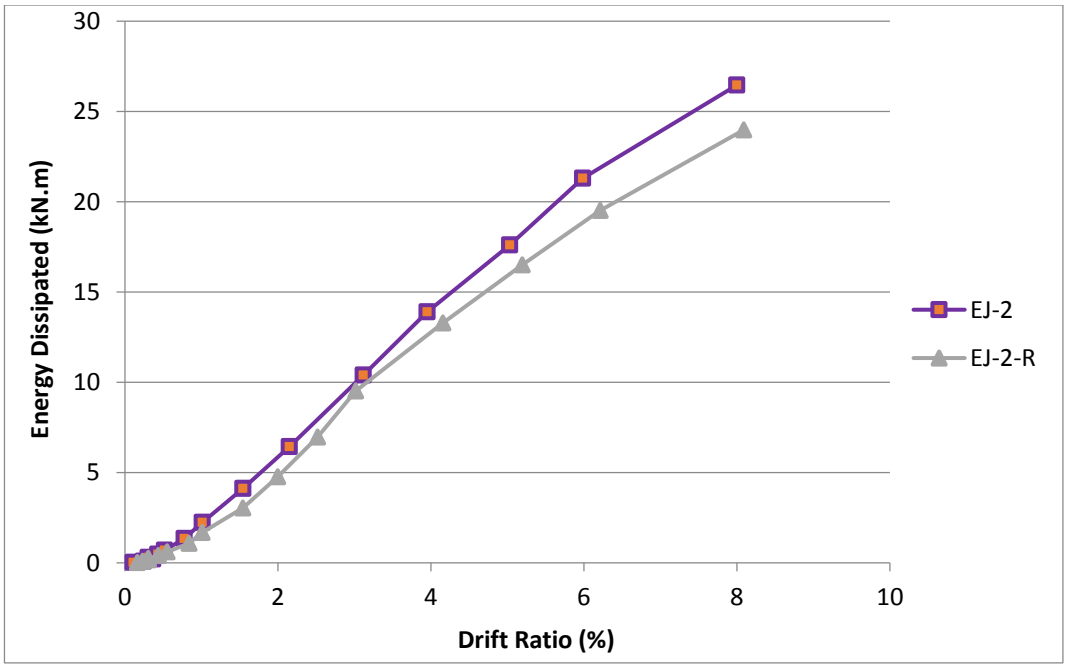

Figure 5.33. Cumulative dissipated energy curves, test series 2

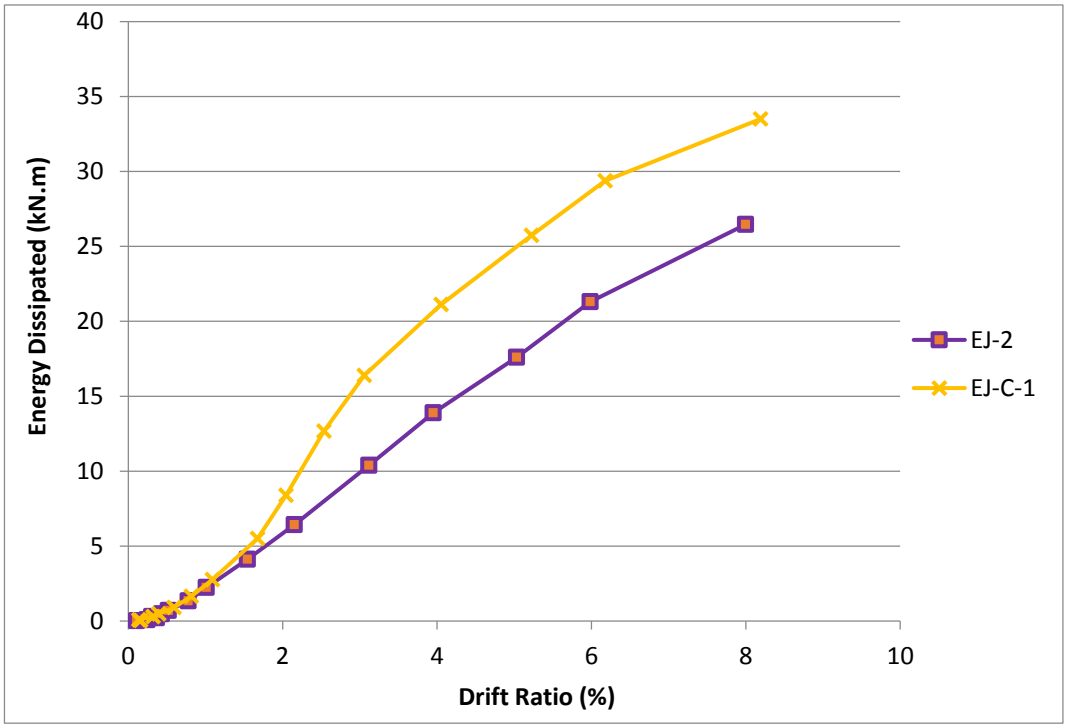

Figure 5.34. Cumulative dissipated energy curves, test series 3

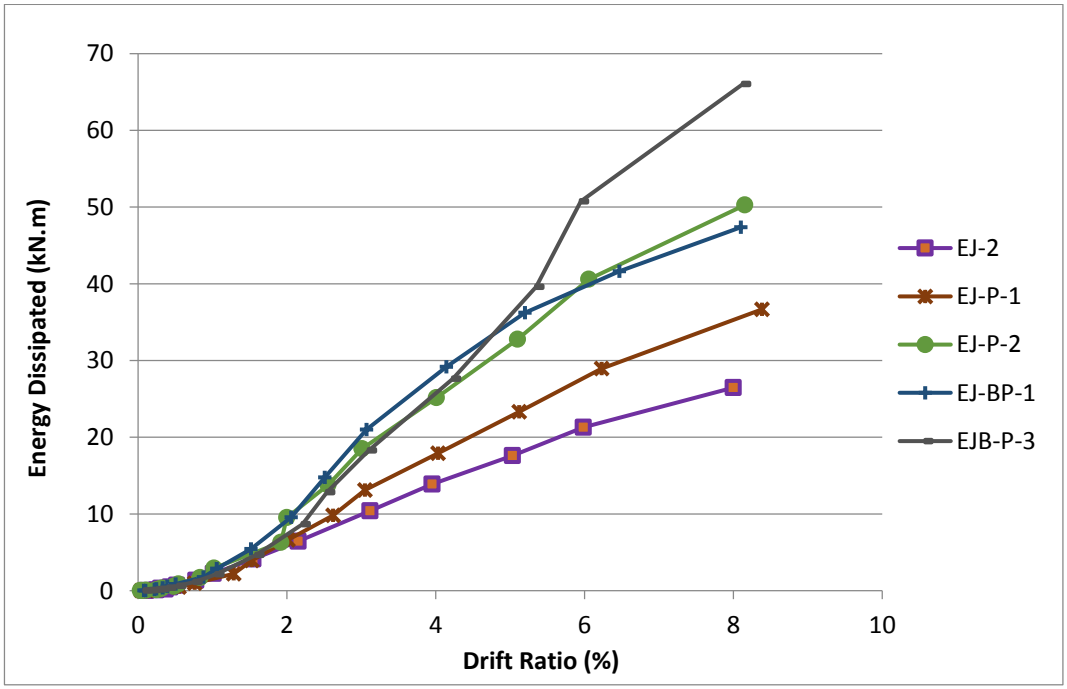

Figure 5.35. Cumulative dissipated energy curves, test series 4

5.8. Joint Shear Strain

Joint shear strain is computed by using cosine theorem with the Equation 5.3 in radian. The displacement measurements obtained from horizontal, vertical and diagonal LVDTs in the beam-column joint were substituted in cosine theorem [59].

$$\gamma = -\frac{\pi}{2} + \arccos\left(\frac{L_v^2 + L_h^2 - L_d^2}{2L_v L_h}\right) \qquad 5.3$$

Where L_v, L_h, L_d are obtained by summing the original length and measured displacement of vertical, horizontal and diagonal LVDTs respectively.

In the first test series, the joint shear strains of EJ-1-R are larger than its reference sample (EJ-1), as shown in Figure 5.36. In the repaired specimen (EJ-1-R) the beam and column capacities are improved with the CRFPs while there was no retrofit attempt in the joint. In EJ-1, damage was concentrated in the beam. After repairing, damage was transferred to the beam-column joint, which results in an increase in the joint shear strains.

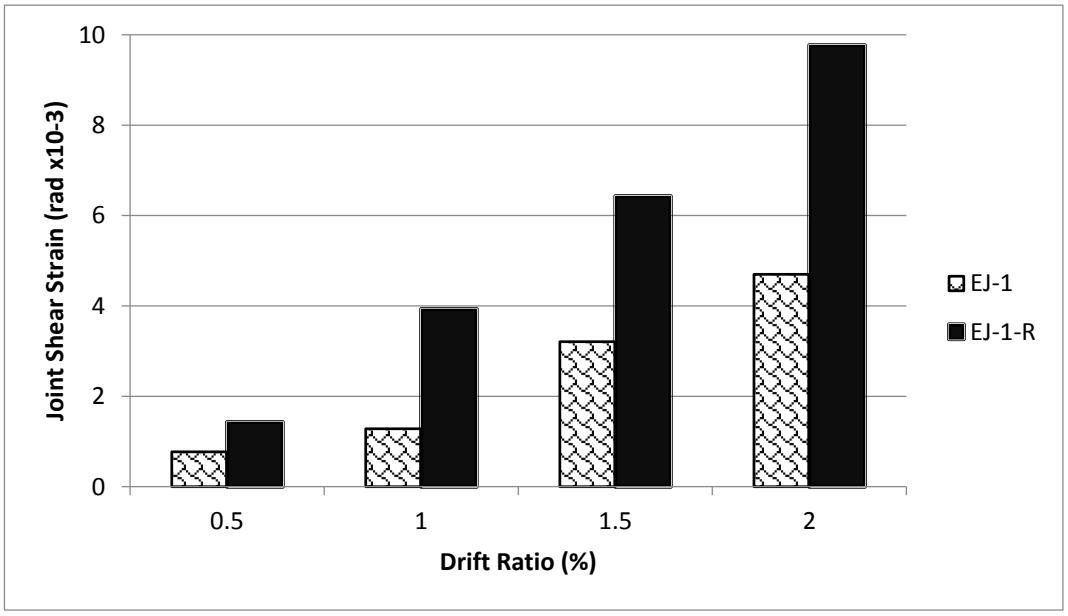

Figure 5.36. Joint shear strain vs. drift ratio, test series 1

Repairing by CFRPs at the deficient beam-column joint led to obtain less joint shear strain in EJ-2-R with respect to its reference sample, EJ-2 (Figure 5.37). This

proves the effectiveness of diagonal CFRPs as a repairing technique for the damaged beam-column joints up to the fracture of CFRP sheets, which correspond to 2% drift ratio in this study.

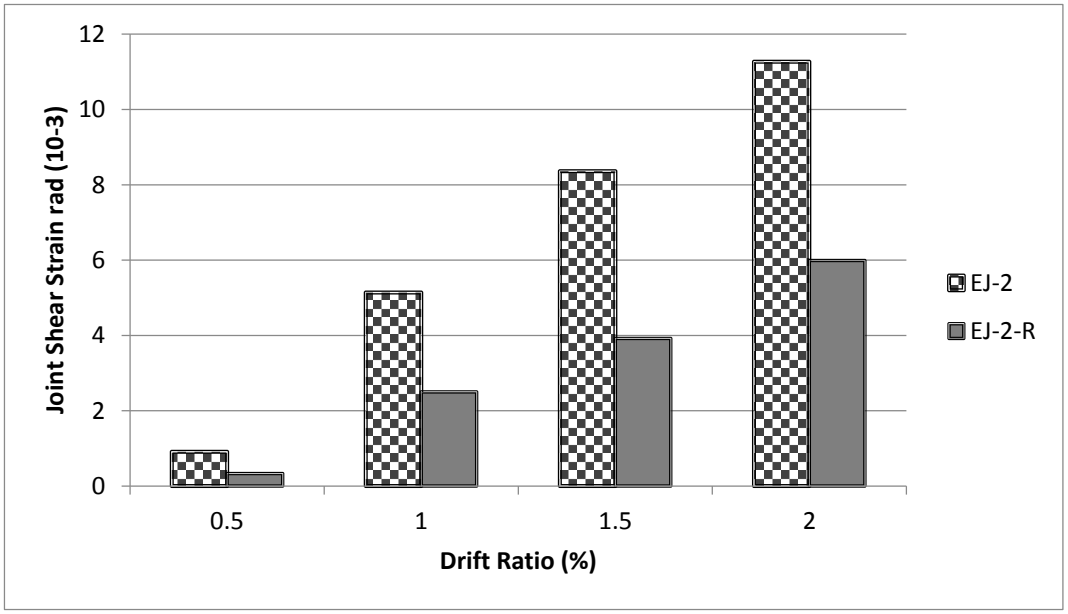

Figure 5.37. Joint shear strain vs. drift ratio, test series 2

Similar to the test series 2, existence of CFRPs in the joint decreased the joint shear strain in the test series 3, which once again proved the knowledge acquired in the test series 2 (Figure 5.38).

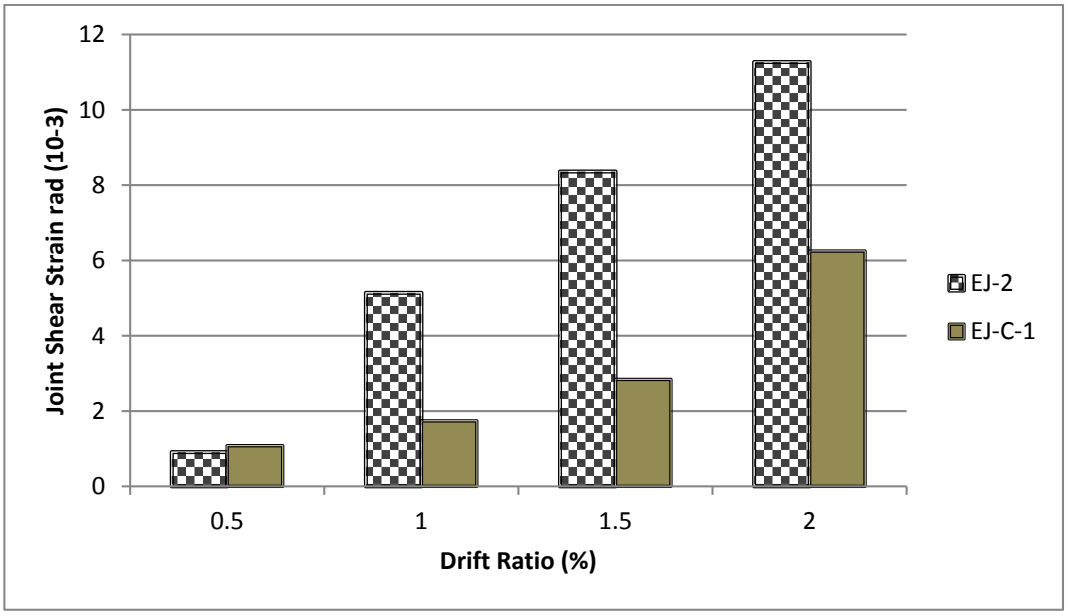

Figure 5.38. Joint shear strain vs. drift ratio, test series 3

It should be noted that the joint shear strain values were not calculated for the specimens of test series 4 since the diagonal displacement transducers were not mounted due to overlapping of rods and LVDTs. It is apparent from the joint damage photographs that a relatively rigid joint panel response was investigated when the joint was retrofitted by the post-tension bars. Application of post-tension bars limited the crack propagation in the joint and decreased the damage level in the joint panel.

5.9. Effect of the Column Back Plate: EJ-P-2 and EJ-BP-1

One major drawback of the retrofit of EJ-P-2 was that no significant strength enhancement in the strength of positive direction was achieved while a satisfactory strength improvement was observed in the negative direction. Investigating the reasons of the significant strength difference in both loading directions has been a continuing concern. However, this inconsistency in the strength can be attributed to additional confinement through column back plate. As the column back plate distributed the load provided by the post-tension rods uniformly, more confined joint area was achieved in the EJ-BP-1. It can be inferred that more confined joint kept the lateral load bearing capacities of both loading directions at nearly the same value by preventing the end anchorage failure and spalling of concrete cover.

Concrete cover was spalled at the column back in the EJ-P-2, as discussed before. Relaxation was occurred in the anchor bolts of the steel angles, which was mounted backside and under the upper story column. As a consequence of this undesirable situation, axial stress in the post-tension rods that substituted the tensile force during the positive displacement first relaxed, and then became almost zero. For this reason, EJ-P-2 behaved like the specimen without post-tension (EJ-P-1) in positive direction.

5.10. Effect of the Transverse Beam: EJ-BP-1 and EJB-P-3

EJ-BP-1 responded in a similar way with EJB-P-3 in terms of strength. On the other hand, there was no sufficient enhancement in the ductility of EJ-BP-1. It was known from the previous studies that confinement provided by transverse beam improves the joint shear strength at least 1.2 times [60]. The ductility enhancement can therefore attributable to the presence of transverse beam since the joint strength was increased. The results reported here appear to support the assumption that strength enhancement was provided by not only transverse beam but also torsional stiffness of transverse beam since there were torsional cracks in the transverse beam. During the experiment, torsional cracks in the transverse beam were observed. Then, the reasons of such cracks were investigated in depth. As the movement of the post tension rods was restricted by the transverse beam, the post tension rods could not move freely in the specimen constructed with transverse beam. During the deformation of the beam-column assembly, the post-tension rods for the other specimens (EJ-P-1, EJ-P-2 and EJ-BP-1) can move freely in the subsequent drift levels. This also causes the relaxation in the rods. However, as the movement of the post-tension rods was restricted by the transverse beam in EJB-P-3 specimen, the post-tension rods could not move freely. The unbalanced force in the rods was transmitted to the transverse beam. The force creates additional internal stresses in the transverse beam, which causes the cracks. Due to the restriction in the relaxation of the axial force in the rods, a relatively less decrement in the axial load (especially in positive direction) was observed. It therefore increases the joint shear capacity

Table 5.3 summarizes the experimental results and their outcomes.

Table 5.3. Summary of experiment results

Test No	DOL	V_{max} (kN)	Yield Properties V_y (kN)	μ	Energy (kN.m)	Joint Panel Results τ_j	σ_t (MPa)	σ_c	Failure Type
EJ-1	+	117.0	111.9	2.1	30.4	5.19	4.32	6.24	Beam
	-	108.7	97.7	2.3		5.02	4.16	6.08	
EJ-1-R	+	116.8	112.9	1.6	33.9		N/A		CFRP fracture
	-	117.3	108.4	1.7					
EJ-2	+	47.0	42.9	4.3	26.5	2.37	1.94	2.90	Joint shear
	-	46.8	42.2	5.5		2.31	1.88	2.84	
EJ-2-R	+	37.3	34.8	4.6	23.9		N/A		CFRP fracture
	-	35.2	32.4	5.4					
EJ-C-1	+	59.7	52.2	4.4	33.5	2.87	2.34	3.39	CFRP fracture
	-	62.1	54.5	4.5		2.99	2.56	3.52	
EJ-P-1	+	52.0	47.4	5.3	36.7	2.62	2.18	3.14	Joint shear
	-	62.7	56.6	4.1		2.83	2.39	3.35	
EJ-P-2	+	54.6	48.8	6.4	50.3	2.55	2.11	3.07	Joint shear
	-	71.8	63.0	4.1		3.39	2.95	3.91	
EJ-BP-1	+	67.5	63.5	4.1	47.4	3.20	2.76	3.72	Beam-joint
	-	73.9	68.4	3.6		3.46	3.02	3.98	
EJB-P-3	+	81.0	77.4	5.7	66.1	3.52	3.07	4.03	Beam
	-	73.9	68.6	5.3		3.46	3.01	3.97	

DOL: Direction of loading

CHAPTER 6

6. ANALYTICAL STUDY

This chapter briefly presents an analytical model on the response of the beam-column joints. The implemented model is used to predict the joint strength in the reference and retrofitted specimens. The analytical model provides to calculate the joint shear capacity handily.

6.1. Reference Specimens of Test Series 1 and 2

Theoretical shear capacity of joint is computed by an algorithm based on truss analogy. The formation of tension strut in the joint induces the cracks when the principal tensile stress, which can be calculated by using Mohr Theorem, exceeds the concrete tensile strength. It was known from the Mohr Theorem, the maximum and minimum normal stresses are the highest and lowest points of circle which has a radius, R, on the horizontal axis. The magnitude of principal stresses, which is given by Mohr Theorem, is obtained by Equation 6.1.

$$\sigma_{1,2} = \frac{(\sigma_x - \sigma_y)}{2} \pm \sqrt{(\frac{\sigma_x - \sigma_y}{2})^2 + {\tau_{xy}}^2} \quad 6.1$$

While calculating the tensile strength of concrete which is also a limit value of joint failure, $0.5\sqrt{f_c}$ proposed by İlki et al [54] was used. By rearranging the Equation 6.1, the estimated horizontal joint shear stress can be calculated by Equation 6.2. Then, estimated joint shear force is the multiplication of Equation 6.2 by the cross sectional area of joint as shown in Equation 6.3 [54].

$$\tau_{xy} = 0.5\sqrt{f_c}\sqrt{1 + [\frac{\sigma_y}{0.5\sqrt{f_c}}]} \quad 6.2$$

$$V_{jh} = \tau_{xy} A_c \quad 6.3$$

The estimated effect of transverse reinforcement to the joint shear force can be obtained according to TSI-500 [61] from Equation 6.4 for the specimen with transverse reinforcement in the joint, EJ-1.

$$V_t = A_{st} f_y \frac{d}{s} \tag{6.4}$$

The total theoretical shear capacity of the first reference specimen (EJ-1) is the sum of Equation 6.3 and Equation 6.4. In the reference specimen of test series 2, EJ-2, joint capacity was equal to the value obtained by Equation 6.3 only due to the absence of transverse reinforcement.

6.2. Test Series 3

Truss analogy proposed by Pauley and Priestley [56] was used for the specimen retrofitted by CFRPs to predict the contribution of CFRPs to the total joint shear capacity. Axial load bearing capacity of the CFRP, which resist along the fibers' direction, can be computed by Equation 6.5. Then, the shear force compensated by the CFRP is the horizontal component of F_{CFRP}, since the CFRP was wrapped in the form of X pattern (Equation 6.6) [54].

$$F_{FCRP} = E_{CFRP} \times \varepsilon_{CFRP} \times A_{CFRP} \tag{6.5}$$

$$V_{CFRP} = F_{CFRP} \times \sin(45°) \tag{6.6}$$

The total joint shear capacity is assumed to be the sum of Equation 6.3 and Equation 6.6.

6.3. Test Series 4

The contribution of axial force in the post-tension rods can be estimated by Equation 6.7 for the retrofitted specimens. As the post-tension rods were placed diagonally, the contribution of post-tension rod to the total shear capacity is horizontal component of the axial force in the one post-tension rod.

It should be noted that there were two post-tension rods in the both side of the joint in same direction. Therefore, it is the twice of the calculated value as shown in Equation 6.7.

$$V_{PT} = 2 \times P \times \sin(45°) \quad 6.7$$

The total theoretical joint shear capacity of the retrofitted specimens of the test series 4 can be calculated as a sum of 6.3 and Eq. 6.7.

6.4. Comparison of Experimental and Predicted Joint Shear Stress

The joint shear stress obtained by experiments was compared with the predicted joint shear stress that was determined theoretically as well as the code specified values in Table 6.1. The results were normalized with respect to square root of concrete strength for comparison purposes. It should be emphasized that the concrete strength was slightly different for each specimen.

Since EJ-2 was designed with several structural deficiencies, experimentally obtained joint stress should be compared with non-current code, which considers only the concrete tensile strength in the joint. Therefore, ACI 352-1976 [62] was used for the reference specimen. On the other hand, the results of the specimen complying with current code requirement (EJ-1) as well as the retrofitted specimens are compared with the current codes such as TEC 2007 [4] and ACI 352-2002 [3], where the experimental results and code predictions are in good agreement.

Retrofitted specimens are expected to perform in accordance with the current code requirements. Comparing the results with current code requirements is therefore the only way to determine whether joint response is sufficient or not.

The results presented in Table 6.1 indicate that the shear strength requirements specified by the current codes are in parallel with the test results and the theoretical results of the retrofitted specimens. This clearly shows the efficiency of the proposed retrofitting method in terms of strength.

Table 6.1. Comparison of experimental and predicted joint shear stress

Specimen	Shear Stress				TEC 2007 (MPa)
	Experimental, $\tau_j/\sqrt{f_c}$	Predicted, $\tau_{xy}/\sqrt{f_c}$	τ_j/τ_{xy}	ACI (MPa)	
EJ-1	$1.24\sqrt{f_c}$	$1.14\sqrt{f_c}$	1.09	[b] $0.99\sqrt{f_c}$	$1.97\sqrt{f_c}$
EJ-2	$0.81\sqrt{f_c}$	$0.65\sqrt{f_c}$	1.25	[a] $0.34\sqrt{f_c}$	N/A
EJ-C-1	$0.94\sqrt{f_c}$	$0.79\sqrt{f_c}$	1.19	[b] $0.99\sqrt{f_c}$	$1.38\sqrt{f_c}$
EJ-P-1	$0.87\sqrt{f_c}$	$0.82\sqrt{f_c}$	1.06	[b] $0.99\sqrt{f_c}$	$1.36\sqrt{f_c}$
EJ-P-2	$0.83\sqrt{f_c}$	$1.01\sqrt{f_c}$	0.82	[b] $0.99\sqrt{f_c}$	$1.38\sqrt{f_c}$
EJ-BP-1	$1.02\sqrt{f_c}$	$0.99\sqrt{f_c}$	1.03	[b] $0.99\sqrt{f_c}$	$1.42\sqrt{f_c}$
EJB-P-3	$1.07\sqrt{f_c}$	$0.98\sqrt{f_c}$	1.09	[b] $0.99\sqrt{f_c}$	$1.45\sqrt{f_c}$

[a]ACI 352-1976, [b]ACI 352-2002

CHAPTER 7

7. SUMMARY AND CONCLUSION

7.1. Summary

This study sets out to determine the response of seven 1:1 scale beam-column joint specimens under the combined effect of axial load and quasi-static cyclic loading. The investigation can be grouped into three different actions. These are (i) response of either well-designed or substandard joint (ii) repair of damaged joints through CFRPs (iii) retrofit of substandard joints by means of either CFRPs or externally applied post-tensioned rod.

The specimens were classified into two groups according to their mechanical properties. The specimen of the first group complied with the current earthquake code principles, whereas the specimen of the second group contained several deficiencies resulting from the lack of transverse reinforcement in the joint and poor material properties including low strength concrete and presence of plain round bars.

The first section involves the response of well-designed and substandard joints with two specimens.

In the second section, the damaged specimens were structurally repaired by wrapping the damaged components by CFRP sheets with different configurations depending on the damage type. After repeating the same tests for the repaired specimens, the effectiveness of the repairing techniques applied for the damaged specimens were investigated.

The third action is to investigate response of the retrofitted specimens, which have certain deficiencies in the joint. These deficiencies can result in brittle type of shear failure, which adversely affect the overall seismic behavior of the RC structures. For this reason, non-seismically designed specimens were retrofitted by either CFRPs or externally applied post-tension rods. Nevertheless, proposed retrofit strategy enhanced the lateral strength of the test specimens considerably.

7.2. Conclusion

Based on the results obtained in this study, the following conclusions can be drawn for the test series 1 and 2.

The earthquake code compliant specimen (EJ-1) displayed a ductile response with the damage concentration in the beam while the rest of the components were mostly undamaged. The experimental results indicated that the applied repairing scheme for the damaged component of the first specimen is quite effective in terms of strength, stiffness and energy absorption capacity to attain the corresponding capacities of the reference specimen. The flexural and shear capacities of the damaged beam were recovered by wrapping the member with longitudinal CFRP sheets at the top and bottom surfaces by anchoring them with transverse CFRP sheets as to improve the shear capacity of the damaged member.

The reference deficient beam-column assembly (EJ-2) displayed a brittle type of failure due to the severe damage in the joint, while the rest of the components were slightly damaged. Ultimate load capacity of the reference specimen could not be attained by the applied repairing due to the fracture of diagonal CFRPs resulting from the eccentricity in the section of CFRP sheet. Since the whole area of CFRP sheet did not work as it was designed, the tearing of the CFRP sheet caused the fracture starting from the CFRP sheet side with greater axial stress. For a further improvement in the behavior, the amount of CFRP sheets wrapped in joint should be increased. Although the fractured CFRPs in EJ-2-R did not improve the capacity of the reference specimen, the application of diagonal CFRPs at the beam-column joint has changed the behavior of the beam-column assembly and flexural deformations in the beam amplified and preceded the overall response before the fracture of CFRPs. This indicates that, if the fracture of CFRP sheets was prevented, a more ductile behavior can be achieved.

The initial stiffness of the reference specimens is higher than the ones for repaired specimens due to pre-formed cracks occurred after testing the reference specimens. The degraded stiffness sustained at each loading cycle was also higher in the reference specimens. The dissipated energy in the first repaired specimen was almost the same with the first reference specimen for the investigated drift ratios which show the efficiency of repairing. However, in the second specimen, due to

the fracture of diagonal CFRP sheets at the joint, the energy dissipated in the repaired specimen is less than the reference specimen. Therefore, more layers of diagonal CFRP sheets should be applied in order to prevent the fracture of CFRPs due to eccentric stress distribution.

The shear strains measured from the experiment decreased in the second repaired specimen before the fracture of CFRPs compared to the second reference specimen. Therefore, the deformation in the beam-column joint region has diminished with the employed repairing technique. However, the situation is just the opposite for the first specimen. With the application of CFRP sheets at the beam and column only, the deformations in the joint increased compared to the first reference specimen. This indirectly indicates the effectiveness of the repairing technique for EJ-1 by improving the damaged beam and hence observed deformations in the beam was less. Improvement in the beam deformations lead to increase in the deformations of unrepaired components, which is the beam-column joint in this case.

The test results of the reference test series revealed the importance of transverse reinforcement in the beam-column joint once again. Due to the lack of joint transverse reinforcement, deficient beam-column joint can be exposed to brittle type of shear failure, which adversely affects the overall seismic behavior of the RC structures.

In the test series 3, the same amount of CFRPs used in EJ-2-R were applied to EJ-C-1. Therefore, the strength enhancement was not sufficient enough to reach the beam flexure capacity. Then, a ductile performance with the yielding of the beam reinforcement was not monitored in this specimen.

In the last test series, while a ductile response was observed in the specimen with transverse beam (EJB-P-3), beam flexural capacity is almost attained for the specimen with column back plate (EJ-BP-1). However, it could keep its strength up to 3% drift ratio and then a sharp decrement was observed when the concrete crushing was occurred in the joint.

Whilst the rest of the retrofitted specimens (EJ-P-1, EJ-P-2) did not have sufficient enhancement in ductility, retrofit technique did partially substantiate the efficiency in the strength. When the joint is only retrofitted by rods (without post-

tension) in the specimen EJ-P-1, the overall performance was still dominated by joint panel. In contrast to EJ-P-1, beam-joint failure in negative direction and joint failure in positive direction were appeared in EJ-P-2. This indicates that, if the relaxation of post-tension system was prevented, behavior that is more ductile can be achieved in both loading direction of EJ-P-2.

Due to additional material in the joint region, the initial stiffness of retrofitted specimens is higher than the reference specimen. Although the degraded stiffness, which was sustained at each loading cycle, was almost similar up to elastic region, it differs explicitly in the post-elastic region of the retrofitted specimens as loading scheme progressed. A dramatic difference was found in the rate of increment of dissipated energy between retrofitted and reference specimens, which shows the efficiency of retrofit scheme.

The measured joint strain in horizontal direction decreased in the retrofitted specimens. Therefore, the deformation in the beam-column joint region has diminished with the employed retrofit technique. Decline in the joint strains thus led to increase in the beam deformation.

The applicability of the proposed retrofitting scheme with post-tension bars was tested successfully by a test specimen with a transverse beam (EJB-P-3). The transverse beam was drilled diagonally without damaging any longitudinal reinforcement bars. In actual applications, there will be slab over the beams. Although it is not tested in the laboratory, the drilling of slab can be also done easily, as is the case for the transverse beam.

7.3. Future Research

This study shows the efficiency of the application of the external post-tension. Therefore, it can be implemented to the non-seismically designed joints for retrofit purposes. Based on the information gathered in this research, additional research is recommended as follows.

The finite element model (FEM) of the specimens should be generated to better understand the effect of joint flexibility. The dynamic response can also be investigated via FEM analysis, which could help us to understand the role of damage in the joint to the overall response. In addition, a rigorous analytical model can be developed for the retrofitted specimens by mean of FEM analysis.

The effect of different level of axial force in the joint should also be investigated in depth. Due to limited time and number of test specimens, it could not be conducted in this study.

A further development can be conducted in the steel angles holding the post-tension rods to increase the possibility of viability. In addition, the proposed method could be implemented to the interior beam-column joints.

The efficacy of proposed retrofit method should be investigated in full-scale complete frame. The response can therefore be confirmed.

REFERENCES

[1] Yılmaz, N. and Avşar, Ö. "Structural damages of the May 19, 2011 Kütahya-Simav earthquake in Turkey". *Nat. Hazards*, **69**, 981-1001, 2013.

[2] Pampanin, S., Christopoulos, C. and Chen, T.H. "Development and validation of a metallic haunch seismic retrofit solution for existing under-designed RC frame buildings". *Earthq. Eng. Struct. D.*, **35**, 1739-1766, 2006.

[3] ACI Committee 352R-02. Recommendations for design of beam-column connections in monolithic reinforced concrete structures (ACI 352R-02), Detroit, USA: American Concrete Institute, 2002.

[4] Turkish Earthquake Code. Specification for structures to be built in disaster areas (TEC2007), Turkey: Ministry of Public Works and Settlement Government of Republic of Turkey, 2007.

[5] Maheri, M.R. "Recent advances in seismic retrofit of RC frames". *Asian J. Civil Eng.*, **6**, 373-391, 2005.

[6] Thermou, G.E. and Elnashai, A.S. "Seismic Retrofit Schemes for RC Structures and Local–Global Consequences". *Earth. Eng. Struct. Dyn.*, **8**, 1-15, 2006.

[7] Ilki, A. *FRP Strengthening of RC Columns, in retrofitting of concrete structures by externally bonded FRPs with special emphasis on seismic applications*. FIB Bulletin 35, Sprint-Digital-Druck, Stuttgart, 2006.

[8] Engindeniz, M. *Repair and strengthening of pre-1970 reinforced concrete corner beam-column joints using CFRP composites*. PhD Thesis, Georgia Institute of Technology, Georgia, USA, 2008.

[9] Girgin C.S., Mısır S.İ., Özçelik Ö., Kahraman S. and Baran T. "Kolon Kiriş Birleşim Bölgelerinin Güçlendirilmesine Yönelik Çalışmalar". *IMO İzmir Şubesi Bulteni*, **154**, 28-31, 2010.

[10] Park R. and Paulay, T. "Reinforced Concrete Structures". *John Wiley & Sons, First Edition*, 769, 1975.

[11] Doğangün, A. “Performance of reinforced concrete buildings during the May 1, 2003 Bingöl earthquake in Turkey”. *Eng. Struct.*, **26**, 841–856, 2004.

[12] Sezen, H., Whittaker, A.S., Elwood, K.J. and Mosalam, K.M. “Performance of reinforced concrete buildings during the August 17, 1999 Kocaeli, Turkey earthquake, and seismic design and construction practice in Turkey”. *Eng. Struct.*, **25**, 103-114, 2003.

[13] Said, A.M. and Nehdi, M.L. "Use of FRP for RC frames in seismic zones – Part I: Evaluation of FRP beam-column joint rehabilitation techniques". *App. Comp. Mat.*, **11**, 205-226, 2004.

[14] Yurdakul, Ö. and Avşar, Ö. "Structural repairing of damaged reinforced concrete beam-column assemblies with CFRPs". *Struct. Eng. Mech.*, **54**, 521-543, 2015.

[15] Hassan, W.M. *Analytical and experimental assessment of seismic vulnerability of beam-column joints without transverse reinforcement in concrete buildings*. PhD Thesis, University of California, Berkeley, USA, 2011.

[16] Pantelides, C.P., Hansen, J., Nadauld, J.D. and Reaveley, L.D. *Assessment of reinforced concrete building exterior joints with substandard details*. Technical Report PEER 2002-18, Pacific Earthquake Engineering Research Center (PEER), University of California, Berkeley, 2002.

[17] Wong, H.F. *Shear strength and seismic performance of non-seismically designed reinforced concrete beam-column joints*. PhD Thesis, The Hong Kong University of Science and Technology, 2005.

[18] Bedirhanoglu, I., Ilki, A., Pujol, S. and Kumbasar, N. "Behavior of joints built with plain bars and low-strength concrete". *ACI Struct. J.*, **107**, 300-10, 2010.

[19] Park, S. and Mosalam K.M. "Experimental investigation of nonductile RC corner beam-column joints with floor slabs". *J. Comp. Const.*, **139**, 1-14, 2013.

[20] Kotsovou, G. and Mouzakis, H. "Exterior RC beam-column joints: New design approach". *Eng. Struct.,* **41**, 307-319, 2012.

[21] Burak, B. and Wight, J.K. "Experimental investigation of eccentric reinforced concrete beam-column-slab connections under earthquake loading". In: 13th World Conference on Earthquake Engineering, Vancouver, B.C. Canada, 2004.

[22] Unal, M. and Burak, B. "Performance of beam-to-column connection of a well-detailed RC moment frame building under pseudodynamic loading". *J. Struct. Eng.,* **136**, 886-896, 2013.

[23] Karayannis, C.G., Chalioris, C.E. and Sideris, K.K. "Effectiveness of RC beam-column connection repair using epoxy resin injections". *J. Earth. Eng.*, **2**, 217-240, 1998.

[24] Sezen, H. "Repair and strengthening of reinforced concrete beam-column joints with fiber-reinforced polymer composites". *J. Comps. Const.,* **16**, 449-506, 2012.

[25] Engindeniz., M., Kahn., L. F. and Zureick A. "Performance of an RC corner beam-column joint severely damaged under bidirectional loading and rehabilitated with FRP composites". *ACI*, **258**, 19-36, 2008.

[26] Ghobarah, A. and Said, A. "Shear strengthening of beam-column joints". *Eng. Struct.,* **24**, 881-888, 2002.

[27] Tsonos, A. G. "Effectiveness of CFRP-jackets and RC-jackets in post-earthquake and pre-earthquake retrofitting of beam–column subassemblages". *Eng. Struct.*, **30**, 777-793, 2008.

[28] Alcocer, S.M. and Jirsa, J.O. *"Reinforced concrete frame connections rehabilitated by jacketing"*. Report University of Texas at Austin, Texas USA, 1991.

[29] Said, A. and Nehdi, M. "Rehabilitation of RC frame joints using local steel bracing". *Struct. Inf. Struct. Eng.,* DOI:10.1080/15732470600822033, 2008.

[30] Topcu, I. *"Experimental research on seismic retrofitting of R/C corner beam-column-slab joints upgraded with CFRP sheets"*. MSc Thesis, Graduate Program in Civil Engineering, Bogaziçi University, Istanbul, Turkey, 2008.

[31] Coskun, C., Comert, M., Demir, C. and Ilki, A. FRP retrofit of a full-scale 3D RC frame. In: 6th International Conference on FRP Composites in Civil Engineering (CICE 2012), Rome, Italy, 2012.

[32] Del Vecchio, C., Di Ludovico. M., Balsamo. A., Manfredi. G. and Dolce, M. "Experimental investigation of exterior RC beam-column joints retrofitted with FRP systems". *J. Comps. Constr.*, **18**, 04014002, 2014.

[33] Akguzel, U. and Pampanin, S. "Effects of variation of axial load and bidirectional loading on seismic performance of GFRP retrofitted reinforced concrete exterior beam-column joints". *J. Compos. Construct.*, **14**, 94-104, 2010.

[34] Bedirhanoglu, I., Ilki, A. and Kumbasar, N. "Precast fiber reinforced cementitious composites for seismic retrofit of deficient rc joints – A pilot study". *Eng. Struct.*, **52**, 192-206, 2013.

[35] Shafaei, J., Hosseini, A. and Marefat, M.S. "Seismic retrofit of external RC beam–column joints by joint enlargement using prestressed steel angles". *Eng. Struct.*, **81**, 265-268, 2014.

[36] Kam, W.K. and Pampanin, S. Experimental validation of selective weakening approach for the seismic retrofit of exterior beam-column joints. In: New Zealand Society of Earthquake Engineering (NZSEE) Conference Christchurch, New Zealand, 2009.

[37] Parvin, A., Altay, S., Altay, C. and Kaya, O. "CFRP rehabilitation of concrete frame joints with inadequate shear and anchorage details". *J. Comps. Constr.*, **14**, 72-82, 2010.

[38] Chaimahawan, P. and Pimanmas, A. "Seismic retrofit of substandard beam-column joint by planar joint expansion". *Mat. Struct.*, **42**, 443-459, 2009.

[39] Lee, J.Y., Kim, J.Y. and Oh, G.J. "Strength deterioration of reinforced concrete beam column joints subjected to cyclic loading". *Eng. Struct.*, **41**, 2070-2085, 2009.

[40] Biddah, A., Ghobarah, A. and Aziz, T.S. "Upgrading of non-ductile reinforced concrete frame connections". *J. Struct. Eng.*, 123, 1001-1010, 1997.

[41] Hadi, N.S.M. and Tran, T.M. "Retrofitting nonseismically detailed exterior beam–column joints using concrete covers together with CFRP jacket". *Constr. and Build. Mat.*, **63**, 161-173, 2014.

[42] Le-Trung, K., Lee, K., Lee, J., Lee, D.H. and Woo, S. "Experimental study of RC beam–column joints strengthened using CFRP composites". *Comps. Part:B*, **41**, 76-85, 2010.

[43] Bindhu, K.R., Jaya, K.P. and Manicka Selvam, V.K. "Seismic resistance of exterior beam-column joints with non-conventional confinement reinforcement detailing". *Struct. Eng. and Mech.*, **30**, 733-761, 2008.

[44] Elsouri, A.M. and Harajli, M.H. "Repair and FRP strengthening of earthquake-damaged RC shallow beam-column joints". *Advan. Struct. Eng.*, **18**, 237-250, 2015.

[45] Fisher, M.J. and Sezen, H. "Behavior of exterior reinforced concrete beam-column joints including a new reinforcement". *Struct. Eng. and Mech.*, **40**, 867-883, 2011.

[46] Garcia, R., Jemaa, Y., Helal, Y., Maurizio, G. and Pilakoutas, K. "Seismic strengthening of severely damaged beam-column RC joints using CFRP". *J. Comps. Constr.*, **18**, 04013048, 2014.

[47] Lee, W.T., Chiou, Y.J. and Shih, M.H. "Reinforced concrete beam-column joint strengthened with carbon fiber reinforced polymer". *Comps. Struct.*, **92**, 48-60, 2010.

[48] Li, B. and Kai, Q. "Seismic behavior of reinforced concrete interior beam-wide column joints repaired using FRP". *J. Compos. Constr.*, **15**, 327-338, 2011.

[49] Karayannis, C.G., Chalioris, C.E. and Sirkelis, G.M. "Local retrofit of exterior RC beam–column joints using thin RC jackets-An experimental study". *Earthq. Eng. Struct. Dyn.*, **37**, 727-746, 2008.

[50] Kim, J. and LaFave, J.M. "Key influence parameters for the joint shear behaviour of reinforced concrete (RC) beam–column connections". *Eng. Struct.*, **29**, 2523-2539, 2007.

[51] Antonopoulos, C.P. and Triantafillou, T.C. "Experimental investigation of FRP-strengthened RC beam-column joints". *J. Compos. Constr.*, **7**, 39-49, 2003.

[52] Haach, V.G., El Debs, A.L.H.D.C. and El Debs, M.K. "Evaluation of the influence of the column axial load on the behavior of monotonically loaded R/C exterior beam-column joints through numerical simulations". *Eng. Struct.*, **30**, 965-975, 2008.

[53] Arıoğlu, E., Arıoğlu, N. and Girgin, C. Normal ve yüksek dayanımlı betonlarda şekil-boyut etkisi. *Hazır Beton* (1999).

[54] Ilki, A., Bedirhanoglu, I. and Kumbasar, N. "Behavior of FRP-retrofitted joints built with plain bars and low-strength concrete". *J. Compos. Const.*, **15**, 312-326, 2011.

[55] El-Amoury, T. and Ghobarah, A. "Seismic rehabilitation of beam–column joint using GFRP sheets". *Eng. Struct.*, **24**, 1397-1407, 2002.

[56] Paulay, T. and Priestley, M. J. N. "Seismic design of reinforced concrete and masonry buildings". *Wiley*, New York, 1992.

[57] Akın, E. *Strengthening of brick infilled RC frames with CFRP reinforcement-general principles*. PhD Thesis, METU, Ankara, Turkey, 2011.

[58] Park, R. "Evaluation of ductility of structures and structural assemblages from laboratory testing". *New Zealand Nat. Soc. Earthq. Eng. Bull.*, **22**, 155-156, 1989.

[59] Canbolat, B.B. and Wight, J.K. "Experimental investigation on seismic behavior of eccentric reinforced concrete beam-column-slab connections". *ACI Struct. J.*, **105**, 154–162, 2008.

[60] Kitayama K., Otani S., and Aoyama, H. *Development of design criteria for RC interior beam-column joints. Design of Beam-Column Joints for Seismic Resistance (ACI SP-123).* Michigan USA, American Concrete Institute, 1991.

[61] TSI-500. Requirements for design and construction of reinforced concrete structures, Turkish Standards Institute, Ankara, Turkey, 2000.

[62] ACI Committee 352R-76. *Recommendations for design of beam-column connections in monolithic reinforced concrete structures (ACI 352R-76)*. Detroit, USA: American Concrete Institute, 1976.